VYSOKÉ UČENÍ TECHNICKÉ V BRNĚ
BRNO UNIVERSITY OF TECHNOLOGY

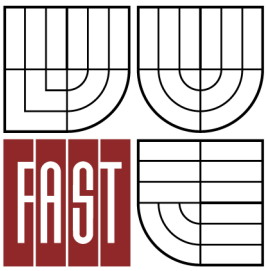

FAKULTA STAVEBNÍ
ÚSTAV TECHNOLOGIE STAVEBNÍCH HMOT A DÍLCŮ

FACULTY OF CIVIL ENGINEERING
INSTITUTE OF TECHNOLOGY OF BUILDING MATERIALS AND COMPONENTS

BEHAVIOR OF CONCRETE AT HIGH TEMPERATURES

STUDIUM CHOVÁNÍ BETONU PŘI PŮSOBENÍ VYSOKÝCH TEPLOT

DIPLOMOVÁ PRÁCE
MASTER'S THESIS

AUTOR PRÁCE — ING. MICHAELA FIEDLEROVÁ
AUTHOR

VEDOUCÍ PRÁCE — Ing. LENKA BODNÁROVÁ, Ph.D.
SUPERVISOR

BRNO 2014

VYSOKÉ UČENÍ TECHNICKÉ V BRNĚ
FAKULTA STAVEBNÍ

Studijní program	N3607 Stavební inženýrství
Typ studijního programu	Navazující magisterský studijní program s prezenční formou studia
Studijní obor	3607T020 Stavebně materiálové inženýrství
Pracoviště	Ústav technologie stavebních hmot a dílců

ZADÁNÍ DIPLOMOVÉ PRÁCE

Diplomant	Ing. MICHAELA FIEDLEROVÁ
Název	Studium chování betonu při působení vysokých teplot
Vedoucí diplomové práce	Ing. Lenka Bodnárová, Ph.D.
Datum zadání diplomové práce	31. 3. 2013
Datum odevzdání diplomové práce	17. 1. 2014

V Brně dne 31. 3. 2013

v.z. N. Žižka

prof. Ing. Rostislav Drochytka, CSc.
Vedoucí ústavu

prof. Ing. Rostislav Drochytka, CSc.
Děkan Fakulty stavební VUT

VYSOKÉ UČENÍ TECHNICKÉ V BRNĚ fakulta stavební DĚKANÁT - 1 -

Podklady a literatura

Designing Concrete Structures for Fire Safety, ACI, SP-255
Bradáčová, I. Stavby z hlediska požární bezpečnosti. ERA group, s.r.o. Brno 2007. ISBN 978-80-7366-090-1.
Bodnárová, L. Kompozitní materiály, učební opora VUT Brno, FAST, 2007
Drochytka, R. Trvanlivost stavebních materiálů, učební opora VUT Brno, FAST, 2008
ČSN EN 1992-1-2 Eurokód 2: Navrhování betonových konstrukcí – Část 1-2: Obecná pravidla – Navrhování konstrukcí na účinky požáru.
Sborníky z tuzemských a zahraničních konferencí (r. 2008-2013). České a zahraniční normy.
Internetové zdroje.

Zásady pro vypracování (zadání, cíle práce, požadované výstupy)

Předmětem diplomové práce je studium chování cementových betonů při působení vysokých teplot.
V teoretické části popište chování cementových betonů při působení vysokých teplot. Zaměřte se zejména na explosivní odprýskávání betonu. Uveďte příčiny explosivního odprýskávání a možnosti jeho eliminace.
Na základě rešerší literatury definujte požadavky na vhodný typ kameniva, cementu, přísad a příměsí pro prostředí s možným působením vysokých teplot.
V experimentální části diplomové práce připravte vzorky s vybraným typem cementu a rozptýlenou výztuží z polypropylenových (PP) vláken.
Proveďte zatěžování těchto vzorků na různé teplotní stupně.
Popište zvolenou metodiku teplotního zatěžování vzorků.
Proveďte sledování změn vlastností zkušebních vzorků po působení vysokých teplot.
Zhodnoťte vliv PP vláken na vlastnosti zkušebních vzorků po působení vysokých teplot.

Struktura bakalářské/diplomové práce

VŠKP vypracujte a rozčleňte podle dále uvedené struktury:

1. Textová část VŠKP zpracovaná podle Směrnice rektora "Úprava, odevzdávání, zveřejňování a uchovávání vysokoškolských kvalifikačních prací" a Směrnice děkana "Úprava, odevzdávání, zveřejňování a uchovávání vysokoškolských kvalifikačních prací na FAST VUT" (povinná součást VŠKP).
2. Přílohy textové části VŠKP zpracované podle Směrnice rektora "Úprava, odevzdávání, zveřejňování a uchovávání vysokoškolských kvalifikačních prací" a Směrnice děkana "Úprava, odevzdávání, zveřejňování a uchovávání vysokoškolských kvalifikačních prací na FAST VUT" (nepovinná součást VŠKP v případě, že přílohy nejsou součástí textové části VŠKP, ale textovou část doplňují).

.....

Ing. Lenka Bodnárová, Ph.D.
Vedoucí diplomové práce

Abstract

Increasing intensity of road and railway transport and thus a higher risk of accidents leads to a constant increase of safety standards in tunnels. Fire development in enclosed area such a tunnel is unpredictably fast and gasoline-fuelled fire temperature can rise up to 1100°C. Fire tests undertaken in past showed that with increasing temperature evaporation of chemically and physically bounded water lead to explosive spalling. Small or greater parts spall and it complicates the evacuation of people during fire as well as leads to loss of reinforcement cover or even rapid decrease of load-bearing capacity and subsequent collapse of structure. Owing to the increasing temperature, water contained in the concrete is converted to water vapour which is associated with built up of pore pressure. If the impermeable structure of concrete does not allow the escape of water vapour the pore pressure will increase and results in development of micro-cracks, respectively macro-cracks. This problem leads to the theme "Influence of permeability on explosive spalling". The term permeability represents the rate of transmission of media or energy flows and is a measure of the porosity of the concrete. Due to the density and compactness of high performance concrete (HPC) in comparison with ordinary concrete (OC) is impermeable and therefore sensitive to spalling caused by creation of high pore pressure. Additions of polymer fibres have been proved to be most effective solution to avoid explosive spalling in the event of fire. Various types of polymer and fibre dimensions and geometries have been testing at fire test since 1990´s. Polypropylene (PP) fibre has been ascertained as the most sufficient to avoid explosive spalling.

The master thesis is focused on analysis of behaviour of cement composite materials (concrete) exposed to high temperatures. Concrete specimens with different polypropylene fibres (standard and modified) of different dosage were exposed to thermal load with a high initial temperature increase of 1100°C in first 30 minutes and then constant temperature 1100°C hold up to 120 minutes (HydroCarbon curve). Experimental work was focused on different behaviour and physical mechanical properties of concrete without and with polypropylene fibres and verification of function of concrete with modified polypropylene fibres. Using the modified fibers with lower dosage of 0.9 kg/m^3 reduces a negative effect of fibers on workability and processability of fresh concrete.

After exposition to high temperature load, physical mechanical properties of fibre reinforced concrete were observed and compared to reference specimens without PP-fibres and simultaneously were compared specimens with addition of standard PP-fibres with melt flow index 25 (MFI 25) and dosage 2.0 kg/m^3 and modified PP-fibres with MFI 2500 and dosage 0.9 kg/m^3. Surface of tested specimens was analysed by photogrammetry analysis and damage of surface was defined. Mode of action of

polypropylene fibres was observed with high temperature microscopy and video with melting properties of standard and modified fibres were gained as result. Subsequent comparison of videos show different points of softening and melting of standard fibres with MFI 25 and modified fibres with higher MFI 2500. Softening starts with difference of about 10°C. PP-fibres with lower MFI 25 start to melt at 160°C and build a drop at temperature 174°C whereas modified PP-fibres with higher MFI 2500 start to melt in the range 147 - 150°C and build a drop at temperature 160°C. This mode of action has been proven in permeability measurement when permeability of samples with modified fibres increased at temperature around 150°C and around 175°C in samples with standard fibres. Concrete permeability at different temperatures and pressures has been measured in cooperation with Technical University in Vienna. Permeability was measured at temperatures of 20°C, 90°C, 150°C, 175°C, 200°C, 225°C and 250°C and at pressure of 0.2, 0.4 and 0.6 MPa.

Keywords

explosive spalling, polypropylene fibres, Melt Flow Index (MFI), thermal load, HydroCarbon temperature curve, high performance concrete, permeability of concrete

Rozšířený český abstrakt

Se stále se zvyšující intenzitou silniční a železniční dopravy se zvyšuje i riziko nehodovosti, což vede ke zvyšování bezpečnostních požadavků v tunelech a podzemních konstrukcích. Vznik a vývoj požáru v uzavřeném prostoru, jako například v tunelu, je nepředvídatelně rychlý a benzínem živený požár má vysoký počáteční nárůst teploty, která dosahuje až 1100°C v prvních třiceti minutách. Při rychlém teplotním zatížení betonové konstrukce dochází k přeměně fyzikálně a chemicky vázané vody ve vodní páru, což vede k nárůstu pórového tlaku. Problematika explosivního odprýskávání vyvstala s požadavkem na zvyšování pevnosti betonu. Hutnější, méně propustnější struktura betonu sebou přináší i jisté nevýhody, jako např. křehkost. Impermeabilní struktura betonu neumožňuje únik vodní páry a tak dochází při požáru k nárůstu pórového tlaku, který kromě explosivního odprýskávání vede ke vzniku mikro a makro trhlin. Malé či větší úlomky odprýskávají od povrchu a komplikují evakuaci osob během požáru, dochází ke ztrátě krycí vrstvy výztuže a následnému omezení nosné kapacity konstrukce, což může vést až ke kolapsu celé konstrukce. Tato problematika tedy vede k tématu „Vliv permeability betonu na explosivní odprýskávání“, které je řešeno v experimentální části společně s tématem „Explosivní odprýskávání vysokopevnostního betonu exponovaného teplotnímu zatížení“. Permeabilita, jako měřítko pórovitosti betonu, představuje míru transmise média nebo energetických toků materiálem. Již je známo, že malé množství polypropylenových vláken přidávaných do betonové směsi efektivně ovlivňuje vlastnosti betonu proti účinkům požáru zvyšováním jeho permeability, ale negativně ovlivňuje jeho zpracovatelnost. Tato problematika zpracovatelnosti by mohla být eliminována snížením dávky vláken. Nová modifikovaná vlákna s vyšším indexem toku taveniny MFI 2500 (Melt Flow Index), patentovaná německou firmou BAUMHÜTER, umožňují snížení dávky na 0,9 kg/m^3 oproti vláknům standardním.

V experimentální části této práce byly porovnávány mechanicko-fyzikální vlastnosti betonu bez přídavku polypropylenových vláken (dále jen PP-vláken), s 2 kg/m^3 standardních PP-vláken s MFI 25 a s 0,9 kg/m^3 modifikovaných PP-vláken s MFI 2500. Explosivní odprýskávání bylo zkoušeno na zkušebních tělesech o rozměrech (600x600x300)mm vystavených uhlovodíkové teplotní křivce po dobu 120 min. Exponovaná plocha o rozměrech (600x600)mm byla paralelně zahřívána horizontálním a vertikálním olejovým hořákem v peci o objemu 1 m^3. Sledovaný povrch zkušebních těles byl podroben fotogrammetrii před i po zkoušce ohněm a tyto snímky slouží k následnému porovnání. Na snímcích je zřetelná plocha a hloubka odprýsknutého povrchu i makro-trhliny. Pro objasnění mechanismu účinku standardních PP-vláken s MFI 25 a modifikovaných vláken s MFI 2500 byla vlákna pozorována pod vysokoteplotním

mikroskopem. Z pořízeného videozáznamu bylo možné stanovit bod měknutí a tání PP-vláken a objasnit tak způsob účinku jednotlivých druhů PP-vláken.

Druhá část experimentální práce byla zaměřena na stanovení permeability betonu o stejné receptuře a s různým dávkováním PP-vláken jako v případě explosivního odprýskávání. Zkušební tělesa byla umístěna v ocelovém prstenci o průměru cca 100 mm a výšce cca 50 mm. Permeabilita byla zkoušena laboratorně pomocí stlačeného vzduchu na zkušebním zařízení sestrojeném na Technické Universitě ve Vídni, které umožňuje měření permeability za různých teplot a současně za různých tlaků. Propustnost byla měřena při teplotě 20°C, 90°C, 150°C, 175°C, 200°C, 225°C a 250°C a tlaku 0,2, 0,4 a 0,6 MPa.

Doposud získané poznatky této problematiky jsou podrobně zpracovány v části teoretické. Faktory mající dominantní vliv na explosivní odprýskávání a jeho mechanismus jsou popsány v kapitole č.2. Mechanismus explosivního odprýskávání je procesem dvou paralelně probíhajících procesů: termo-mechanický a termo-hydraulický. Dále je zde uveden podrobný výčet standardů a norem pro požární ochranu ostění tunelů včetně sumarizace specifických kritérií. Ve stručnosti byl popsán vhodný návrh jednotlivých komponent betonu se zaměřením zejména na příměsi ve formě rozptýlené výztuže z polypropylenových vláken, jež se ukázala jako velmi efektivní ochrana proti odprýskávání. Polypropylenová vlákna, druhy, dávkování a především jejich mechanismus působení v betonu exponovaného požáru je popsán v kapitole č.6 a č.7.

Klíčová slova

explosivní odprýskávání, polypropylenová vlákna, index toku taveniny (MFI), teplotní zatížení, uhlovodíková teplotní křivka, vysokopevnostní beton, permeabilita betonu

Bibliografická citace VŠKP

Ing. Michaela Fiedlerová *Studium chování betonu při působení vysokých teplot.* Brno, 2014. 98 s.,7 s. příl. Diplomová práce. Vysoké učení technické v Brně, Fakulta stavební, Ústav technologie stavebních hmot a dílců. Vedoucí práce Ing. Lenka Bodnárová, Ph.D..

Prohlášení:

Prohlašuji, že jsem diplomovou práci zpracoval(a) samostatně a že jsem uvedl(a) všechny použité informační zdroje.

V Brně dne 10.1.2014

……

podpis autora
Ing. Michaela Fiedlerová

Acknowledgements

I would like to express my thanks of gratitude to my supervisor Ing. Lenka Bodnárová, Ph.D.as well as Dipl.-Ing. Klaus Pistol and Dr. Ing. Frank Weise who gave me the golden opportunity to do this interesting project on the topic *Explosive spalling of concrete exposed to elevated temperature*. Secondly I would also like to thank to Ass.Prof.Dipl.-Ing.Dr.techn. Heinrich Bruckner, who helped me with measurement of concrete permeability and gave me valuable advices in this topic. Finally I would also like to thank my parents and friends who helped me a lot in finishing this project within the limited time. This diploma thesis has been prepared with the financial support of the project "SUPMAT - Promotion of further education of research workers from advanced building material centre". Registration number CZ.1.07/2.3.00/20.0111. The project is cofunded by European Social Fund and the state budget of the Czech Republic. This diploma thesis has been made under the internship which increased my knowledge and interest of research.

CONTENT

AIM OF THE STUDY

The aim of this diploma thesis is to focus on the resistance of concrete exposed to high temperatures especially with focus of resistance against explosive spalling as well as clarifying the mode of action of polypropylene fibres. The theoretical part is an introduction to the issues of explosive spalling, its mechanisms and majority influencing factors. Further description of the processes taking place in the structure of concrete under extreme thermal load, distribution and size of pores in concrete, thermal load, temperature-time curves and their applications, methods of elimination of negative behaviour of concrete exposed to thermal loading (passive and active methods), mode of action of polypropylene fibres and more is also included in the theoretical part. The main aim of experimental part is to verify the function of polypropylene fibers of various Melt Flow Indexes (MFI) and dosage. Primarily, the test samples with content of the PP-fibers are compared to the reference sample without fibers. Secondarily, the samples with standard PP-fibers (with MFI 25) with dosage 2.0 kg/m^3 are compared to samples with modified PP-fiber (with MFI 2500) of dosage 0.9 kg/m^3. Photogrammetric images were used for evaluation and comparison of spalled surface and its depth. Determination of the softening temperature and melting point of the modified and standard PP-fibers was made by using a high temperature microscope video. The second part of the experimental work was to determined concrete permeability at different temperatures and pressures. Permeability was measured at temperatures of 20°C, 90°C, 150°C, 175°C, 200°C, 225°C and 250°C and at pressure of 0.2, 0.4 and 0.6 MPa.

I. THEORETICAL PART

1 Introduction

Concrete as the world´s most widely used building material offers advantages in civil engineering due to its versatility, durability, processability to desired shape and strength. Despite the favourable properties of this material there is still an effort to optimize its properties to different conditions which may occur during the usage and lifetime of the constructions. Although its incombustibility, the fire exposure changes the mechanical behaviour of concrete especially in case of high performance concrete due to its density and low porosity. However, if concrete structure is exposed to high temperature due to fire, explosive spalling is generated. Explosive spalling leads to significant deterioration in the load resistance of structures, drastically reduces their lifetime, and in some cases, can lead to the collapse of construction. Damages of construction caused by fire are fatal especially regarding the underground construction as tunnels, metro, where the possibility of early and urgent intervention, escape of people and subsequent repairs are impeded. Therefore, many researches dealing with fire exposure of concrete has been undertaken in last decades.

A method to improve the fire resistance of concrete is the use of a special type concrete which can fully avoid explosive spalling during a fire. The addition of polypropylene fibres (PP-fibres) to concrete is one way to decrease or even avoid spalling of concrete exposed to fire ([1]-[4]). Due to thermal decomposition of the PP fibres the permeability of concrete is increased and transport system is provided for the escaping water vapour [2]. Additionally, it has been proven that type of aggregate has also significant impact on the physical characteristics of concrete exposed to high temperatures [3]. The results showed that the density of concrete has the greatest impact on explosive spalling. This makes high performance concrete (HPC) more sensitive than ordinary concrete (OC) due to its impermeable structure.

1.1 Fire protection requirements standards for tunnels and underground structures

The fire protection of underground structures (road, rail and mass-transit tunnels) is an important criterion for the design of such structures in the recent years, since it has been showed that damage could be very serious not only in terms of loss of human lives, but also the subsequent large direct and indirect cost of repairs Increased attention is paid to the risks of fires due to occurrence of accidents in recent years (e.g. King's Cross in 1987 – 31 dead and many injured, Mont Blanc in 1999 - 39 dead, Tauern – Salzburg in 1999 – 12 dead and 49 injured, St. Gotthard in 2001 – 11 dead [6], [7]).

The aim of proposed measures is to guarantee a certain time for strength and stability of concrete structures and supporting its integrity in order to ensure safe escape of persons, evacuation of animals and property as well as allowing interference for rescue teams during and after a fire. It is necessary to prevent both the spread of fire inside the building and transfer of fire from a burning structure on the adjacent (opposite or adjacent) structure ([8]-[13]).

In this chapter the main European standards and guidelines for the fire protection of tunnel linings and their specific criteria are summarized as well as the most common general temperature-time curves will be showed and briefly described.

1.1.1 Superior European Directives for tunnel safety

EU Tunnel Directive 2004/54/EC [7]

- Document provides minimum general requirements and specifications for the safety of road tunnels with the trans-European road network.
- Directives includes mainly the tunnel general layout, escape routes and emergency exits, safety installations, water supply, monitoring system, etc. with no specific requirements for structural fire resistance except for the requirement of no collapse of important neighbouring structures (cascading effect).

EU Decision 2008/163/EC (TSI – Guideline)

- Technical specification in term of International multi-system operability relating to safety in railway tunnels in the trans-European conventional and high-speed rail system provides minimum safety requirements including structural requirements under fire.
- Requirement of no collapse of the structure during evacuation.
- Fire resistance of the tunnel surface to fire impact for a time of 170 min.

1.1.2 Relevant Eurocodes for fire protection design

Eurocode EN 1991-1-2: Actions on structures [10]

- Defines general loading assumption and general rules for the analysis of structures under the high temperature

Eurocode EN 1992-1-2: Design of concrete structures [11]

- Provides general material requirements of concrete and steel reinforcement that vary with increasing temperature and detailed and simplified methodologies for the design of concrete structures under the impact of fire.

Eurocode EN 13501-1:2007+A1:2009: Fire classification of construction products and building elements [12]

- Fire classification of construction products and building elements.

1.1.3 Application documents for fire safety in Czech Republic

ČSN 73 7507 Desing of road tunnels [13]

- Provides requirements for the design, spatial layout and equipment of tunnels on the road, highways and local roads.
- Chapter 13 specified requirements for design of tunnels for fire safety.

1.2 Temperature-time curves for fires in tunnels

Large deal of research of international scale has been undertaken with aim to specify the types of fire which could occur in tunnel and underground spaces. It has been tested in both real, disused tunnels and laboratory conditions. As a result of the data gained from these experiments, a series of temperature-time curves for the various exposures have been developed ([12]-[14]). The most common general temperature-time curves are showed in Figure 1-1.

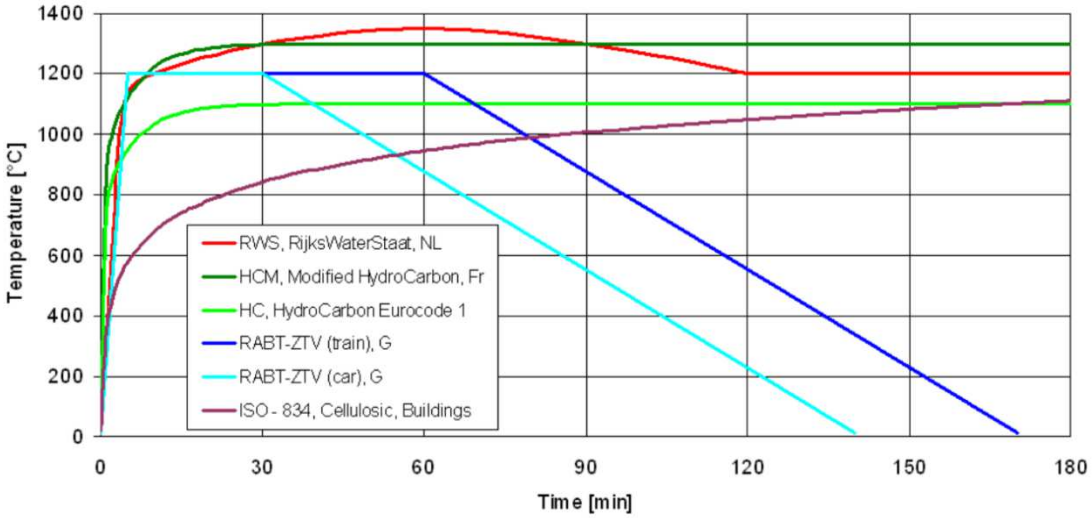

Figure 1-1: Temperature-time curves for fires in tunnels [17]

The fire scenarios and the application of the different temperature-time curves has been investigated in the past recent years in different projects and Eurocode EN 13501-1[12] has applied individual fire scenarios and fire classification of construction products and building elements. The different temperature-time curves correspond to individual fire scenarios (Figure 1-2 to Figure 1-5).

1.2.1 Cellulosic curve ISO – 834

This cellulosic ISO-based curve is based on the burning rate of the materials found in general building materials and contents and it is used in standards throughout the world (Figure 1-2). It is a model of a ventilated controlled natural fire, i.e. fires in a normal building. The increase of temperature after 30 minutes is 842°C and temperature increase up to 1110°C in 180 minutes [14].

ISO 834 specifies the temperature T (°C) as:

$$T = 345 \cdot \log_{10}(8t+1) + T_o \qquad 1.1.$$

t….. *time (min)*

T_o… *ambient temperature (°C)*

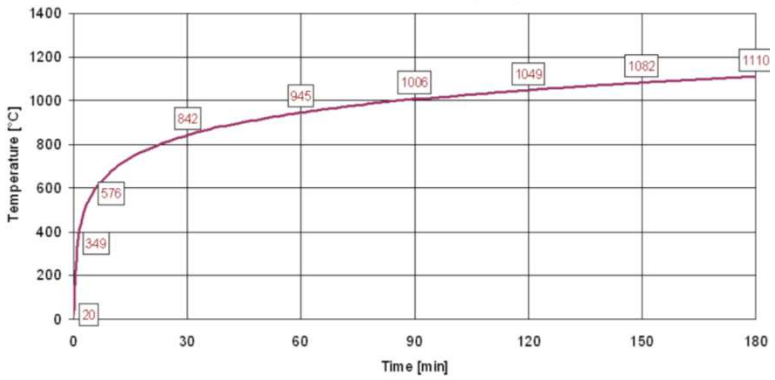

Figure 1-2 : Cellulosic temperature-time curve [17]

1.2.2 HydroCarbon curve

Although the Cellulosic curve has been in use for many years, it soon became apparent that the burning rates for materials such a petrol gas, chemicals and etc. have a different temperature-time load. Therefore, there was a need to develop an alternative exposure for the purpose of carrying out the experiments on structures and materials used within the petrochemical industry. The HydroCarbon temperatute-time curve (Figure 1-3) was determined as a simulation of a ventilated oil fire with a high initial temperature increase of 1100°C after 30 minutes and then constant temperature 1100°C hold up to 180 minutes [14].

The temperature T (°C) in hydrocarbon fire curve is given by:

$$T = 1080 \cdot (1 - 0.325 \cdot e^{-0.167t} - 0.675 \cdot e^{-2.5t}) + T_o \qquad 1.2.$$

t….. *time (min)*

T_o… *ambient temperature (°C)*

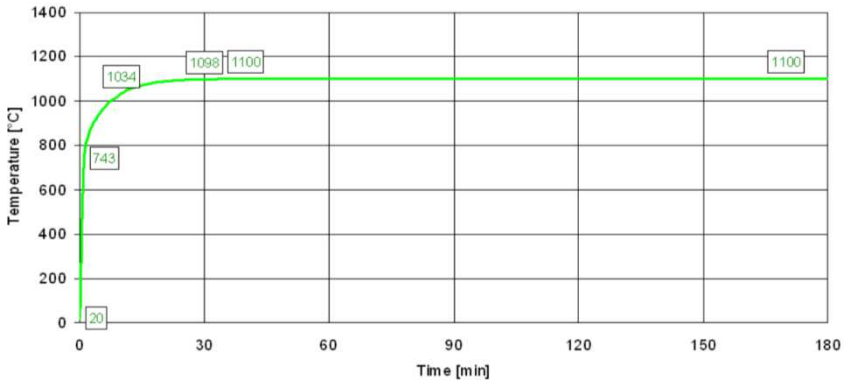

Figure 1-3: HydroCarbon temperature-time curve [14]

1.2.3 RABT curve ZTV

RABT curve (Figure 1-1) developed in Germany as a result of a series of test programmes such as the Eureka Project EU 499: Firetun [15]. In the RABT Curve (car, train), the temperature rise is very rapid up to 1200°C within 5 minutes. The duration of the 1200°C exposure is shorter than other curves with the temperature drop off starting to occur at 60 minutes for cars and 30 minutes for trains [14].

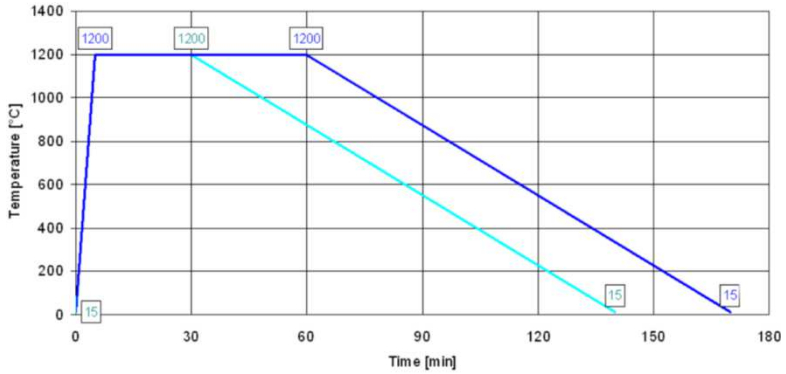

Figure 1-4: Figure 4: RABT temperature-time curve (car, train) [14]

1.2.4 RWS curve

RWS curve, model of petroleum based fire of 300 MW fire load in an enclosed area developed by the Rijkswaterstaat, Ministry of Transport in the Netherlands is specified for use in tunnels (Figure 1-5). This curve is based on the assumption that in a worst case scenario, a 50 m³ fuel, oil or petrol tanker fire with a fire load of 300 MW could occur, lasting up to 120 minutes. It is internationally accepted. The temperature increase after 30 minutes is 1300°C. Temperature reaches 1350°C (melting point of concrete) for short duration in 60 minutes and then drop off starting to occur after 60 minutes. After 120 minutes temperature is constant up to 180 minutes.

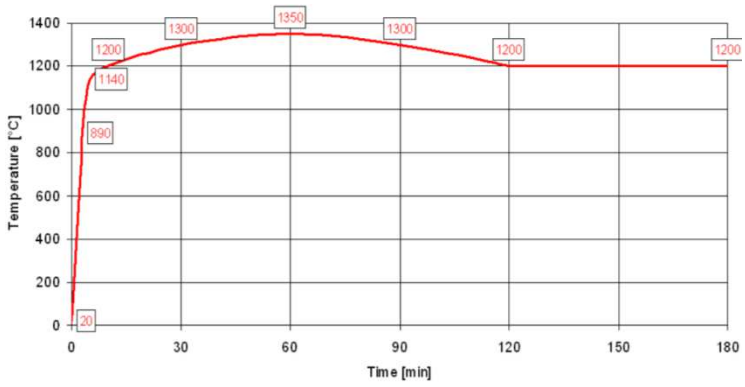

Figure 1-5: RWS temperature-time curve [14]

2 Explosive spalling of HPC due to fire exposure

In last year's, concrete was improved to provide better performance in term of higher strength, early strength increase, rheology of fresh concrete and better durability due to changes in composition of mixture such as reduction of water cement ratio compensate by using superplasticizers, addition of fibres and etc., which can also leads to brittle behaviour foremost of high performance concrete exposed to fire. The brittle behaviour of HPC exposed to fire leads to explosive spalling due to thermo-hydraulical and thermo-mechanical mechanisms (Figure 2-1 to Figure 2-2). It is likely that both contribute to spalling but the relative importance depends upon the concrete design, moisture content, section size, external load and pressing level, content of reinforcement and permeability associated with concrete strength. Small or greater parts spall and it complicate the evacuation of people during fire as well as leads to loss of reinforcement cover or even rapid decrease of load-bearing capacity and subsequent collapse of structure (Figure 2-3). Several technological solutions can be applied to reduce this negative effect [11]:

- Application of protective layers for which it is demonstrated that no spalling of concrete occurs under fire exposure (external protection),
- modification of mix design - addition of 2 kg/m^3 monofilament propylene fibres has been proved as effective way,
- use of a type of concrete for which it has been demonstrated (by local experience or by testing) that no spalling of concrete occurs under fire exposure (eliminate use of HPC in the zone where the risk of fire is high),
- modification of design of structures and elements itself, so that the thermal stress is reduced.

Besides explosive spalling the other types of spalling are distinguish such as (a) violent spalling related to pore pressure, compression due to thermal gradient and internal cracking due to different thermal expansion of aggregates and cement paste (b) local corner spalling caused by internal cracking due to different thermal deformation of concrete and steel (c) post-cooling spalling and (d) sloughing off caused by strength loss due to chemical transition and cracking due to different thermal expansion of aggregates and cement paste. The study will be focus mainly on explosive spalling.

Spalling can be also categorized according the size of spalled pieces to [32]:

- Explosive spalling – destructive spalling of a few large pieces of concrete,
- local spalling – small pieces of some local points e.g. corners, edges,
- gradual spalling of cross section - take place at very high temperature and with lightweight aggregate concrete,
- sloughing off – spalling of small pieces of concrete from the surface.

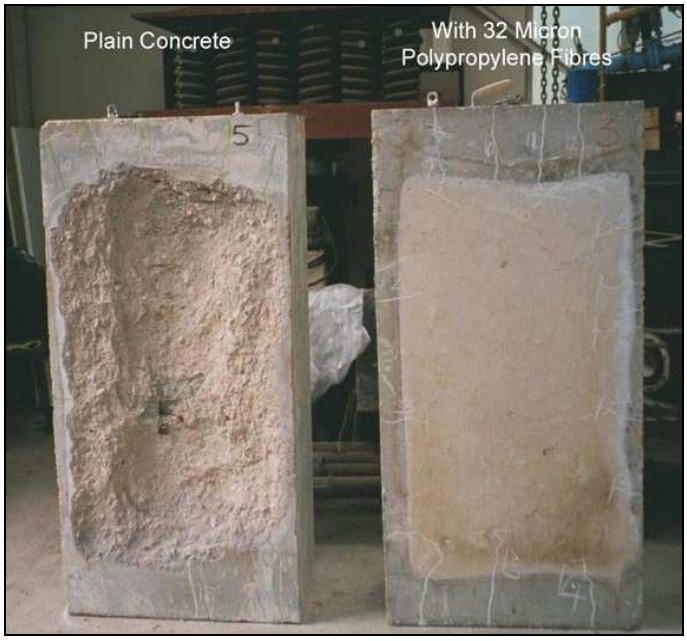

Figure 2-1: Spalled surface of concrete without PP fibres and with PP fibres [16]

Figure 2-2: left: Uncovered reinforcement due to explosive spalling; right: Collapse of structure due to explosive spalling [17]

2.1 Mechanism of explosive spalling

Mechanism of explosive spalling can be explained as follow (Figure 2-3). With increasing temperature load on the surface of concrete desorption of physically bounded water occurs at first and the gel water and crystal water from aggregate is released subsequently. One part of water vapour emerge in the concrete escape through the pores of the concrete via free surface into atmosphere and the other part moves into the internal concrete body. When this water vapour flow reaches the cooler zone it begins to condense and an accumulation of condensed water forms so called “Moisture Clog”. This moisture clog is completely saturated front that does not allow migration of vapour through. This results to build-up of large pore pressure at saturated front and leads to explosive spalling due to enormous pore pressure and thermal stress.

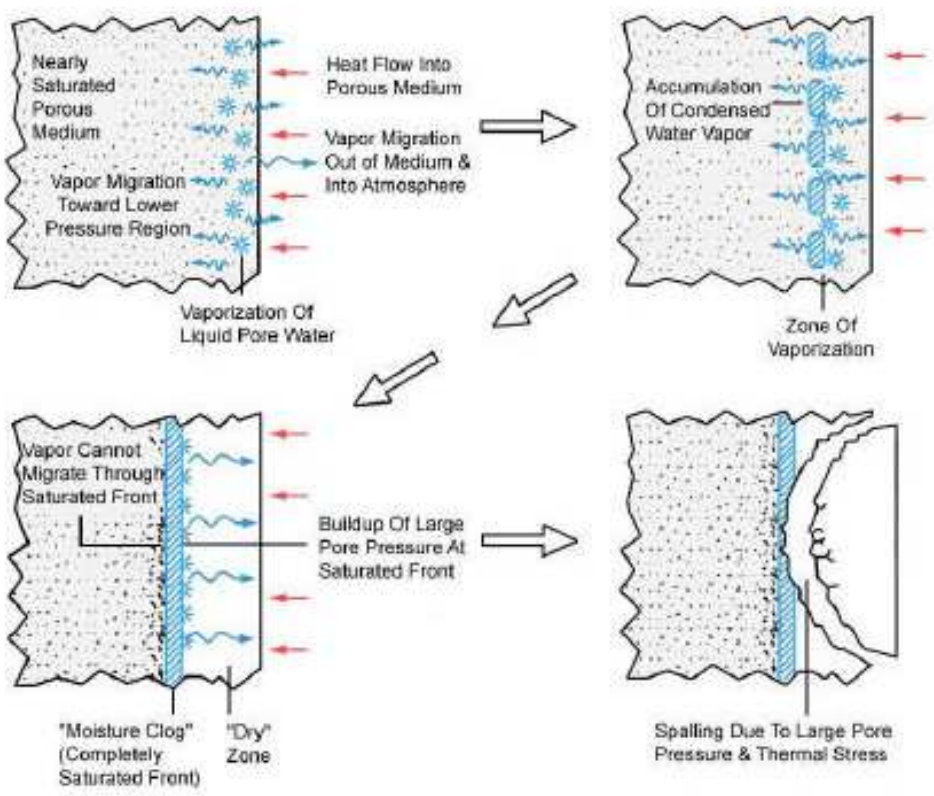

Figure 2-3: Schematic diagram of explosive spalling caused by thermo-hydraulical processes [32]

The total pore pressure is a result of the summarization of the partial pressures of all phases involved, i.e. water, vapour, air and melted fibres [32]:

$$P_{tot}(T) = P_W(T) + P_V(T) + P_A(T) + [P_F(T)] \quad (1.3.)$$

Due to dense impermeable structure of high performance concrete the saturated front is formed near to the surface which leads to the faster heating up of the water zone and faster increase of build-up pore pressure (Figure 2-4). Probability of explosive spalling is therefore higher than in ordinary concrete.

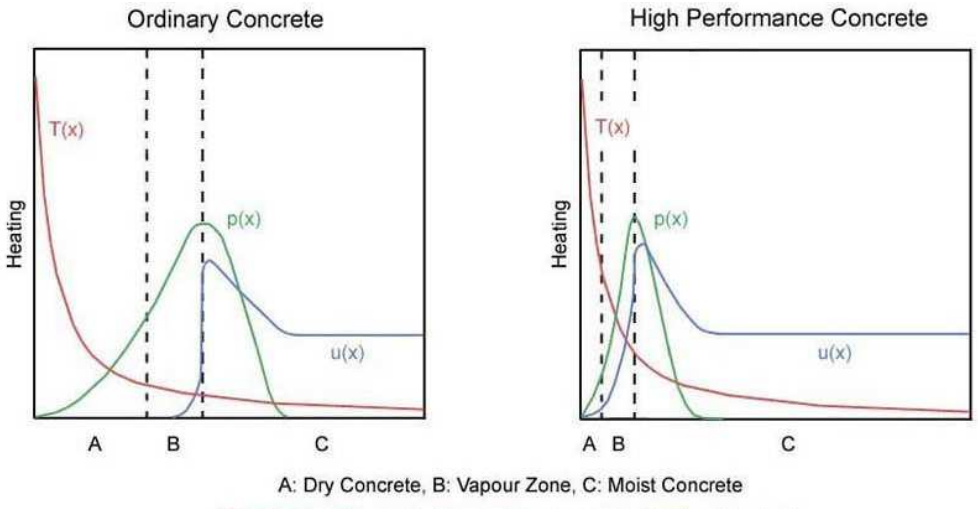

Figure 2-4: Difference of pressure and moisture distribution in Ordinary Concrete [32]

2.2 Factors influencing spalling

Many aspects have been investigated in past to clarify and interpret explosive spalling mechanism as:

- different heating condition,
- section size and shape,
- moisture content and age of concrete,
- permeability of concrete and the associated pore pressure,
- different concrete (mix proportion, aggregate, curing condition, quality of concrete),
- content and cover to reinforcement,
- additives (polypropylene fibres),
- external load and pressing level.

Those aspects will be closely described below.

2.2.1 Heating rate

Generally, the risk of spalling and its severity increases with heating rate. However, probability of spalling arises with the heating rate doesn´t has to be rule. Higher heating rate may generate occurrence of macro-cracks, damages which helps to increase permeability and allow transport of vapour and therefore reduce build-up pore pressure. Contrary to that, lower heating rate reduce a formation of macro-cracks, therefore water vapour cannot easily vaporize from core of element and explosive spalling would occur due to higher pore pressure.

In general, the heating rate is crucial and has a dramatic effect on the spalling mechanism. Thermal shock cause water vapour generation and expansion of aggregates culminated in explosive spalling.

2.2.2 Section size

Very thin section (few millimetres) enable moisture content to escape more readily and thus preventing the build-up of pore pressure and therefore spalling is eliminated.

Spalling volume varies within loaded size of section. Effect of the dimension is closely describe in research undertaken in BAM focussed on effect of the dimension of a fire exposed surface upon the spalling of concrete specimen (HPC without PP-fibres) [48]. Heated surface was partly blocked by the plate of insulating material (vermiculite plate) with circular cut-outs of different diameter in the middle. Specimens of size 600x600x300 mm with cut-outs of dimensions 120 mm, 180 mm, 240 mm and 360 mm were exposed to cellulosic ISO-based curve ISO 834. Mix design of concrete is shown in Table 10-1 (without fibres). Photogrammetry pictures in Figure 2-5 shows different spalling volume and crack formation. Explosive spalling was not observed in sample with exposed surface of 120 mm. Spalling occurred in exposed section of diameter 180, 240 and 360 mm where the most striking spalling depth was observed in sample with cut-out of diameter 240 mm.

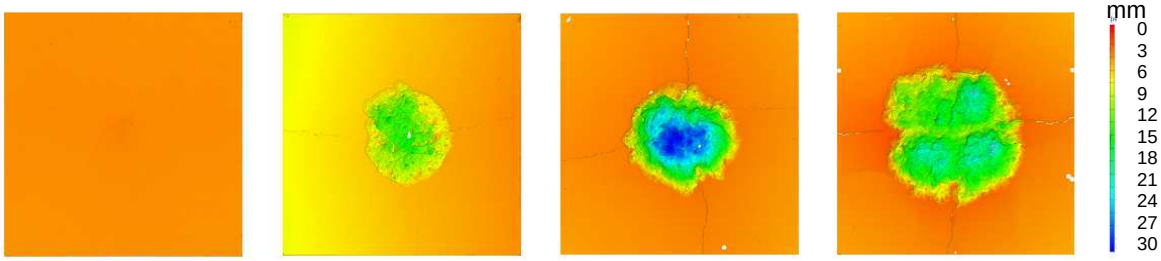

Figure 2-5: Explosive spalling and crack formation [48]

It may be conclude that tendency to spalling and spalling volume increase with heated area. Another interesting phenomenon was observed in sample with exposed area of 360

mm. Spalled surface was divided into 4 parts with shape of cloverleaf where spaling depth was significant in the centre of each part (leaf).

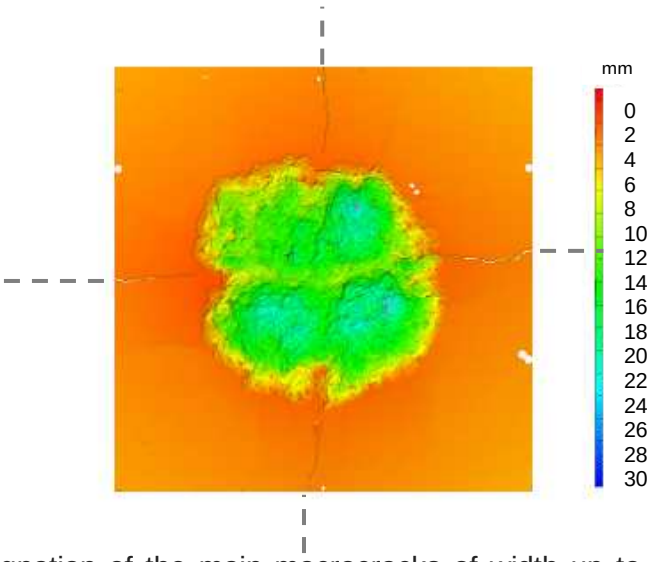

Figure 2-6: Designation of the main macrocracks of width up to 4 mm which result in significant pore pressure decrease and thus minimize explosive spalling in adjacent area [48]

2.2.3 Section shape

The higher the jaggedness (segmentation) of cross-section is the higher sensitivity to spalling due to higher thermal stresses. Plain surfaces and rounded corners seem to be the more stable.

2.2.4 Moisture content in concrete

Moisture content of concrete normally decreases with age as a result of hydration. It is also dependent on initial water-cement ratio which varies with type of concrete and its desire strength characteristic. Higher water content is higher sensitivity to spalling. Explosive spalling of self compacting concrete (SCC) with strength in range 50-70 N/mm^{-2} was tested by Schneider et al. [46] and higher spalling volume was observed at sample stored in water. Both water stored and air stored specimen were without fibres.

This issue is further discussed in Chapter 4**.**

2.2.5 Pore pressures

Owing to the increasing temperature, water contained in the concrete is converted to water vapour and with increasing temperatures the expansion and the associated upsurge in pore pressure. If the impermeable structure of the concrete will not allow the escape of

water vapor the pore pressure increased and results in development of micro-cracks, respectively macro-cracks.

Testing device for simultaneous measurements of pressure and temperature at various concretes heated on one face up to 800°C was designed by Kalifa et al. [23]. Ordinary concrete (OC) and high performance concrete (HPC) were tested. Both tested concretes demonstrated a similar thermal behaviour as was supposed. The pore pressure curves exhibit a very well-marked peak where pressure in HPC at 50 mm reached 37 bars and 18 bars in OC. Another interesting phenomenon is an increasing trend of pore pressure in HPC measured from 10 to 50 mm which is not recorded in OC. Total mass loss was measured simultaneously with increasing temperature and total mass loss of OC was higher than in HPC due to a different initial water content (initial water content of OC was 3.9 %vol and 2.95 %vol in HPC). Comparison of pore pressure and mass loss of OC and HPC is illustrated in Figure 2-7.

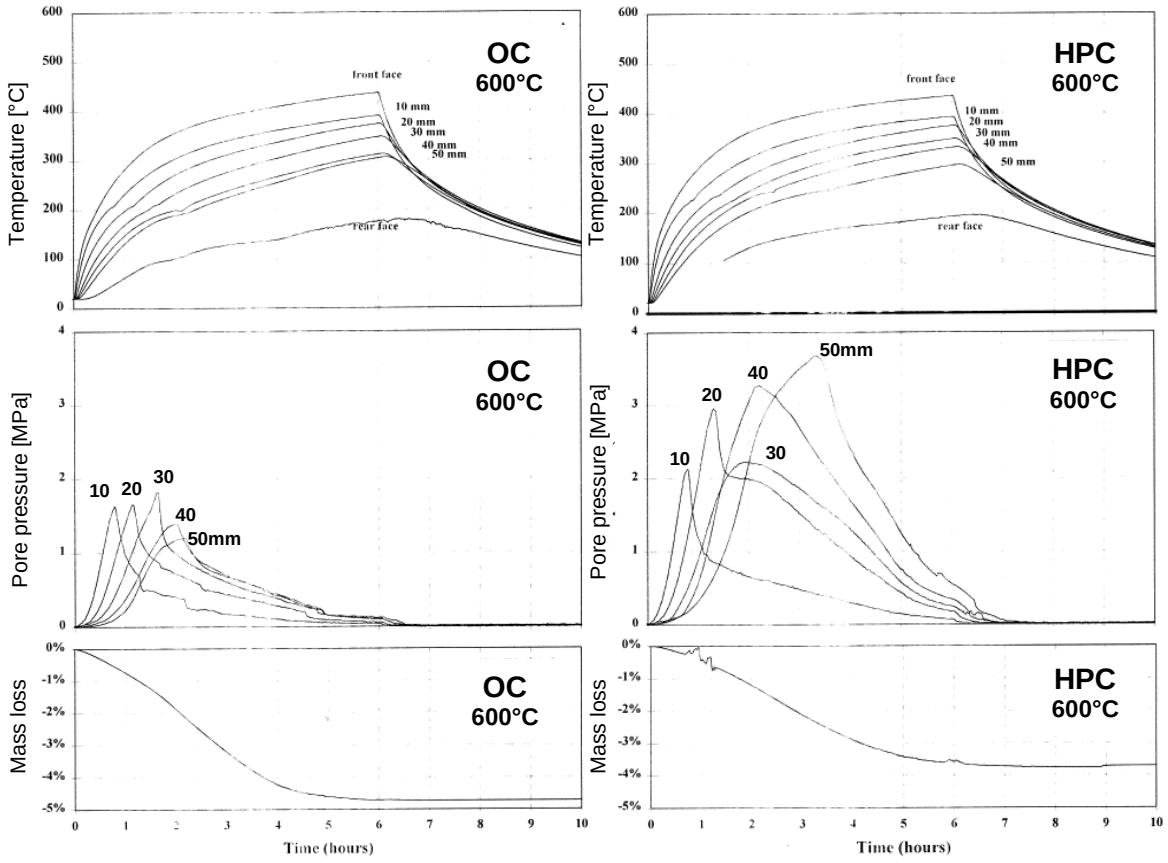

Figure 2-7: Temperature, pore pressure and mass loss vs. time of ordinary concrete (left) and high performance concrete (right) [23]

Anomaly that is noticeable in the pressure curve at 30 mm measured in HPC has been identified as damage of o-ring connector or as a result of crack formation at the interface between the pressure gauge and concrete. These significant differences in the pore

pressure levels are the explanation for the different behavior of OC and HPC exposed to high temperatures and subsequent explosive spalling.

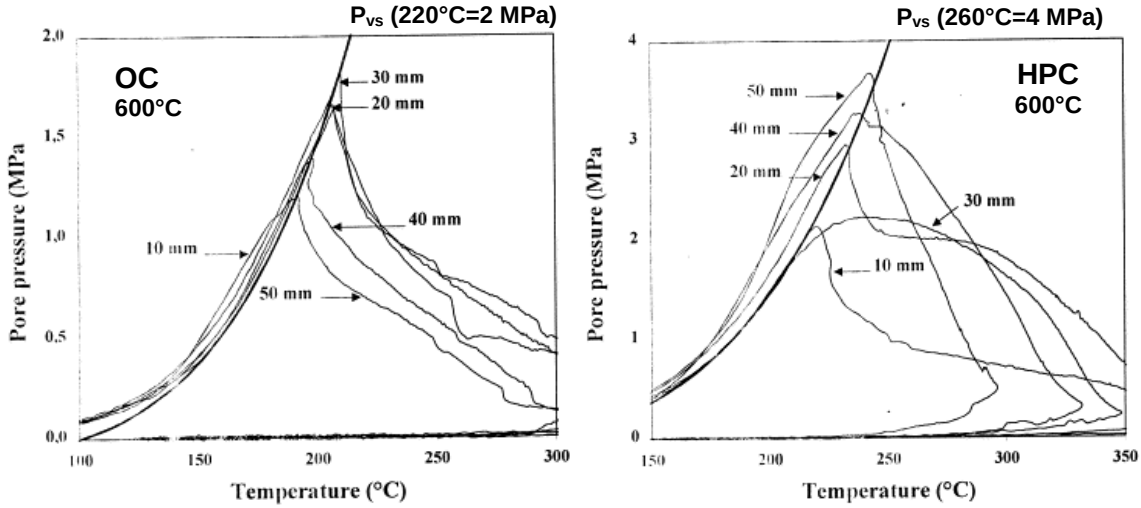

Figure 2-8: Pressure vs. temperature diaframs for OC and HPC, plotted together with the saturating vapour pressure Pvs(T) [23]

From Figure 2-8 the most striking differences observed between OC and HPC lays in the height of the pressure peak and pressure gradients are higher in HPC in comparison to OC. This explains a higher sensitivity to explosive spalling of HPC.

2.2.6 Permeability of the concrete

Permeability as influencing factor affects the rate of vapour release as a result of critical pressure level is significant foremost in term of HPC. Due to the density and compactness of HPC is in comparison with OC impermeable and therefore sensitive to spalling caused by creation of high pore pressure.

This issue is further discussed in Chapter 4: Permeability and porous network in concrete.

2.2.7 Concrete age and storing

With the age of concrete the moisture content decreases as a result of hydration. This may vary according to location and use of construction. Tested specimens of dimensions (300x500x600)mm with compressive strength in range 50 – 70 N/mm^2 tested after different storing conditions (air stored, water stored) showed explosive spalling and cracking in both cases but it different range. Water stored specimen demonstrated more significant cracks and surface damage in for of explosive spalling [46].

2.2.8 Concrete strength, mix and quality

With the increasing quality of the concrete its porosity (permeability) is reduced and therefore its density, strength and durability increased. Paradoxically, it increases its brittleness and susceptibility at elevated temperatures. It was observed that dense high performance concrete showed an increased sensitivity to explosive spalling over ordinary concrete. Explosive spalling of high performance concrete (HPC) has been already observed at concrete with compressive strength around 50 Mpa [46]. Water/cement ratio plays also significant role in term of spalling. Capillary pores are formatted in concrete with w/c ratio over 0,30 and therefore increased permeability of concrete overcome tendency to spalling by itself.

Explosive spalling of self-compacting concrete (SCC) has been observed by Horvarh et al within concrete with compressive strength in range 50 – 70 N/mm^2 [46].

2.2.9 Type of aggregate

The aggregate occupies 60-80% of the volume of concrete and therefore its properties at high temperature are substantial. A key factor in the thermal behaviour of concrete exposed to fire is the physical and chemical stability of aggregates. Increasing temperature leads to increase in the volume of aggregates and thus thermal expansion is an important characteristic of aggregates. Thermal expansion of the aggregate depends on the mineralogical composition and therefore all the minerals vary in the amount of thermal expansion as shown in Figure 2-9.

Aggregates with low thermal expansion and a negligible residual strain appear to be suitable for concrete with a potential risk of exposure to high temperatures [20].

Aggregates like flint, gneiss, slate and lightweight aggregates cause local or gradual spalling but only at very high temperatures. Addition of lightweight aggregates in concrete mixture can eliminate explosive spalling due to its porosity which enables water vapour escape. Suitable aggregate for concrete exposed to high temperature are blast furnace slag, basalt, diabase and andesite [32].

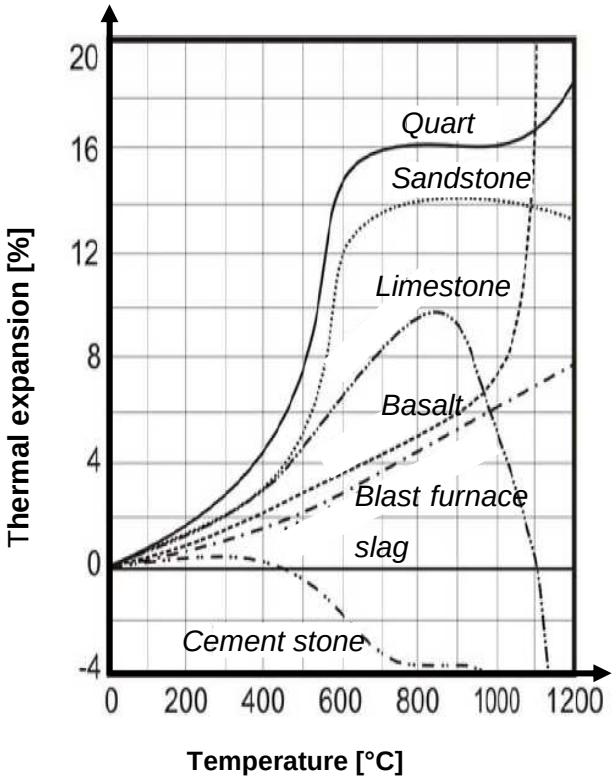

Figure 2-9: Thermal expansion as a function of temperature [19]

2.2.10 Thermal expansion of components

The aggregate volume during heating increases and simultaneously cement paste surrounds aggregate shrinkage. This leads to cracks through aggregates and cement paste and to cracks in interfacial transit zone (ITZ).

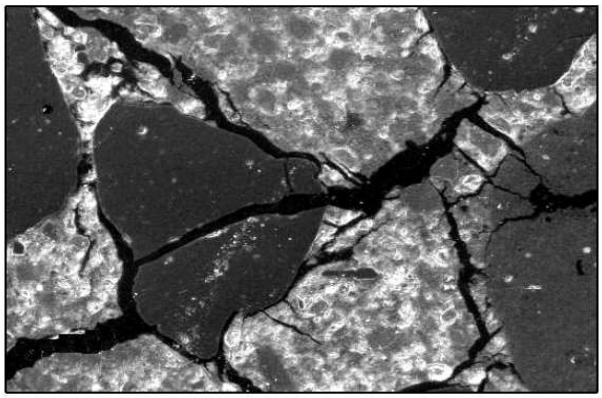

Figure 2-10: The structure of HPC (fc = 75 N/mm^2) composed of silicate-lime aggregates heated up to 600 °C (MEB, 50x) [20]

This issue is further discussed in Chapter 3: Thermo-mechanical and thermo-hydraulic mechanisms.

2.2.11 Cover to reinforcement

The reinforcement of concrete must be protected so long as it is possible in case of fire. From this point of view the thickness of reinforcement cover is crucial and must keep the temperature of reinforcement below 450 °C. Concrete in the cover layer of reinforcement has to be well compacted without any local defects in the form of small cracks or pores which may affect the behaviour of reinforced concrete structures. Hot gases generated in case of fire can easily penetrate into these cracks in the covering layer and heat up the reinforcement. Due to the high thermal conductivity of steel (125-195 $kJ \cdot m^{-2} \cdot h^{-1} \cdot °C^{-1}$) in the temperature range from 0°C to 600°C the heat flux can quickly transmitted to the reinforcement bars. Concrete thermal conductivity (6-8 $kJ \cdot m^{-2} \cdot h^{-1} \cdot °C^{-1}$) is much lower than thermal conductivity of steel and therefore a thermal gradient is generated. Once the bond between steel and concrete can no longer resist to the increasing tensile stress generated by the thermal gradient, the bond breaks and cover to reinforcement and reinforcement separate [4].

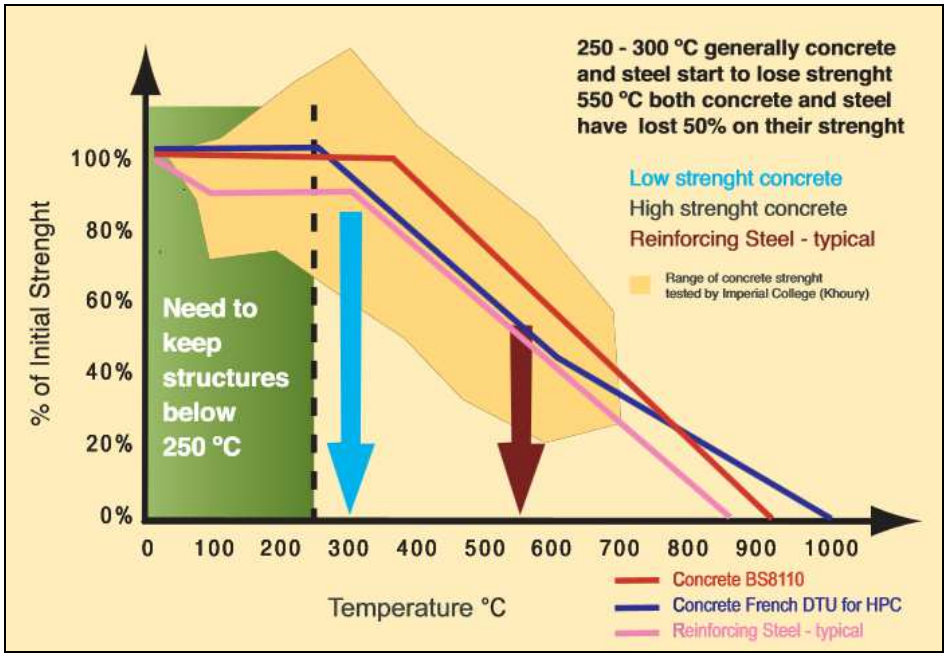

Figure 2-11: Effect of temperature on concrete and steel reinforcement (adapted from ITA 2004 and Khoury 2005) [37]

The long sections of reinforcement easily reach the critical temperature of 500 ° Cd to the high thermal conductivity of the reinforcement and lead to the risk of collapse. This type of failure can be significantly reduced by increased the thickness of the cover layer. The risk of local cracks reaching the reinforcement and cause the collapse of construction is decreased with increased thickness of cover [4].

2.2.12 Polypropylene fibres

The science behind this method is in development and sufficient experiments have been undertaken in recent years. It showed that polypropylene fibres added to concrete efficiently (positively) influenced resistance against fire. The PP-fibres melt at about 170°C thus creating micro channels for transport of water vapour and thereby decrease pore pressure build-up in the element ([1],[3],[21]). Melted fibres due to thermo-oxidative decomposition are partly absorbed by cement matrix and therefore create network more permeable than cement matrix itself and results in the reduction of pore pressure. The important point are melting point at 171°C, vaporization point at 341°C and the burning point at 457°C showed in Figure 6-1 [22]. The mode of action of PP-fibres will be closely described in chapter 6.

3 Thermo-mechanical and thermo-hydraulic mechanisms

Explosive spalling is a result from two parallel processes: (a) thermo-mechanical process, associated with gradients of thermal deformation (dilatation/shrinkage) due to stress generated within element during heating and (b) thermo-hydraulic process as a result of build-up of gas pressure in the porous network due to enclosed air and water vapour [23].

Table 3-1: Properties of cementitious composites at high temperatures [24], [32].

Temperature range	No.	Changes in cement matrix	Result
30 – 120°C	1.	Evaporation of free water from coarse and air pores up to 100°C (150°C)	Explosive spalling and cracks formation
110 – 140°C	2. 3.	Disintegration of hydrates and loss of chemically bonded water Degradation of gypsum, dehydration of calcium-aluminate-hydrates, decomposition of C-S-H (gel reduction) and ettringite	
180 – 300°C	4.	Evaporation of the physically bounded water at 180°C Evaporation of the chemisorbed water at 220°C-300°C Dehydration and degradation of C-S-H gels and C-A-H	
450 – 550°C	5.	Degradation of portlandite $Ca(OH)_2 \rightarrow CaO + H_2O$	Cracks formation
600 - 900°C	6.	Decomposition (decalcination) of calcite $CACO_3 \rightarrow CaO + CO_2$	
1100 – 1200°C	7.	Formation of Wollastonite β ($CaSiO_2$)	
1200 - 1300°C	8.	Beginning of the melting of cement stone	
≥ 1300°C	9.	Cement stone is available as vitreous glasses	Total disintegration of concrete

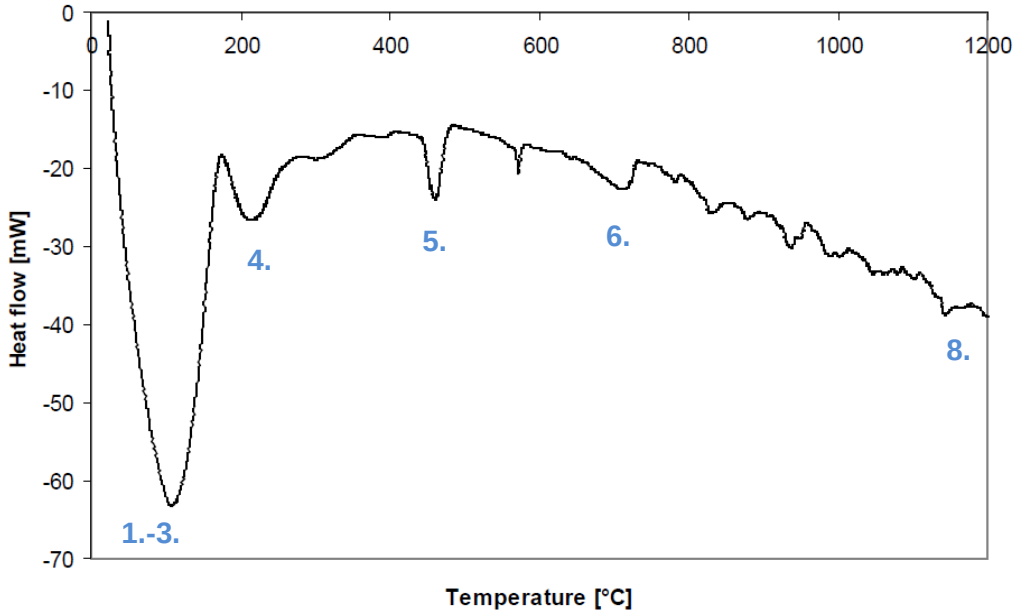

Figure 3-1: DTA of Portland cement mortar [24]

Changes in water content and material composition

In the first stage, the heating of concrete leads to the rapid loss of free and physically bounded water. Evaporation of free and physically tied water is nearly being finalized at 150°C. Thereafter disintegration of hydrates and loss of chemically bonded water take place. First step of dehydration of C-S-H (gel reduction) occurs. Evaporation of the chemisorbed water occurs from 220°C and fairly finishes at 300°C. Second step of C-S-H degradation occurs after 250°C whereby decomposition of Portlandite ($Ca(OH)_2$) at 450°C - 550°C is of major interest. When the temperature exceeds 600 ° C, the final phase of C-S-H dehydration occurs. Wollastonite β ($CaSiO_2$), α-C_2S, β-C_2S, etc. may be formed at that stage. This chemical and physical processes lead to significant changes in pore size and pore volume and completely new micro- and sub-micro structures which can result to internal cracks or formation of local crack. Exceeding 1200°C melting of cement stone and total disintegration of concrete occur.

3.1 Thermo-hydraulic mechanism

As it was mentioned above, thermo-hydral process is associated with transfer of water, vapour phases and air. Due to the rapid increase of temperature the free and bounded water is transferred into water vapour. Water evaporates and subsequently pressure is build-up inside the element. Build-up of high pore pressure is one of the major factors responsible for explosive spalling (Figure 3-2).

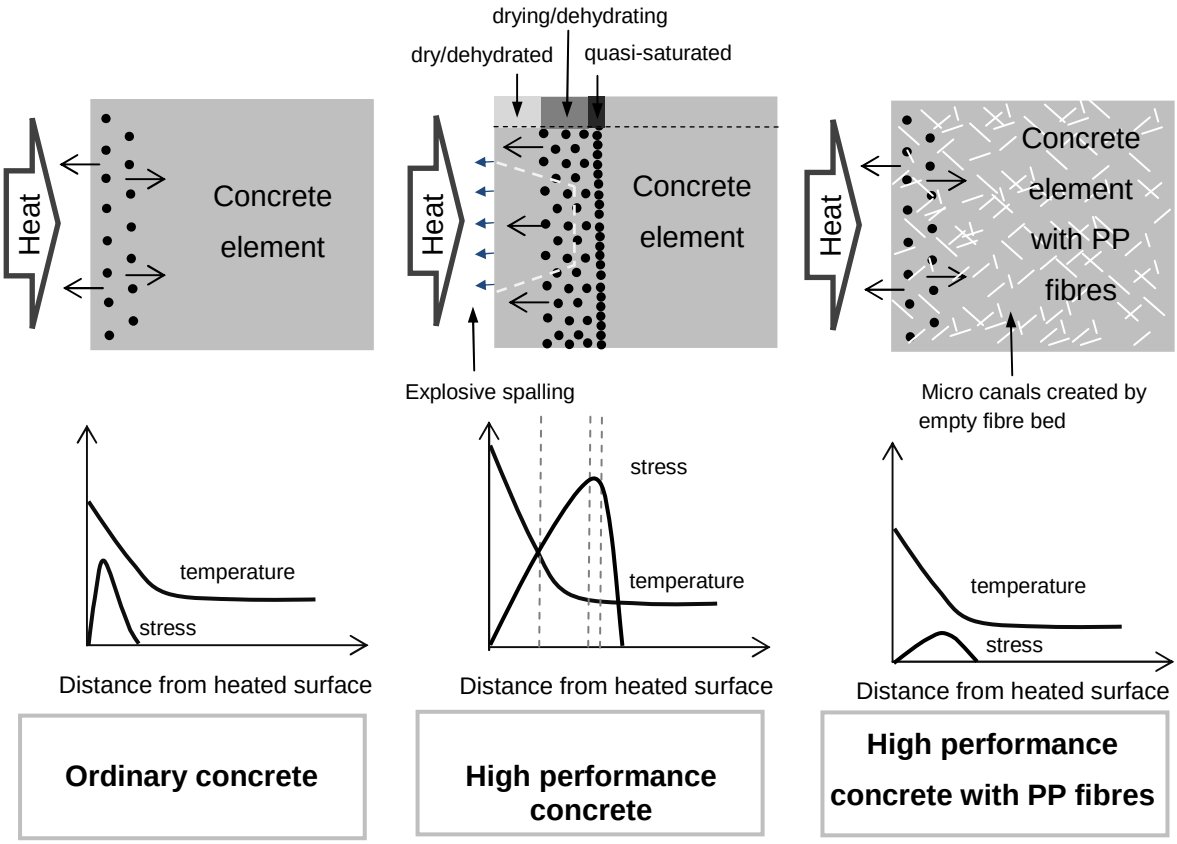

Figure 3-2: Schema of build-up of pressure process ([23], adapted by author)

"*Under the effect of pressure gradient, the water vaporized in the zone close to the heated face is transported (mainly by Darcy flow) not only towards the outside, but also the inside, of the concrete element at a lower temperature. It condenses again and a quasi-saturated layer is progressively formed, which impedes further mass transport in the inner direction*", as explained by P. Kalifa et al. [23].

3.2 Thermo-mechanical mechanism

Thermo-mechanical mechanism is a result of strain-incompatibilities of aggregates and hydrated cement paste. During the heating of the concrete, local incompatibilities appear between hydrated cement paste and aggregates, which may leads to structured tensions in the interfacial transition zones (ITZ). While the aggregates expand with increasing temperatures (a_T = $5 \cdot 10^{-6} \cdot K^{-1}$ to $12 \cdot 10^{-6} \cdot K^{-1}$ according to aggregate type), the cement hardened paste, (a_T = $8 \cdot 10^{-6} \cdot K^{-1}$ to $23 \cdot 10^{-6} \cdot K^{-1}$), after an initially extension shrinks because of the desiccation depending on the moisture content [32].

Simultaneously the aggregate conversion occurs with higher temperatures, dehydration reactions occur within different types of aggregates as well as mineral conversions (Figure 2-9). This may leads to an increase of spalling.

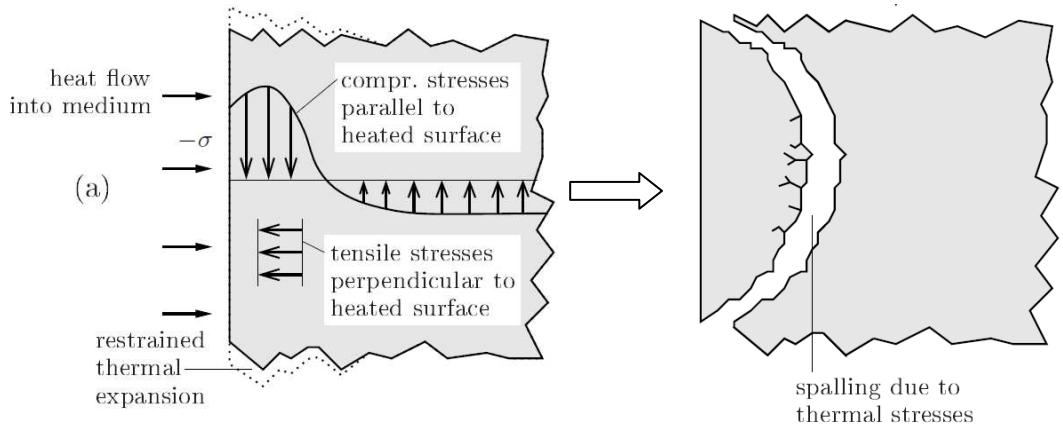

Figure 3-3: The mechanism of violations due to the thermal expansion: The temperature gradients induce gradients of thermal dilatation, which in turn generates tensile stresses perpendicular to the heated surface [49]

The decalcination of the limestone (Table 3-1) leads to a fired limestone aggregate. From 1200 to 1300 °C some components of the concrete begin to melt. Different concrete aggregates, for example gush rock, like certain basalts, show inflation effects, i.e. the gases which were locked during the rock formation process do escape during the melting [32].

4 Porous network in concrete

Concrete is a porous material with spatially heterogeneous structure. Pore size, their overall content and layout greatly affects its properties both in a positive and negative. With decreasing porosity of the concrete becomes more compact, impermeable, and thus more resistant to outside influences that affect his durability and life dependent on the transport of aggressive substances through hardened concrete. With the increasing demands for concrete structures the development of better performances of concrete take place in last 30 years. Changes in the composition of concrete mixtures as reduction of water content, addition of fibers (polymer, steel, natural, etc.), optimization of grain size, use of particles with pozzolanic activity etc. lead to better properties of concrete. This evolves ordinary concrete to high performance concrete with improve properties such as strength, compactness (density), reduce permeability, early strength increase, but also lead to brittle behaviour of impermeable HPC in fire condition ([25]-[27], [32]). Water content in concrete elements exposed to fire is transformed into water vapour and build-up pore pressure. If concrete with reduced pores and cavities is not permeable enough it will lead to serious damages.

Porosity is an important factor influencing the permeability of concrete. Characteristic properties of concrete change significantly with increase temperature:

- Changes in pore space and pore structure – empting of water-filled pores and capillaries
- Modification in pore space and pore structure – phase transition as recrystallization, dehydration, melting, thermal decomposition
- Changes in individual phases in the pore system

Detailed list of changes is shown in Table 3-1: Properties of cementitious composites at high temperatures in Chapter 3.

4.1 Classification of pores in concrete:

Sorting of pores in concrete in general (Table 4-1):

- Pores in the hydrated cement paste
- Pores in aggregates
- Capillary pores filled with water
- Pores due to imperfect compaction
- Pores associated with the Interfacial Transition Zone (ITZ)

Table 4-1: Classification of pores in concrete ([29]-[31], [34])

Type of pore		Description	Size
I.	**Compacting pores**	Coarse pores (caverns)	2 – 3 mm
II.	**Air pores**	Macrocapillary	50 µm – 2 mm
III.	**Capillary pores**	Capillary	15 µm – 50nm
		Microcapillary	10 – 50 nm
IV.	**Gel pores**	Mesopores	2 nm – 50 nm
		Micropores	< 2 nm
V.	**Others pores**	ITZ*	20 – 50 µm
		Microcracks	50 – 200 µm

** Interfacial Transition Zone*

4.1.1 Compacting and air pores

Caverns and coarse pores can be greater than 3 mm and the air pores 50 µm – 2 mm. They are considerably larger than the capillary pores and play an important role in terms of permeability of concrete ([29]-[31], [34]).

4.1.2 Capillary pores

Capillary pores represent that part of the gross volume which has not been filled with the product of hydration. These pores are of great importance in terms of transport processes and less significance in terms of hydration. The size and amount of capillary pores depend on the water/cement ratio and degree of hydration. The size of pores in hydrated cement paste varies widely, but the size of capillary pores was estimated as range about 15 µm – 50 nm and microcapillary as range around 10 – 50 nm. In term of the permeability, capillary pores play a significant role due to its ability evaporates. Capillary pores form an interconnected system randomly distributed within the cement paste. This interconnected system is mainly responsible for the permeability of the hardened concrete. Increasing water content leads to increase of diameter and amount of the capillary pores ([29]-[31], [34]).

4.1.3 Gel pores

Gel pores are much smaller than capillary pores. Their size varies from range 2 nm – 50 nm for mesopores and less than 2 nm for micropores. This is approximately only one order of magnitude greater than size of water molecule. Gel is considered as a porous due to the fact that it can hold large amount of evaporable water. Gel pores are interconnected interstitial spaces between the gel particles. Due to its small diameter the vapour pressure and mobility of adsorbed water differ from properties of free water. ([29]-[31], [34]).

4.1.4 Interfacial transition zone

Interfacial transition zone (ITZ) is the layer immediately surrounding the larger aggregates, which during compaction of fresh concrete restrict a homogeneous water distribution in fresh concrete. This leads to the so-called wall effect, which cause in the vicinity of large grains a larger amount of water and thus cement matrix is more porous. The result is a high concentration of portlandite ($Ca(OH)_2$) and ettringite (Figure 4-1).

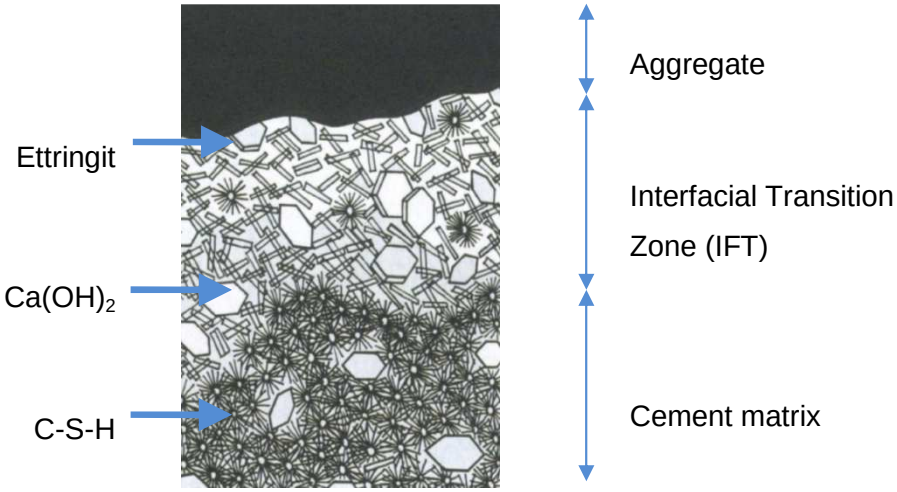

Figure 4-1: Detailed schema of interfacial transition zone (ITZ) [31]

This leads to inhomogenity in the microstructure and significant reduction in strength. If the concrete is exposed to a certain tension, the cracks begin to develop primary in the transition zone (around the stone and gradually interconnect the whole element with microcracks). This mechanism is typically for ordinary concrete. High strength concrete (HPC) has significantly reduced water-cement ratio and therefore there is the emergence of ITZ and that is the formation of microcracks distinctly limited (Figure 4-2). Ordinary concrete exposed to high temperatures enable escape of water vapour through ITZ. In the case of high performance concrete increase of pressure created by converting the water

content into water vapour lead to initiation of cracks running through aggregate grains. This fact has higher degradation mechanism.

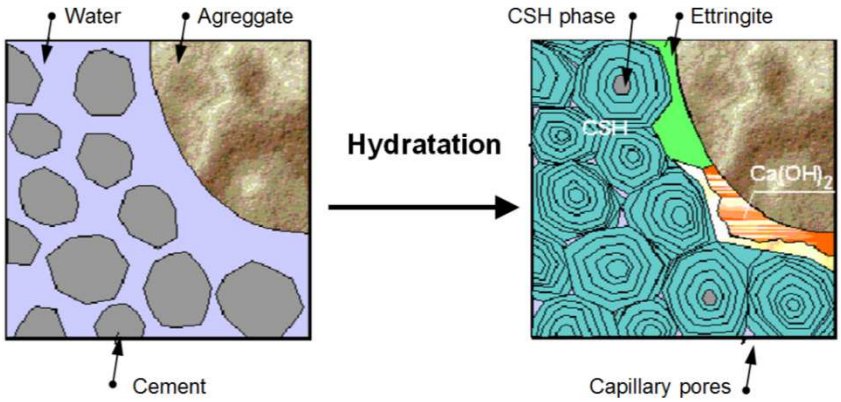

Hydration and ITZ of ordinary concrete [31]

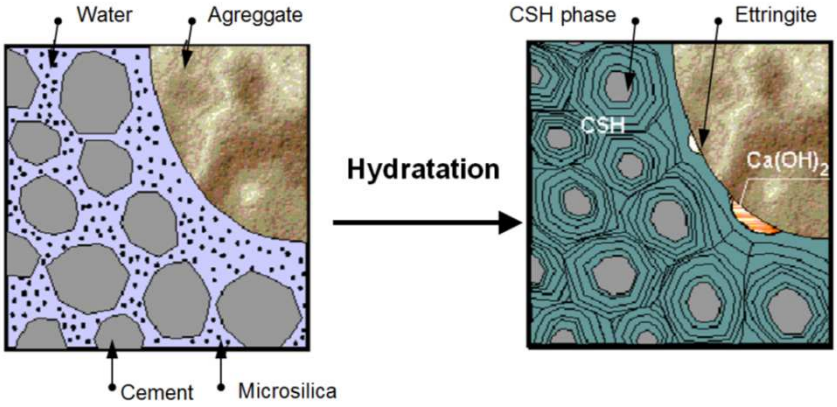

Figure 4-2: Hydration and ITZ of high performance concrete [31]

4.2 Permeability

The term “permeability” represents the flow rate of media or energy through a porous material and is a measure of the porosity of the concrete. The gas permeability is a physical property which describes the transport of gas through material which is dependent on the nature porosity of material.

In essence, the following formula describes permeability as a gas flowing through a solid structure of material. It is directly proportional to the air pressure difference flown through area of two surfaces of the sample (Figure 4-4). Permeability is a material property that describes the gas permeability and viscosity of the gas. Furthermore the flow is inversely proportional to the thickness of the specimen. For the simple case of one-dimensional direction of flow in the x-axis, the equation can be described as follows:

$$q = \frac{qk * Dp * A}{x} \quad \text{1.4.}$$

or as a differential equation:

$$k = -\frac{q * dx}{A * dp} \quad \text{1.5.}$$

q…… flow rate [cm ^{3} / sec] or [l / min]

A…… cross-sectional area of the porous body [cm^2]

Δx..… distance x in the direction of flow [m]

Δp..… pressure difference in Pa [= 100 N / m]

During testing, dry air was injected laterally from the top through cylindrical specimens. Air flow rate was measured with bubble flow-meters. The gas (air) permeability is calculated with Darcy´s law. Darcy's law is a simple proportional relationship between the instantaneous discharge rate through a porous medium, the viscosity of the fluid and the pressure drop over a given distance.

Permeability coefficient k

The gas permeability of concrete can be measured with gases such as oxygen, nitrogen or air, which are applied to the materials. The gas permeability is describe by the specific permeability coefficient *k*. It is specified as a measurement of the open porosity of concrete. The open porosity, in term substantially corresponds to the capillary porosity. In dry concrete under normal conditions, the gas permeability is from 10^{-14} to 10^{-19} m^2. It increases with increasing temperature, decreasing moisture content and increasing porosity.

Viscosity μ

The viscosity of the gas is dependent on the temperature and on the nature of the flowing medium. In general, the formula for the calculation of the viscosity as follows:

$$h = \frac{1}{3} * n * m * v * l \quad \text{1.6.}$$

It is defined by:

l…... free path (= distance traveled by particles without interaction)

m…. mass

v….. average of particle velocity

n….. particle number density of the gas.

- Dynamic viscosity (sometimes referred to as Absolute viscosity) [μ = Pa·s]
- Kinematic viscosity = Dynamic Viscosity / Density [v=$m^2 \cdot s^{-1}$]

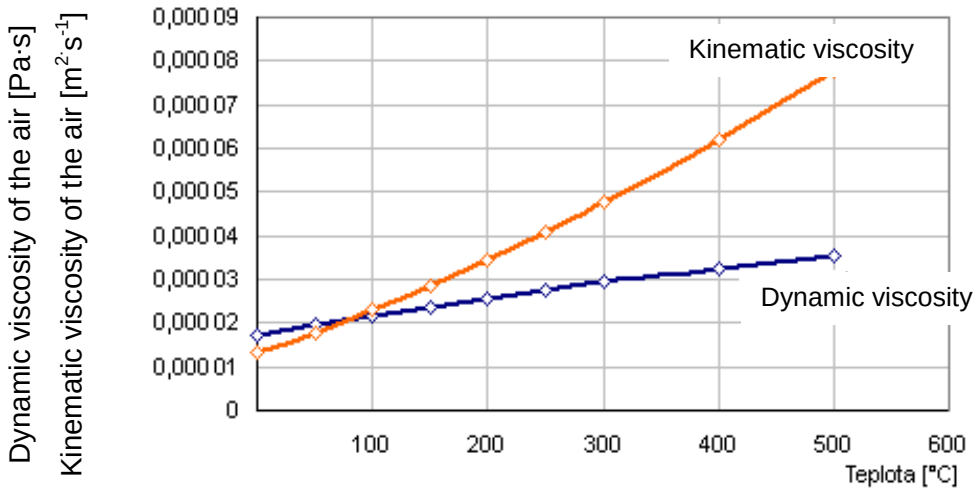

Figure 4-3: Temperature-dependent curve of the air viscosity at 1,013 25 bar

Differential pressure Δ p

The differential pressure is formed by the difference between incoming and outgoing pressure.

$$D_p 0 = p_1 - p_2 \qquad 1.7.$$

p_1…. pressure applied to the one side of specimen (inlet pressure)

p_0…. pressure of air passing through the sample (outlet pressure)

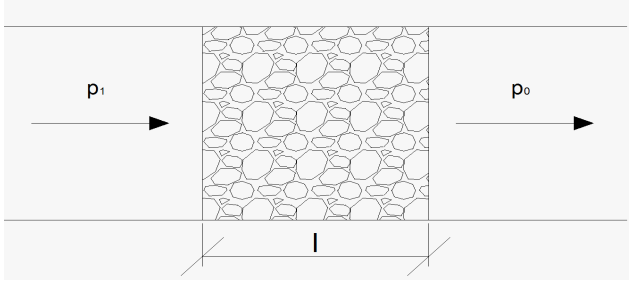

Figure 4-4: Stationary flow of a porous body

Therefore obtained by multiplying the equation with the dynamic viscosity, the specific permeability as follows

$$k_{spez} = -\frac{m * q * l}{A * D * p} \qquad 1.8.$$

$k_{spec..}$ specific permeability [m]

μ….. viscosity of the fluid medium in Centipoise [1 poise = 0.1 Ns / m],

l…… length (width) of the porous body [cm]

A…. cross-section [m^2]

As can be seen from the equation the permeability is temperature and pressure dependent. The unit of measurement for the Darcy permeability is named after the French scientist Henry Darcy (1803-1858), who studied the flow of water through gravel beds in 1856. The permeability is thus defined by Darcy's law. The general definition of equation for the measurement of permeability is in vector notation:

$$J = -K * DY \qquad 1.9.$$

J…flow density vector

K… transport matrix

Ψ… potential function

Darcy's law is thus based on the following significant assumptions:

- The flow is viscous and linear, i.e. the linear velocity and the flow rate is proportional to the pressure difference occurring,
- the gas (liquid) is homogeneous and incompressible,
- the porous medium is homogeneous,
- there is no interaction between gases (fluids) and porous medium,
- the permeability is independent of the sample length in the flow direction,
- The fluid medium (gas, water) must be saturated in the phase up to 100%.

The permeability is used in practice to assess the durability of concrete - and used for quality control of concrete structures - especially in matters of carbonation and corrosion.

4.2.1 Permeability of cement-based materials

The permeability of cement-based materials (cement mortar or concrete) can be determined by using compressible media (gases) or incompressible (liquids). A wide

range of experimental techniques has been performed either on site (in-situ tests) or in the laboratory (laboratory tests).

Using liquids as measurement medium:

- the Initial Surface Absorption Test (ISAT) - The method consists in measuring the amount of water pressure (0.2 bar) flowing into the concrete through an acrylic chambre,
- Covercrete Absorption Test (CAT).

Using gases as measurement medium:

- Figg's test The Air Permeability of Near Surface (APNS) test,
- the CEM-Bureau method,
- the Hassler method,
- tests under changing thermal conditions.

Determining permeability of cement-based materials at different temperature stage is not easy to measure and therefore the application of these test methods was restricted to laboratory-cast specimens.

In order to compare concrete permeability measured under different pressure conditions by different test methods the results must be normalized. For this normalization there are two significant approaches: the Klinkenberg theory which is more widespread and the approach by Carman and Kozeny. The approach of Klinkenberg is based on the boundary layer theory, which states that under certain conditions the surface of a stationary wall (capillary) has only influence on the near-wall boundary layer, but not on the potential flow of the flowing medium in more distant layers. Klinkenberg discovered that permeability to gas is relatively higher than to water, and he interpreted this phenomenon as "slip flow effect" between gas molecules and solid walls. Gas molecules collide each other and to pore-walls during traveling through the pore medium. When the pore radius approaches to the mean free path of gas molecules the frequency of collision between gas molecules and solid walls increases. Therefore this additional flux due to the gas flow at the wall surface, which is called "slip flow", becomes effective to enhance the flow rate (Figure 4-5). This phenomenon is called Klinkenberg effect.

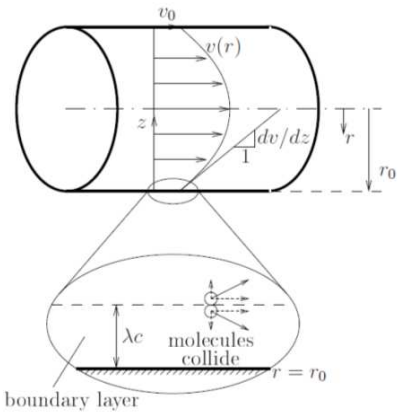

Figure 4-5: Slip flow effect describe by klinkenberg

Klinkenberg defines normalized permeability coefficients (k_{int}) as follow:

$$k_{app} = k_{int} + \left(1 + \frac{\beta k}{P_m}\right) \qquad 1.10.$$

where $P_m = \frac{P_1 + P_1}{2}$ 1.11.

k_{app}…. measured coefficient of permeability from experiments [m^2]

k_{int}…… normalized intrinsic/absolute permeability ($P_m = \infty$) [m^2]

βk…….. Klinkenberg factor [Pa]

P_m……. the average of pressure differences [Pa]

P_1……. inlet pressure [Pa]

P_2…….. inlet pressure [Pa]

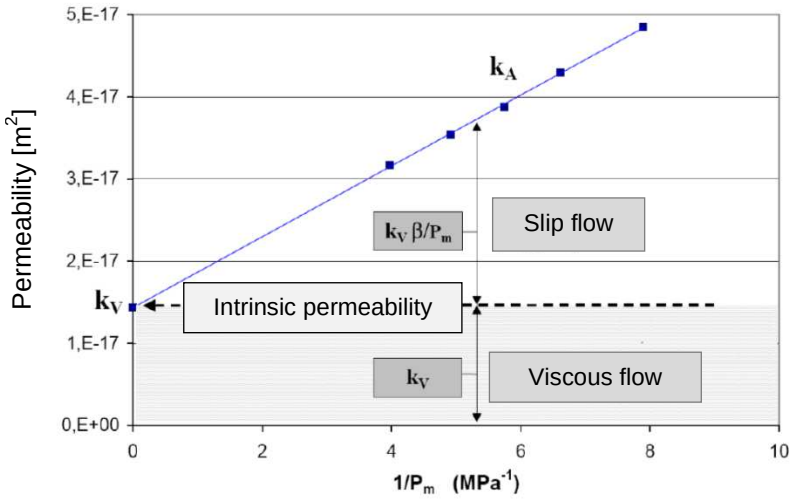

Figure 4-6: The relationship between measured permeability coefficient k_{app} obtained by experiments and the normalized coefficient k_{int}

Considering this slip-flow phenomenon in Darcy's equation, reading for incompressible flow (where k = k_{int}):

$$Q = -k_{int}\frac{A}{\eta}\frac{dp}{dx} \qquad 1.12.$$

the flux of a compressible fluid through porous media is obtained as:

$$Q = -k_{int}\frac{A}{\eta}\frac{dp}{dx} = -k_{int}\left(1+\frac{b}{p}\right)\frac{A}{\eta}\frac{dp}{dx} \qquad 1.13.$$

with the permeability *k* given by: $k = k_{int}\left(1+\frac{b}{p}\right)$. 1.14.

Intrinsic permeability k_{int} [m^2] or so called absolute permeability is a comparable unit for different test methods. This intrinsic parameter describes the pore space of material which is dependent on the medium flowing through the material (liquids as incompressible medium or gasses as compressible). For compressible media (e.g., air or water vapour), the intrinsic permeability is defined as the permeability at infinite pressure, with 1/p=0. The relationship between measured permeability coefficient k_{app} obtained by experiments and the normalized coefficient k_{int} is shown in Figure 4-6.

The approach of Carman and Kozeny is based on the proportion of molecular diffusion which has a theoretically perfect background. Both approaches assume that the measured value must be reduced by the nonviscous proportion to obtain standardized and thus comparable permeability coefficients. According to Carman and Kozeny theory the molecular diffusion in the gel pores has been taken into account. In the basic Carman-Kozeny equation the Mass flow m [kg/m²s], length l [m] of the flow path through the sample, pressure difference ΔP [Pa] and in a complex manner geometric sizes (pore structure of sample) and the physical parameters (characteristics of the gas) are linked.

As was mentioned before, addition of polypropylene fibres significantly reduce explosing spalling of dense concrete exposed to elevated temperature by increasing permeability of concrete body. The influence of amount of fibres at different temperature level was investigated by Kalifa et al. [1] where concrete with different dosage of fibres was treated by elevated temperature up to 400°C and permeability to nitrogen was measured at cooled-down samples treated with 80, 100, 300 and 400°C. The maximum pressure applied was around 1 MPa and the intrinsic permeability was determined by using the Klinkenberg method. Measurement was carried out by two methods: the Hassler method

and Cem-bureau method. Measurements performed with Hassles permeameter yield higher values in comparison with Cem-bureau method. It was assumed that this discrepancy is not caused by different method of measurement, but rather in the difference in the sample size (the bigger specimen, the large thermal gradient at heating and cooling which may induce a larger cracking). This interesting observation raises the question of whether the permeability is also dependent on the size.

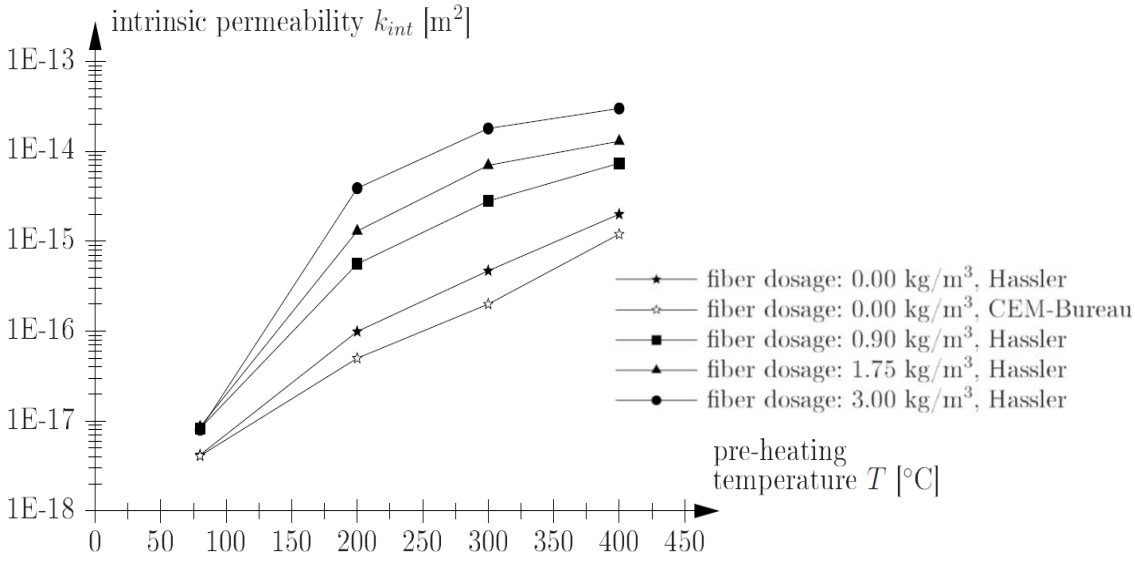

Figure 4-7: Intrinsic permeability of high-performance concrete as a function of temperature and fibre dosage [1]

Figure 4-7shows that permeability of concrete with different amount of PP-fibres is very similar and only two times higher than concrete without PP-fibres. Expected increase of initial permeability of concrete with fibres due „foam effect“ when mixing fresh concrete has not been observed. Whereas k_{int} of concrete without fibres varied one order of magnitude, a variation of k_{int} of two orders of magnitude was observed for concrete with dosage of 0.9 and 1.75 kg/m^3 PP-fibres and three orders of magnitude was observed for concrete with dosage of 3.0 kg/m^3 PP-fibres within a temperature range from 80 to 200°C. The more significant increase of the intrinsic permeability in the range of temperature between 80 and 200°C for concrete with PP-fibres was explained by PP-fibre melting. From 300°C up to 400°C, permeability has not increase as significantly as in temperature range from 80 to 200°C was mainly controlled by cracking. Concrete specimen with addition of PP-fibres exhibit a much higher crack density than the concrete without PP-fibres with very thin cracks (close to 1µm) which form a dense network link between fibre beds and aggregate skeleton. Concrete without PP-fibres represents with thicker cracks (around 10µm) in large distance in between linking a bigger aggregates (Figure 4-8).

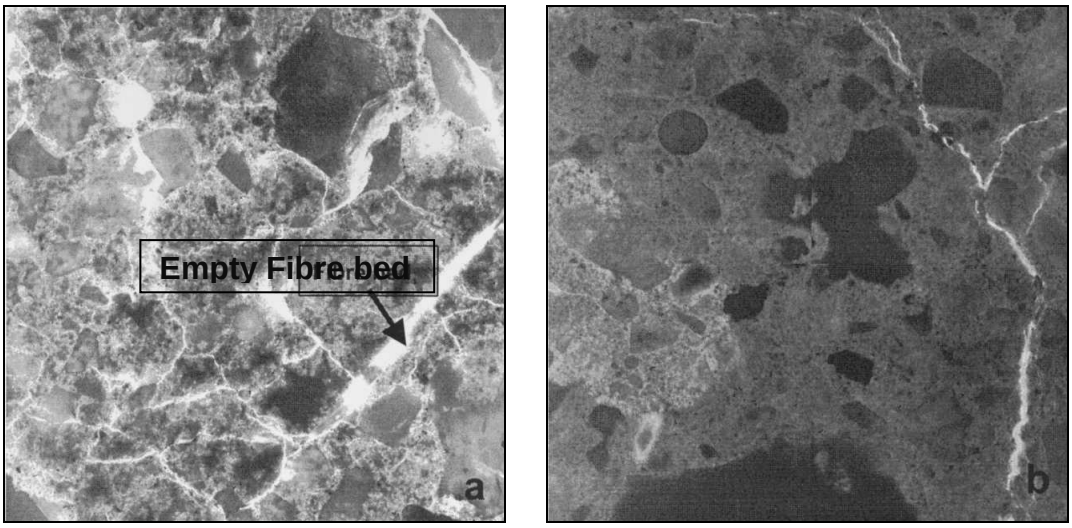

Figure 4-8: left: Concrete with PP fibres (αf = 3 kg/m3) , Right: Concrete without PP fibres, both exposed to 400°C. The images represent a polished surface impregnated with fluorescent resin and observed under blue and polarised light. Cracks and fibres filled with the resin appear in white. These pictures clearly show the difference in damage between concrete with and without PP-fibre [1].

The images of concrete with and without PP-fibres after a fire exposition has been undertaken up to know by using non-destructive testing methods as optical microscopy or scanning electron microscopy. According to assumption that melting point of polypropylene fibres is around 170°C and a point of vaporization and burning between 341°C – 457°C, only this range of temperature treatment has been observed ([1], [21]). There are two different theories about mode of action of polypropylene fibres in concrete exposed to elevated temperature. The first theory is based on the fact that PP-fibres melt at 170°C, whereas explosive spalling occurs between 190°C and 250°C [1]. When melted and partially adsorbed into cement matrix, the fibres create a pathway for gas. This network creation leads to more permeable structure than the matrix itself and therefore allows outward migration of vapours and results in the reduction of pore pressure. The second theory presumes that PP-fibres in concrete exposed to high temperature act just before reaching their melting point by creation of microcracks and their interconnection and therefore prevent explosive spalling.

5 Methods to prevent explosive spalling

The aim of fire protection system is to allow the safe users evacuation as well as allow the rescue units to enter the scene and to limit damages to the tunnel. These systems are constantly being developed with the goal to prevent concrete spalling and heating and melting of steel and metal elements.

With respect to fire protection of structural concrete tunnel linings, this chapter establishes the role of active and passive systems (emergency lighting, escape routes, warning system, active fire protection system etc.). The examples of protective performance will be shown in Figure 5-1.

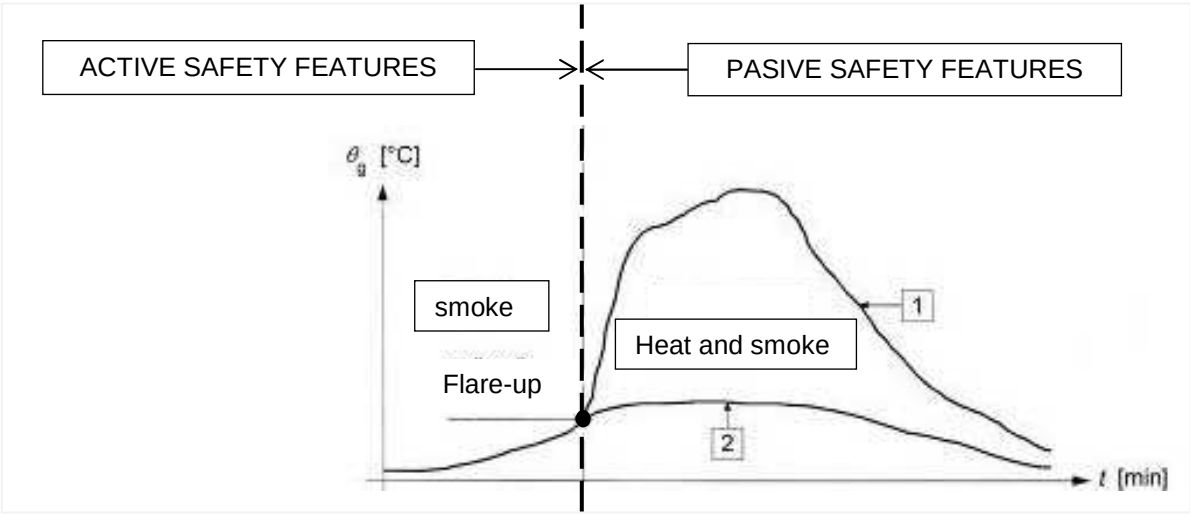

1 temperature in fire section during a fully developed fire in case of failure of active safety features

2 temperature in fire section for undeveloped fire with working active safety features

Figure 5-1: Active and passive safety [47]

5.1. Active methods

Active safety features in tunnels include water sprinklers, foam deluge systems, water mists, smoke and heat ventilation and fire alarm which are activated by early warning sensors in the event of fire in order to reduce the fire before it comes out of control. The problem may arise in the event of their damage and subsequent failure ([35]-[37]).

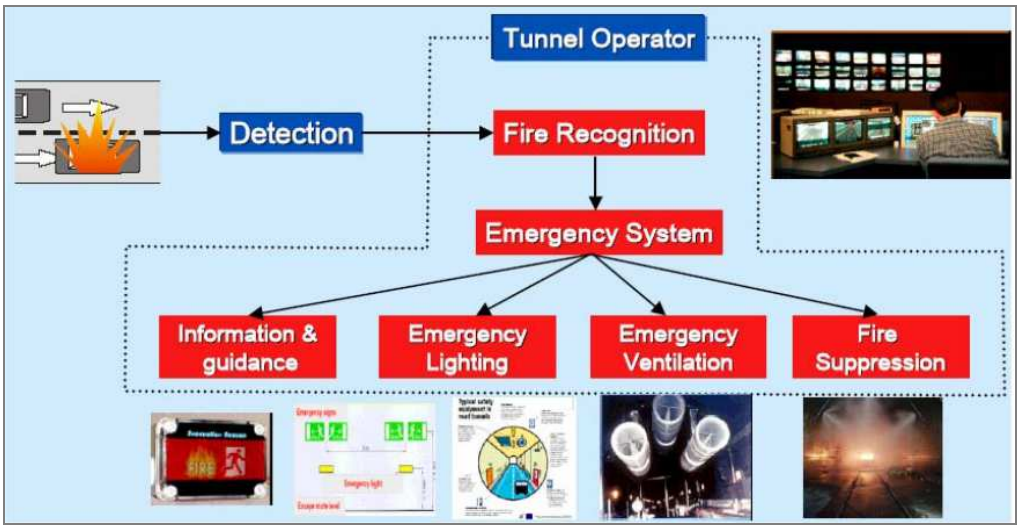

Figure 5-2: Road tunnel fire protection system [47]

5.2 Passive methods

Passive safety features is design to be installed as a shield to protect the structure from fire at any time. Unlike active system the damage cannot occur and therefore passive protection always works. There are essentially following types of fire protection for tunnels (and structures generally) ([35]-[37]).

- Sprayed mortars,
- pre-fabricated boards,
- polypropylene fibre modified concrete
- fire compartmentation,
- safe escape routes,
- limitation of spread of fire to neighboring buildings.

Figure 5-3: Sprinklers [37]

5.2.1 Sprayed mortars

Vermiculite-cement based products applied by hand spraying have been used in past. It was relatively weak material with compressive strength around 2,5 MPa and therefor its

mechanical properties had not been sufficient. It is essential for sprayed mortars to have adequate durability in respect of both physical and chemical attack during the service live. The new development in fire protection materials combines both durability and excellent fire protection and it is based on light weight concrete technology with compressive strength of 15 MPa minimum. These product are designed for easy and effective shotcrete technology allowing application in rate between 150 and 250 m^2/hr depending on the protection thickness requirement ([35]-[37]).

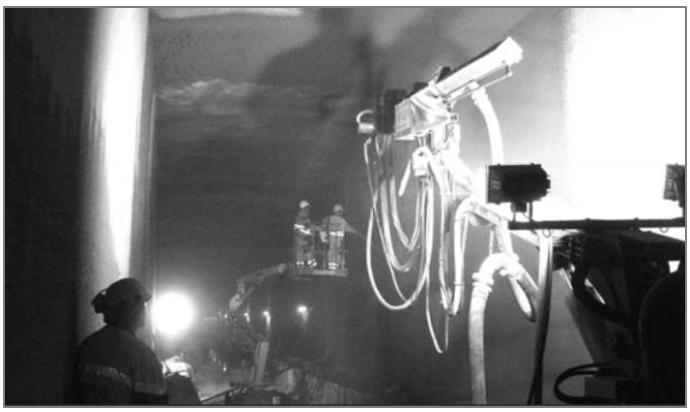

Figure 5-4: Robotic application of spray applied fire protection mortar [37]

5.2.2 Pre-fabricated boards

Pre-fabricated fire protection boards offer a clear advantage for box shaped tunnels where there are no curved tunnel walls or complex geometries e.g. cut and cover and immersed tube tunnels. However, they are not well suited to curved profile tunnels. Also the price is higher than sprayed systems. Apart from their high cost, vehicle collision damage is often considered a maintenance problem in road tunnels using pre-fabricated board protection systems ([35],[37]).

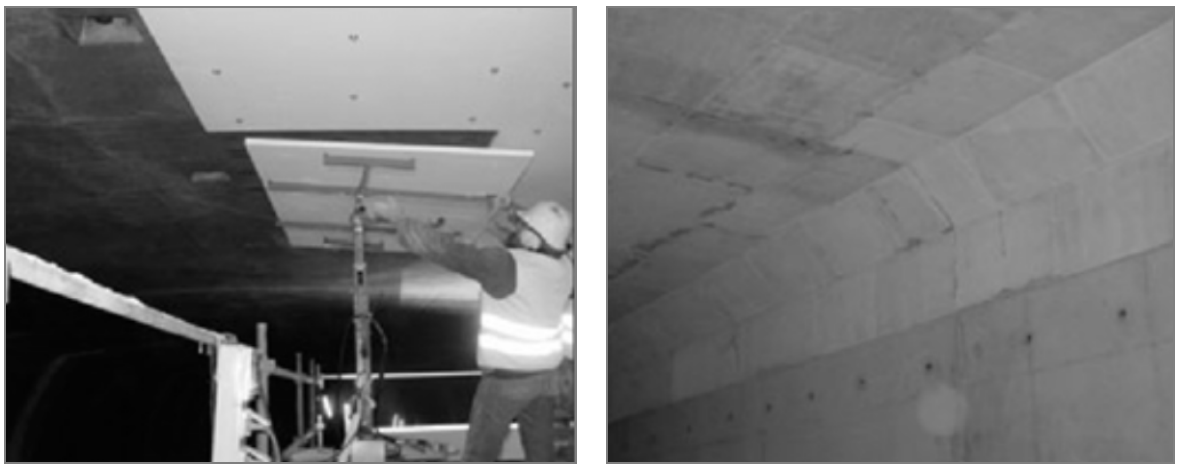

Figure 5-5: Installation of pre-fabricated thermal barrier boards in tunnel lining [37]

6 Polypropylene fibres in fire exposure HPC

The PP-fibres melt at about 170°C thus creating micro channels for transport of water vapour and thereby decrease pore pressure build-up in the concrete element ([1], [3], [21]). Melted fibres due to thermo-oxidative decomposition are partly absorbed by cement matrix and therefore create network more permeable than cement matrix itself and results in the reduction of pore pressure. The important point are melting point at 171°C, vaporization point at 341°C and the burning point at 457°C showed in Figure 6-1 [22]. The mode of action of PP-fibres will be closely described in chapter 8.2.

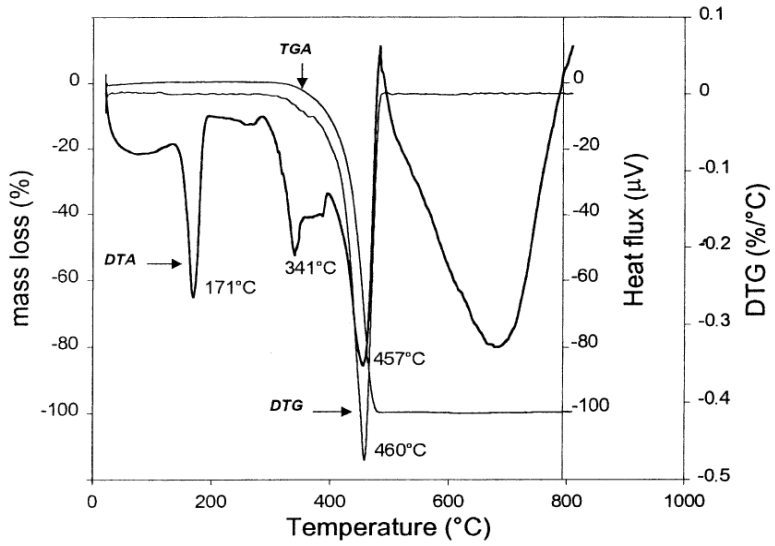

Figure 6-1: DTA, TGA and differential thermo-gravimetric analysis (DTG) [22]

6.1 State of the art of PP-fibres

Polypropylene is a partially crystalline thermoplastic and belongs to the group of polyolefin's. Due to its high resistance to alkali and acid materials, rigidness, strongness, low density and is suitable for use into concrete. Due to its point of softening, melting point and point of decomposition is suitable for concrete with higher fire resistance. According to the method of manufacture PP fibres are distinguishes into two groups:

- Monofilament polypropylene fibers (Figure 6-2)
- Fibrillated polypropylene fibers (Figure 6-3)

Classification according to dimension:

- Microfibers
- Macrofibers

6.1.1 Monofilament polypropylene fibers

Monofilament fibres are produced by fiberizing (shredding) from the melt with length 5-15 mm (32 mm) and a diameter of 10-20 µm. It has sufficient cohesion with concrete and concrete surface is smooth and free of optical defects.

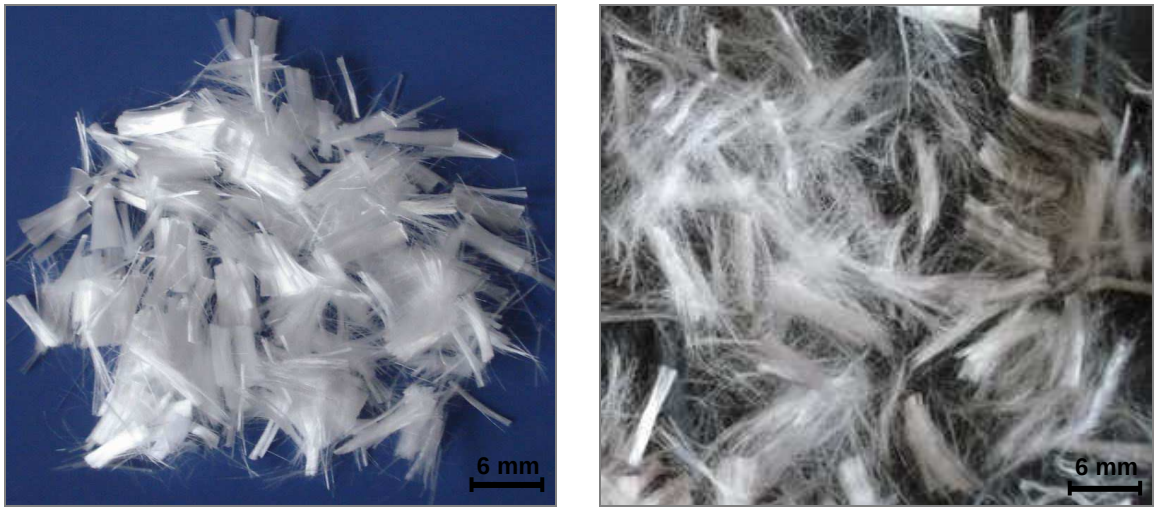

Figure 6-2: Monofilament polypropylene fibers [40]

6.1.2 Fibrillated polypropylene fibers

Fibrillated PP fibres are produced by fiberizing of modified prestressed plastic foil with thickness about 40-200 mm. Fibrillated PP-fibres do not have in the issue of spalling of concrete widespread application such a monofilament fibres due to its dimension. Its dimension is substantially larger than the monofilament fibre and creates a rough surface.

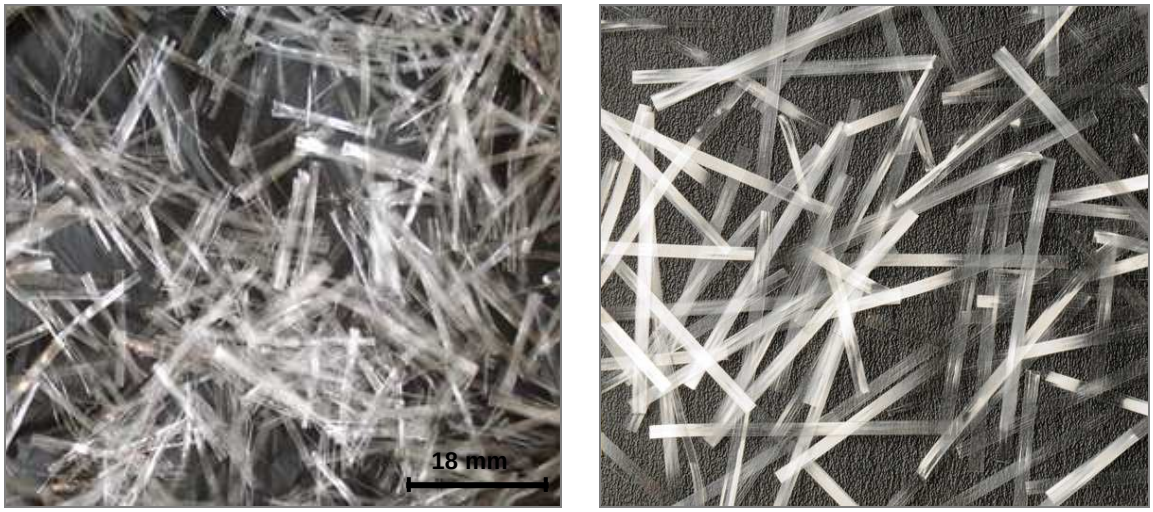

Figure 6-3: Fibrillated polypropylene fibers [41]

6.1.3 Dimensions and content of PP fibres

Diameter of polypropylene fibres used in concrete varies from range 5 µm – 32 µm and leng from 6 to 12 mm. According to statistical basic, Persson suggested a content of 0.7 kg/m^3 for indoor concrete and 1.4 kg/m^3 for tunnel concrete, as sufficient amount to prevent explosive spalling in self-compacting concrete (SCC) [42]. The higher the fibre content, the higher the gas permeability. X. Liu et. al tested self-compacting concrete (SCC) and high-performance cement paste (HPCP) with pp fibre content 0, 0.5 and 1.0 kg/m^3. The influence of PP fibre was more obvious for SCCP than for HPCP. A PP fibre content of 0.5 kg/m^3 in SCCP showed a similar effect as for a fibre content of 1.0 kg/m^3 in HPCP [43]. From the industrial point of view, a dosage of 2.0 kg/m^3, a fibre length in range 10 – 20 mm and a fibre diameter of 50 – 200 µm are generally adopted rules for preventing current high performance concretes from spalling. The experimental studies showed that fibres were efficient at dosage as low as 0.9 kg/m^3. Since the use of fibres significantly affected the workability af fresh concrete, optimization of fibre content is of significant interest.

6.1.4 Melt Flow Index (Melt Flow Rate)

Melt Flow Index (MFI) or Melt Flow rate (MFR) is the amount of material (polymer) in grams extruded in 10 minutes under certain testing conditions through a standardized system (Figure 6-4). The plastic, PP-fibres in our case, is fed into a heated vertical barrel and a known weight is kept on top of the plunger. The amount of plastic that is extruded in 10 minutes is called the MFI or MFR.

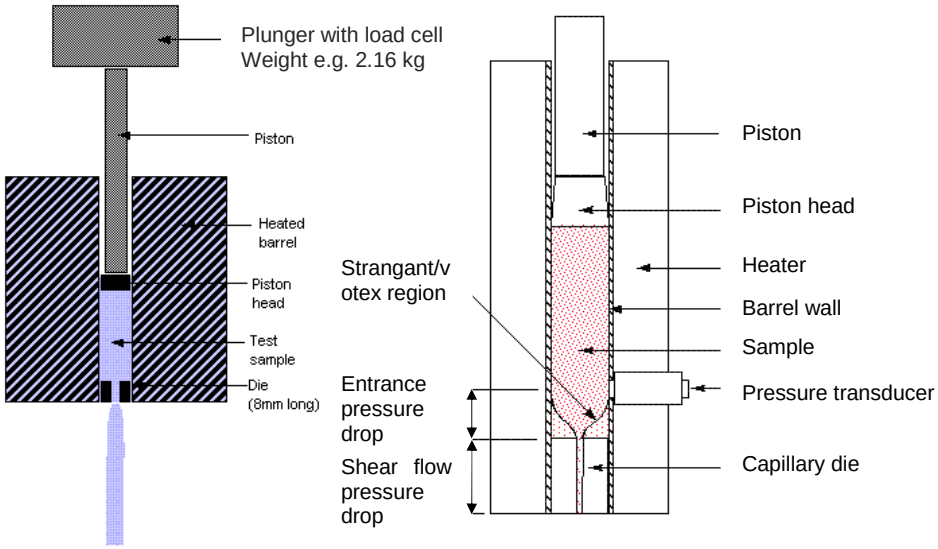

Figure 6-4: left: Melt Flow Index (MFI) equipment; right: screw-driven capillary rheometer [44]

The measurement unit is [g/10 minutes] and the standard that defines all measurement methodology is "ASTM D1238" or "ISO 1133".

Melt flow index (MFI) and viscosity are inversely related:

- High Melt Viscosity = Low MFI
- Low Melt Viscosity = High MFI

6.2 Theories about the mode of action of PP-fibre

6.2.1 Effect of monofilament Polypropylene fibres

Addition of polypropylene fibres has essentially 4 effects on permeation improvement [32]:

o Additional micro pores are created during the addition and mixing of fibres in the fresh concrete mix. Addition of PP fibres influences the porosity due to so called “foaming effect” developed during mixing fresh concrete. The higher amount of fibres the higher porosity (Table 6-1 to Table 6-3). It has been observed that thin and small fibres are more effective than the larger ones. Therefore monofilament PP fibres which are finer than fibrillated fibres are used to avoid spalling.

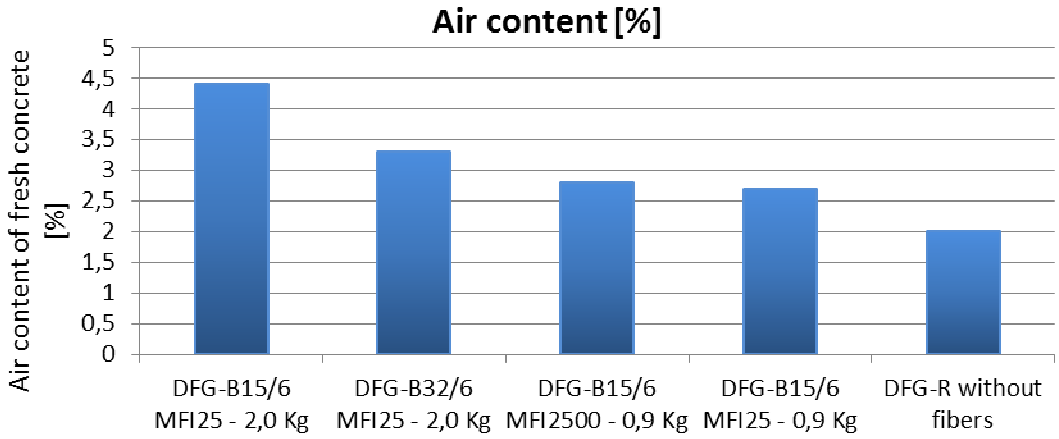

Table 6-1: The air content of fresh concrete [%] related to dosage of PP fibres [kg] [results obtained by the author]

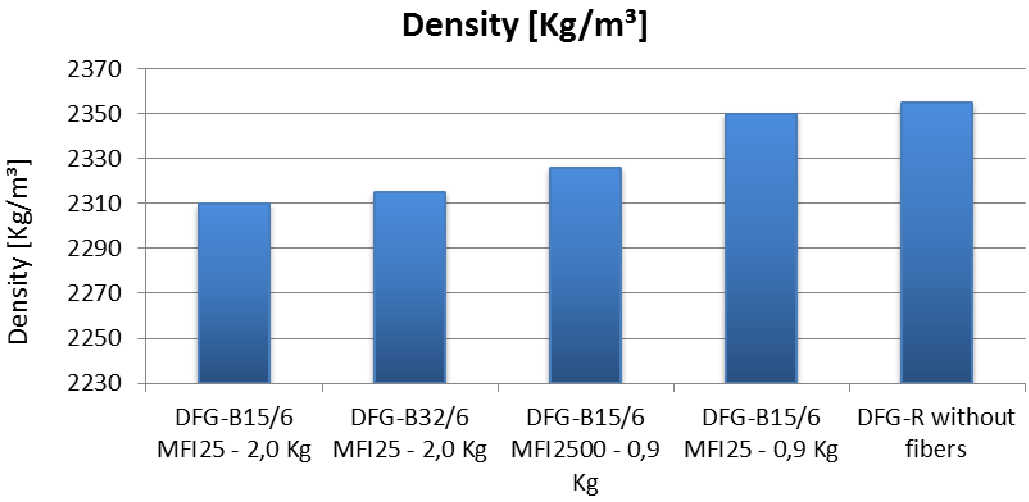

Table 6-2: Density of concrete [kg/m3] related to dosage of PP fibres [kg] [results obtained by the author]

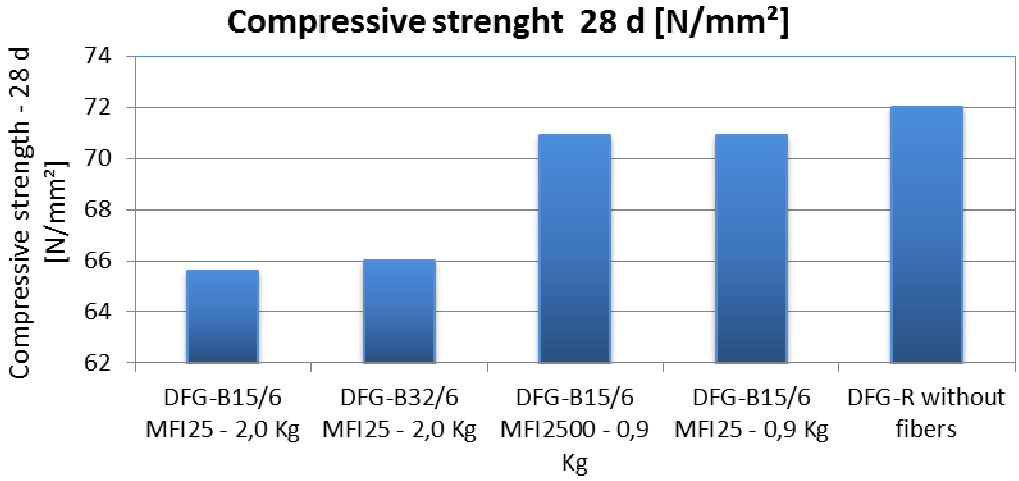

Table 6-3: Compressive strength [N/mm^2] related to dosage of PP fibres [kg] [results obtained by the author]

o Development of diffusion-open transition zones between aggregate and cement matrix. Transition zones around aggregate allow higher transport of vapour and addition of PP fibers this imperfectly connected system improve and thus cause the increase the filtration. Schematic description of this theory is illustrated on Figure 6-5. Thickness of this transition zone is dependent on w/c ratio, cement type and content of micro silica.

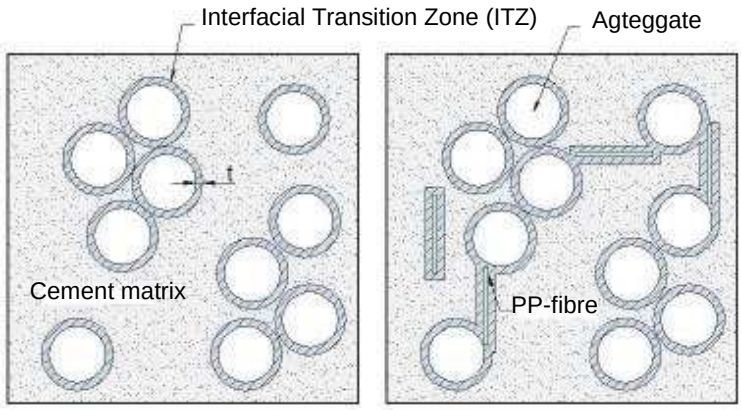

Figure 6-5: Schematic description of “Theory of Permeation“ [32]

- Formation of capillary pores during melting and burning of the fibres. Micro channels for transport of vapour are developed at temperature 171°C which is the melting point of PP fibres and creation of micro channels continue to the temperature 341°C – 457°C when fibres vaporize and burn. Kalifa et al. observed that PP fibres are partly absorbed by cement matrix and therefore create network more permeable than cement matrix itself (Figure 6-1) [22].

  In principle, Schneider has observed the same idea with a little different values of PP fibers disintegration (Figure 6-6) [32].

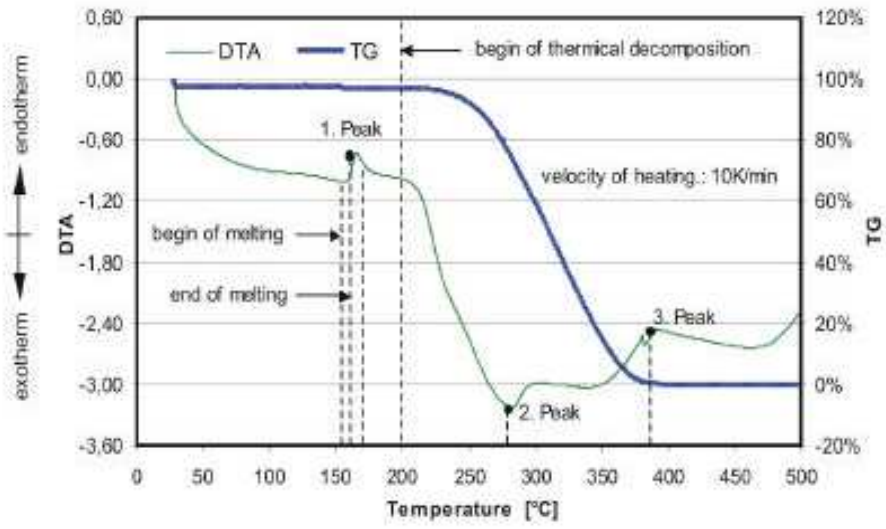

Figure 6-6: Thermogravimetrical investigations of polypropylen fibres by Schneider [32]

- Micro cracks formation at the tip of the PP fibres created during heating up and melting.

6.2.2 Existing theories in research (practice)

The unique testing methodology which has been developed within the framework of an internal research project at BAM shows detailed insights into the existing theories about mode of action of PP fibres. The acoustic emission and ultrasonic measurement during temperature loading was used for testing cylindrical specimen with compressive strength of 110 MPa (with 2 kg/m^3 PP-fibres) and 113 MPa (without PP-fibres). X-ray computed tomography has been used for non-destructive micro structural analysis of cooled down specimens. SEM-analysis showed creation of micro canals and cracks in different temperature level build up by emerging water vapour. Temperature of 170°C has proved as the most significant temperature influencing creation of canals that are essential to build up a micro space. PP-fibre melting in different temperature level is showed in the Figure 6-7 [21].

Initial state of PP-fibres without any changes is clear from first image taken at room temperature (20°C). The second picture taken on cooled-down sample preheated to 200°C already shows signs of shrinkage and partly empty fibre bed. Also crack formation takes place at this range of temperatures. At temperature 250°C the decomposition of PP-fibres take place and the linking crack formation occurs. The empty fibre beds lead to interconnection of micro canals and micro cracks at temperature 300°C. Temperature between 170°C and 350°C is the most significant for PP-fibres.

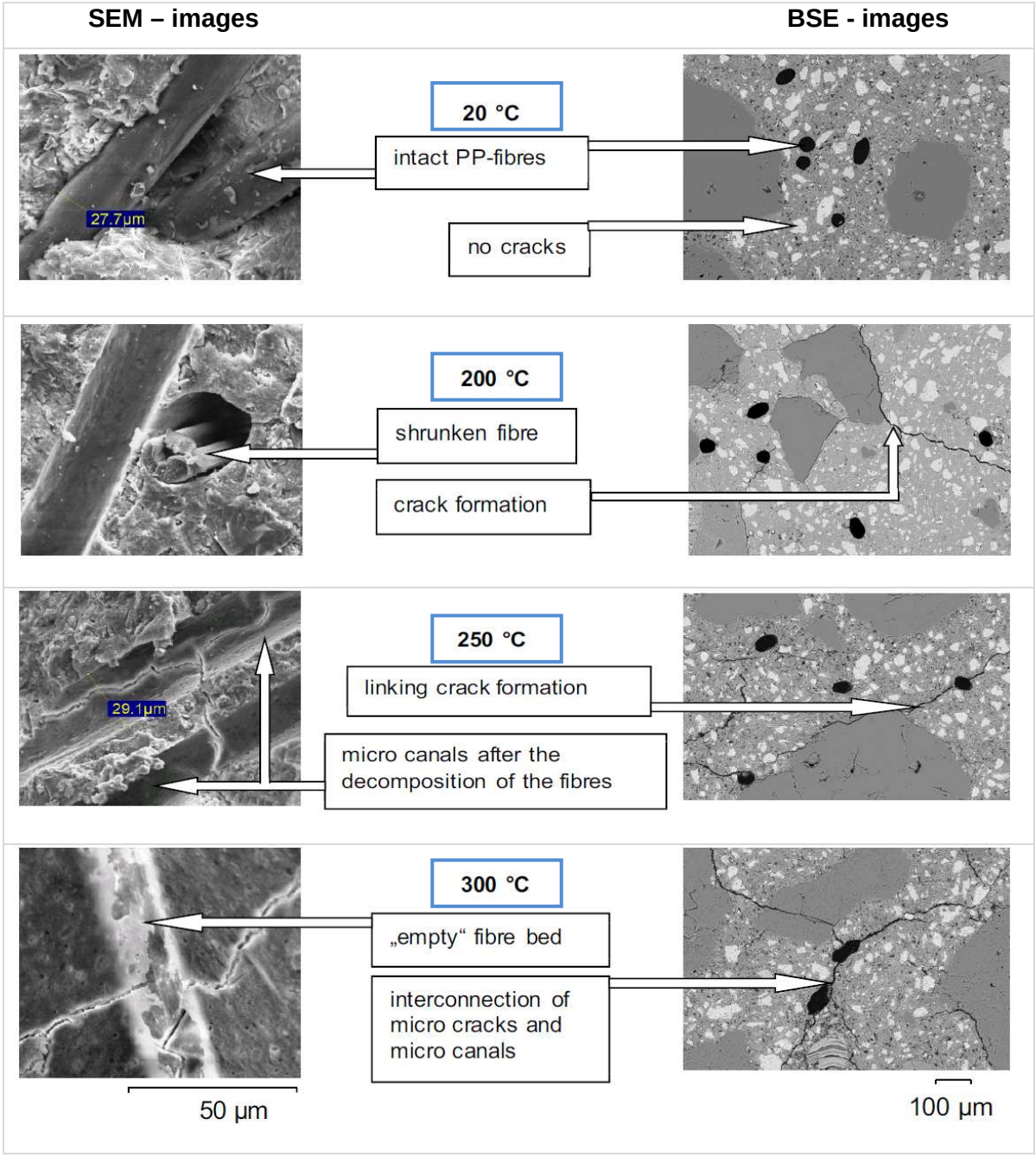

Figure 6-7: Creation of micro canals and micro cracks in concrete exposed to different range of temperature [21]

Initial state of PP-fibres without any changes is clear from first image taken at room temperature (20°C). The second picture taken on cooled-down sample preheated to 200°C already shows signs of shrinkage and partly empty fibre bed. Also crack formation takes place at this range of temperatures. At temperature 250°C the decomposition of PP-fibres take place and the linking crack formation occurs. The empty fibre beds lead to interconnection of micro canals and micro cracks at temperature 300°C. Temperature between 170°C and 350°C showed to be the most significant for PP-fibres.

7 Appropriate design of the individual components of concrete resistant to high temperatures

Appropriate selection of individual components of concrete mixture can positively affect its behaviour in case of fire and ensure adequate durability and fire safety. Concrete as a composite material is composed of coarse granular material (the aggregate or filler) embedded in a hard matrix of material (the cement or binder). The essential components influencing the properties of the final concrete are:

- aggregate,
- cement stone,
- polymer fibres.

7.1 Cement for concrete with higher resistance to high temperatures

The thermo-mechanical and thermo-hydraulic mechanisms occur during the heating of cement paste. Heating of cement paste leads to the evaporation of bound water contained in the capillary and subsequently the water bounded chemically. The nature of the phase change is dependent on:

- mineralogical composition of the cement,
- CaO/SiO_2 ratio,
- the fineness of cement,
- the temperature level,
- and level of pressure.

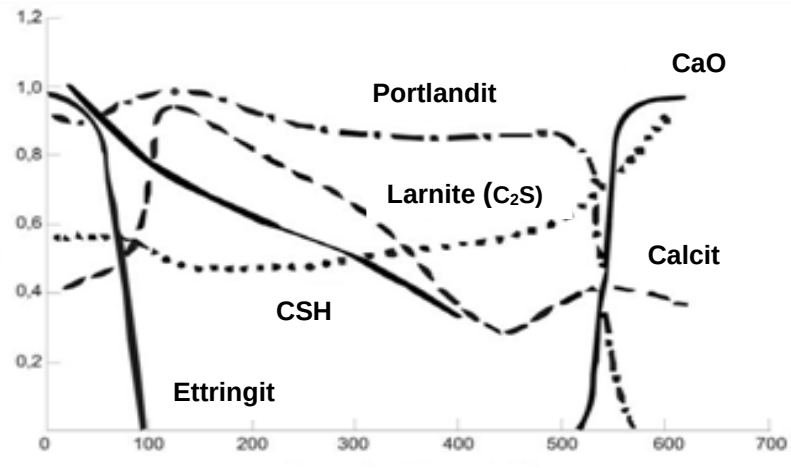

Figure 7-1: Development of normalized intensity of essential minerals of Portland cement paste [45]

Figure 7-1 shows development of changes in amount of essential minerals of Portland cement paste heated up to 700°C with temperature increase of 1°C/min. The following minerals of cement paste have been observed: Portlandit, ettringit, larnite, calcit, CSH gel and CaO. The decomposition of ettringite takes place at temperature around 100°C. CSH gels are being gradually dehydrated since the beginning of heating. Content of portlandit decreases significantly when the temperature around 500°C (550°C) is reached. Chemical bonds and CSH gels significantly affect mechanical properties of cement paste. Dehydration of CSH gels causes decrease of hydrates volume and therefore increase of cement paste porosity. The expansion of cement paste occurs up to 200°C and shrinkage take place when this temperature is exceeded [20].

Concrete which releases less $Ca(OH)_2$ is more resistant at elevated temperature. As it is clear from Figure 7-1, Portlandit decomposes due to high temperature (at 500°C) to water vapor and calcium oxide:

$$Ca(OH)_2 \rightarrow CaO + H_2O \qquad 1.15.$$

In the event of a fire the water sprayed on the surface of structure by fireman negatively contributes to the expansive reactions (slaking), which violates concrete:

$$CaO + H_2O \rightarrow Ca(OH)_2 \qquad 1.16.$$

This leads to an increase in the volume of concrete and thus spalling under the fire. According to this principle, concrete with pozzolanic materials or slag will resist better to fire than concrete with Portland cement due to the lower content of $Ca(OH)_2$.

7.2 Aggregates for concrete with high resistance to high temperatures

Aggregate is a concrete component, which occupies approximately 60-70%, and therefore plays an important role for the optimal design of concrete resistant to high temperatures. Generally, increasing temperature leads to volume expansion of solid materials so as aggregates. Thermal expansion as a function of temperature is an important technical characteristics which establishes the suitability of aggregates for concrete. Linear thermal expansion varies depending on mineralogical and petrographic composition of the rock (mineral). Linear thermal expansion of different types of rocks is given in the Table 7-1.

Table 7-1: Linear thermal strains coefficients of different types of rocks

Type of rock	Linear thermal strains coefficients [10^{-6}/°C]
Granite	1,8 – 11,9
Basalt	3,6 – 9,7
Sandstone	4,3 – 13,9
Limestone	0,9 – 12,2
Dolomite	6,7 – 8,6

In addition to the thermal deformation the metamorphic transformation of minerals may take place, such as conversion of silica aggregates at 574 °C. This change causes volume increase of about 0.84%. Thermal instability of limestone occurs in aggregates heated up to 600 °C. What's more, carbonate aggregate may decomposed to CaO and CO_2 at temperature about 700 °C. During the cooling the forms of CaO can hydrate with the resultant expansion of up to 40%. Suitable aggregates for concrete in response to risk of high temperatures will be aggregates with a low thermal expansion and a negligible residual strain [20].

Some type of limestone has a small thermal expansion at low temperatures and therefore seems to be particularly unsuitable. Different mineral expansions in rocks generate a loss of strength or permanent changes in their volume, especially at high temperatures. Large and irregular dilatation of gravel components may compromise durability of gravel grains as well as release of crystal water and carbon dioxide (calcination). Well proved in the heat seems to be limestone because the burning at temperatures above 500 ° C is limited to the superficial layers, which subsequently protect the core of grain [18]. Stability of aggregates and processes taking place during the heating are given in Figure 7-2.

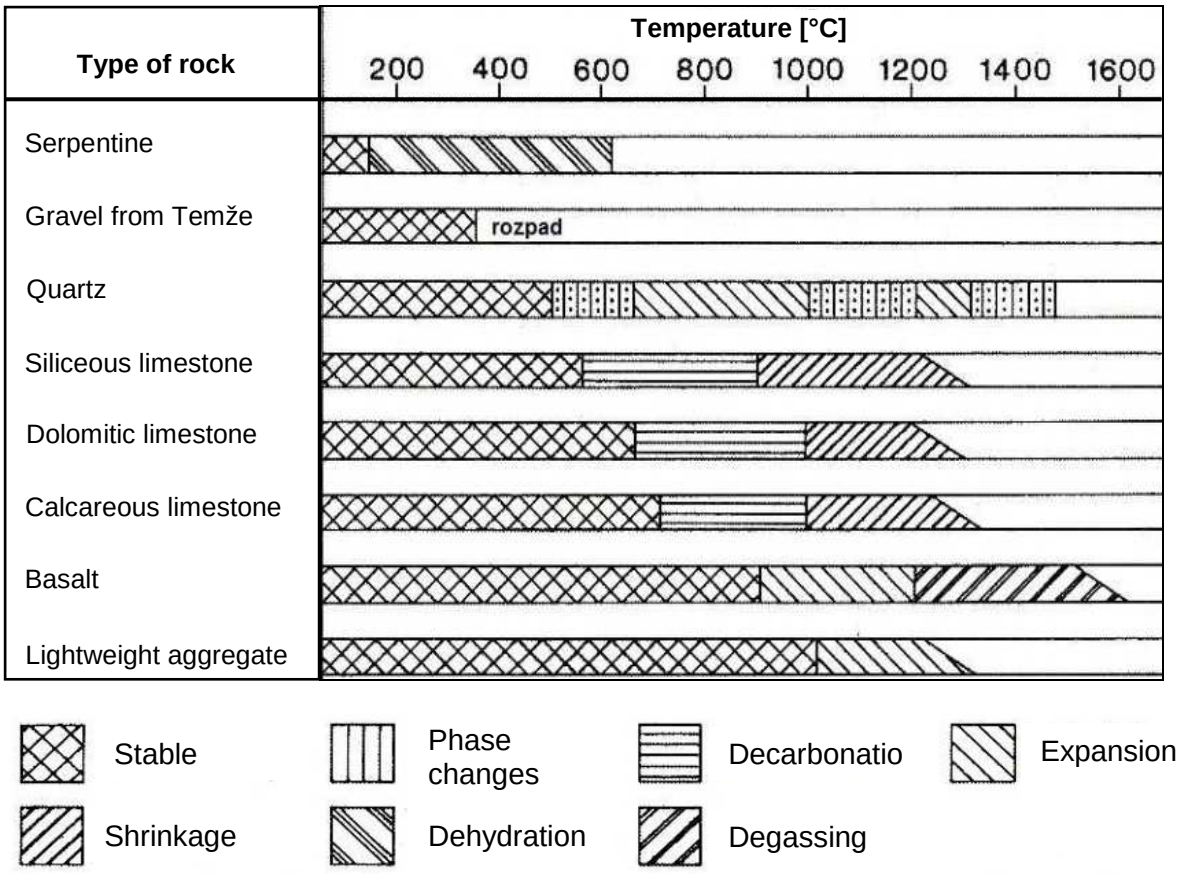

Figure 7-2: Stability of aggregates and processes taking place during the heating [39]

II. EXPERIMENTAL PART

8 Introduction of experimental part

The aim of the experimental work was to compare the behaviour of high performance concrete modified by polypropylene fibers with different arrangements and dosage exposed to high temperatures. Concrete specimens with different polypropylene fibres (standard with MFI25 (Melt Flow Index) and modified with MFI2500) of different dosage were exposed to thermal load of temperatures 1100°C reached in first 30 min and subsequent isothermal dwell of 90 minutes. Experimental part is divided into two main parts: explosive spalling of concrete and permeability of concrete. Concrete mix design was the same for both experiments. Experimental work was focused on different behaviour and physical mechanical properties of concrete without and with polypropylene fibres and verification of function of concrete with modified polypropylene fibres. After exposition to high temperature, physical mechanical properties were tested and compared to reference specimens without PP fibres and simultaneously were compared specimens with addition of standard PP fibres with melt flow index 25 (MFI 25) and dosage 2.0 kg/m^3 and modified PP fibres with MFI 2500 and dosage 0.9 kg/m^3. Surface of testing specimens was analysed by photogrammetry analysis and spall surface was defined.

In the second part of experimental work the permeability of concrete has been tested. Four sets of six samples were testing according a testing plan in testing equipment constructed at TU Wien. This testing device allows measuring permeability at different temperature up to 600°C and simultaneously different air pressure (in our case 0.2, 0.4, and 0.6 MPa). Monitoring temperatures were 20°C, 150°C, 175°C, 200°C, 225°C and 250°C. Each sample was tested at room temperature with applied air pressure of 2 bars, then at target temperature with applied air pressure of 0.2, 0.4 and 0.6 MPa and at the end the permeability of cooled-down specimen with applied air pressure of 0.2 MPa. Thermal load of each sample will be described in detail in methodological procedure for testing in part Permeability of concrete.

9 Methodology of experimental work

Proposal of concrete mix design was based on theoretical knowledge and recommendations from current literature search. Mixtures have been modified by adding two types of dispersed reinforcement in the form of polypropylene fibers from one manufacturer (Baumhüter, Germany). There were all together five proposed mix designs including a reference. Six test samples in the form of cube with dimensions 150 x 150 x

150 mm and test specimen in the form of block with dimensions 600 x 600 x 300 mm were produce from each of the mixtures for experiment A. Explosive spalling. Six test samples in the form of cube with dimensions 150 x 150 x 150 mm and six test specimens placed in steel rings with diameter approx. 102 mm and thickness of approx. 47 mm were produce from each mix design for experiment B. Permeability of concrete. Testing procedures in detail will be described in chapter 10 (testing of explosive spalling) and chapter 11. (testing of concrete permeability).

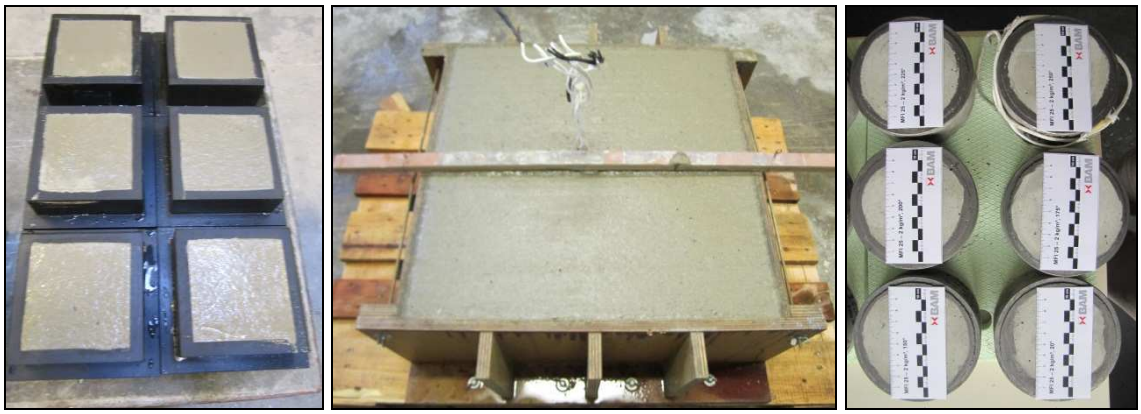

Figure 9-1: From left: cubes (150x150x150)mm, block (600x600x300)mm for explosive spalling test, steel rings for permeability test (by author)

10 Explosive spalling

10.1 Preparation of experiment

Considering the wide scale of the experiment, first of all, it was necessary to ensure the required materials, the persons responsible for the implementation of the specimens, schedule testing dates and book testing laboratories and equipment.

10. 2 Preparation of specimens

Before producing the specimens itself the thermocouples as the sensors for measuring a temperature were prepared (Figure 10-1). It consists of two dissimilar metals in contact, joined together at one end. The thermocouple consists from Nickel-Chromium (Aluminium) with the desired temperature range (20°C – 1200°C). The junctions of these specific alloys have a predictable and repeatable relationship between temperature and voltage. Any junction of diverse metals will produce an electric potential related to temperature. During the heating or cooling process a voltage is produced and correlated back to the temperature.

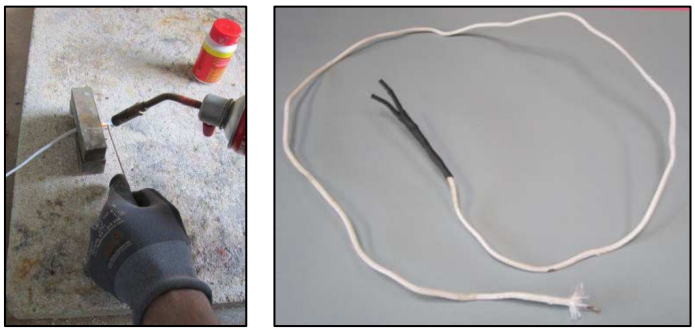

Figure 10-1: Thermocouple preparation (by author)

The preparation involved a simple connection of the ends of two alloys using manual burners and treatment of opposite ends. Thermocouples were placed into the pre-prepared form (mold) in which bores were drilled on the lateral face to ensure the accurate location of thermocouples in relation to the desired distance from the heated surface of the specimen (Figure 10-2).

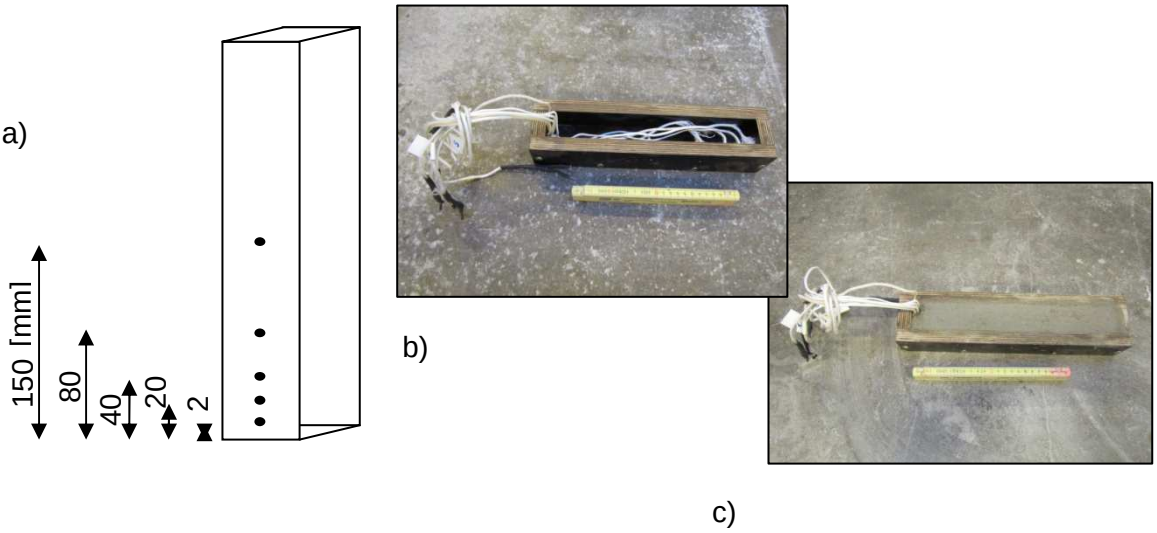

Figure 10-2: a) Scheme of pre-prepared mold, b) Thermocouples placed in mold, c) Pre-prepared mold fulfilled with concrete (by author)

The prisms with thermocouples were located in the middle of framework of dimensions (600x600x300) mm and framework was consequently fulfilled by mixed concrete (Figure 10-3). Demolding of sample took place after 24 for hours and samples were store for 90 days in climate chamber.

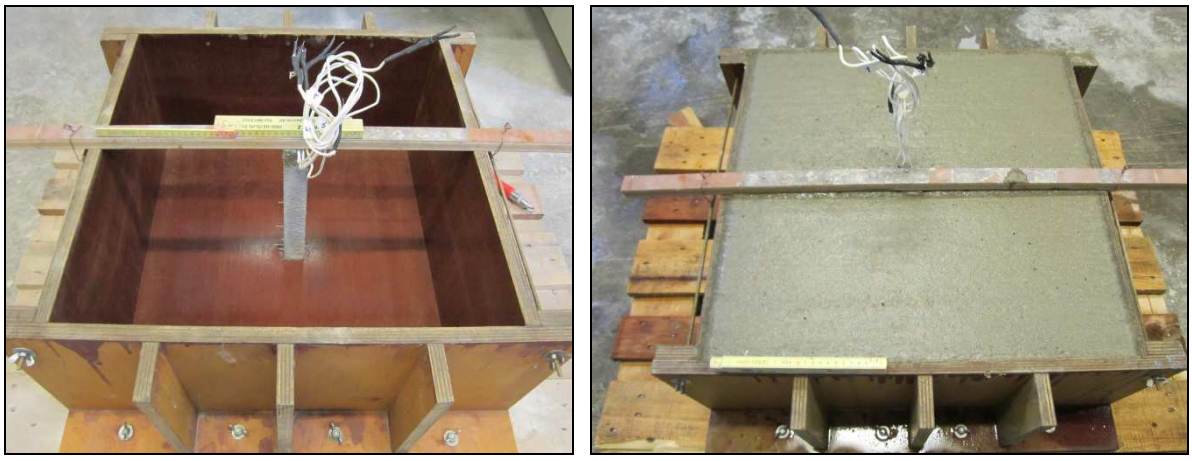

Figure 10-3: from the left: 1)pre-prepared mould with positioned prism with thermocouples, 2) full-filled mould (by author)

The specimen in the form of cube with dimensions 150 x 150 x 150 mm created for determining the mechanical properties in 28 and 90 days age were stored after demolding for 7 days in water with temperature 20°C and. After 7 days water storage were placed in a climate chamber with temperature 20°C and relative humidity of 65% up to 90 days.

Figure 10-4: Storage of specimens in climate chambers with temperature 20°C and relative humidity of 65% for 90 days (by author)

10.3 Materials

Concrete

In this investigation a HPC with siliceous aggregates was created in mixing plants TEKA 250 l with a compressive strength of 66 MPa (for concrete with 2 kg/m^3 of PP-fibres), 71 MPa (for concrete with 0,9 kg/m^3 of PP-fibres) and 72 MPa (for concrete without PP-fibres) measured after 28 days. The water absorption 3.44 mass% for concrete without PP-fibres and 3.5 mass% for concrete with PP-fibres were defined. The specimens were stored after demoulding for 7 days in water with temperature 20°C and then in a climate

chamber with temperature 20°C and relative humidity of 65% up to 90 days. The proportions of the mixtures are given in **Table 10-1**.

Table 10-1: Mix design

PP-Fibres		***DFG-R without fibres***	***DFG-B15/6 MFI25***	***DFG-B32/6 MFI25***	***DFG-B15/6 MFI2500***	***DFG-B15/6 MFI25***
Dosage of PP-fibres [kg/m^3]*		-	2	2	0,9	0,9
Cement CEM I 42,5 R [kg/m^3]		450				
Water [kg/m^3]		167				
Additive FM 21/BV 21 [kg/m^3]		9				
Aggregates (siliceous) [kg/m^3]	**0,0-0,5 mm (Quarz)**	241				
	0,5-1,0 mm (Okrilla)	121				
	1,0-2,0 mm (Okrilla)	155				
	2,0-4,0 mm (Okrilla)	224				
	4,0-8,0 mm (Okrilla)	328				
	8,0-16,0 mm (Dorsten)	655				
Melt flow index of PP fibres		-	25	25	2500	25
Superplasticizer FM 21/BV 21 [kg/m^3]		9	9	10,1	11,2**	9

Aggregate

Siliceous aggregates - dry quartz gravel from Ottendorf – Orilla were used in mix design.

Grain size	**Passing in M-% through the sieve**								**Material**
mm	**0,25**	**0,5**	**1**	**2**	**4**	**8**	**16**	**31,5**	
0 / 0,3	100,0	100,0	100,0	100,0	100,0	100,0	100,0	100,0	Quarz
0,1 / 0,5	40,5	94,5	100,0	100,0	100,0	100,0	100,0	100,0	Okrilla
0,5 / 1,0	0,4	4,1	97,2	100,0	100,0	100,0	100,0	100,0	Okrilla
1,0 / 2,0	0,0	0,1	3,8	98,7	100,0	100,0	100,0	100,0	Okrilla
2,0 / 4,0	0,0	0,1	0,1	1,7	99,7	100,0	100,0	100,0	Okrilla
4,0 / 8,0	0,3	0,3	0,4	0,8	2,8	100,0	100,0	100,0	Okrilla
8,0 / 16,0	0,1	0,1	0,1	0,1	0,2	4,3	97,9	100,0	Dorsten

		5,5	13,5	21,0	30,0	44,0	63,5	100,0	100,0	4,23

Grading curve components		Passing in M-% through the sieve (Sieve opening in mm)								Grain
[mm]	[%]	0,25	0,5	1	2	4	8	16	31,5	
0 / 0,3	0,0	0,0	0,0	0,0	0,0	0,0	0,0	0,0	0,0	
0,1 / 0,5	14,0	5,7	13,2	14,0	14,0	14,0	14,0	14,0	14,0	
0,5 / 1,0	7,0	0,0	0,3	6,8	7,0	7,0	7,0	7,0	7,0	
1,0 / 2,0	9,0	0,0	0,0	0,3	8,9	9,0	9,0	9,0	9,0	
2,0 / 4,0	13,0	0,0	0,0	0,0	0,2	13,0	13,0	13,0	13,0	
4,0 / 8,0	19,0	0,0	0,0	0,1	0,2	0,5	19,0	19,0	19,0	
8,0 / 16,0	38,0	0,0	0,0	0,0	0,0	0,1	1,6	37,2	38,0	
		0,0	0,0	0,0	0,0	0,0	0,0	0,0	0,0	
Grain curve	100,0	5,7	13,5	21,2	30,3	43,6	63,6	99,2	100,0	4,23
Difference in %		0,2	0,0	0,2	0,3	-0,4	0,1	-0,8	0,0	0,00

Polypropylene fibres

In the study, standard and modified polypropylene fibres have been used. The standard PP fibres used have a length of 6 mm, diameter 32 and 15 µm with and melt flow index 25. The modified fibres treated with radiation have length of 6 mm, diameter 15 µm and melt flow index 2500.

Figure 10-5: PP-fibres (by author)

PB EUROFIBER HPR as modified fibres

PB EUROFIBER HPR is the new, patented PP special fiber to maximize the fire resistance of concrete and minimize concrete spalling. New modified PP fibers provide the required fire protection at a highly reduced fiber dosage (50 - 70 % minimized fiber dosage of PB EUROFIBER HPR achieves the stipulated protection against fire), thereby simplifying the manufacturing process of the concrete. Based on the recommendation of manufacturer's dosage 0.5 – 0.9 kg/m³ of concrete is generally enough which leads to savings for fiber dosage costs (dosage 0.9 kg/m³ is considered as an effective). Reduction of fiber dosage leads to reduction of air void content and consequently optimizing the concrete quality, which is significant for achieving the desired properties of the high performance concrete (HPC).

PB EUROFIBER HPR has a significantly faster ease of flow when melted as compared all other PP fibers available on the market. This special feature works in a fire to allow the fibre to melt much faster within the concrete matrix, leading to a rapid creation of the important micro channels needed to discharge the vapour pressure from the concrete. PB EUROFIBER HPR is distinguished by the low viscosity and oily consistence of its melts.

Table 2: Characteristics PB EUROFIBER HPR

Fiber class:	Polypropylene from 100 % virgin PP
Fiber geometry:	1.7 dtex (15.4 mic), 6 mm cutting length
Fiber quantity per kg:	approx. 1 billion
Fiber length per kg:	approx. 6 million km
Melt flow index (230°C/2,16 kg):	> 1000 (PP-standard fibers= approx. 30)

Standard PP-fibres PB EUROFIBRES

PB EUROFIBRES of standard PP-fibres with recommend dosage 2 kg/m^3 produced by BAUMHÜTER, the same company as PB EUROFIBER HPR, were used in tests.

Table 3: Characteristics PB EUROFIBRES

Fiber class:	Polypropylene from 100 % virgin PP
Fiber colour:	Ecru
Fiber geometry:	Diameter 15 µm and 31 µm, 6 mm cutting length
Fiber form:	round
Fiber density:	0.91 g/cm³
Fiber count:	1-150 dtex (g/10000 m)
Melt flow index (230°C/2,16 kg):	25
Melting point:	Approx.. 165°C

Superplasticizer Woerment FM 21 (FM) / BV 21 (BV)

Free lingosulfonate superplasticizer is suitable for all civil engineering usage as well as for concreting in the tunnel. Raw material based on naphthalene sulfonate and melamine sulfonate.

10.4 Material properties / Results of experimental work

Specimens		***DFG-B15/6 MFI25***	***DFG-B32/6 MFI25***	***DFG-B15/6 MFI2500***	***DFG-B15/6 MFI25***	***DFG-R without fibers***
Dosage of PP-fibers [kg/m^3]		2	2	0,9	0,9	-
The test specimens w_1-w_3 [mm]		150/150/150				
Flow table test [mm] - a		365 (F2)	445 (F3)	425 (F3)	440 (F3)	490 (F4)
Flow table test [mm] - a_{30}		-	-	460 (F3)		390 (F2)
Air void content [%]		4,4	3,3	2,8	2,7	2
Volume density [kg/m^3]	w_1	2334	2358	2352	2337	2343
	w_2	2317	2298	2328	2341	2368
	w_3	2328	2292	2356	2324	2358
Average [kg/m^3]	w_1-w_3	2330	2320	2350	2330	2360
Time of vibration [s]		30				

10.4.1 Properties of fresh concrete

Specimens	*DFG-B15/6 MFI25 - 2,0 Kg*	*DFG-B32/6 MFI25 - 2,0 Kg*	*DFG-B15/6 MFI2500 - 0,9 Kg*	*DFG-B15/6 MFI25 - 0,9 Kg*	*DFG-R without fibers*
Air void content [%]	4,4	3,3	2,8	2,7	2
Volume density [kg/m^3]	2326	2316	2345	2334	2357
Flow table test [mm] - a	365 (F2)	445 (F3)	425 (F3)	440 (F3)	490 (F4)

Figure 10-6: Flow table test [mm] (by author)

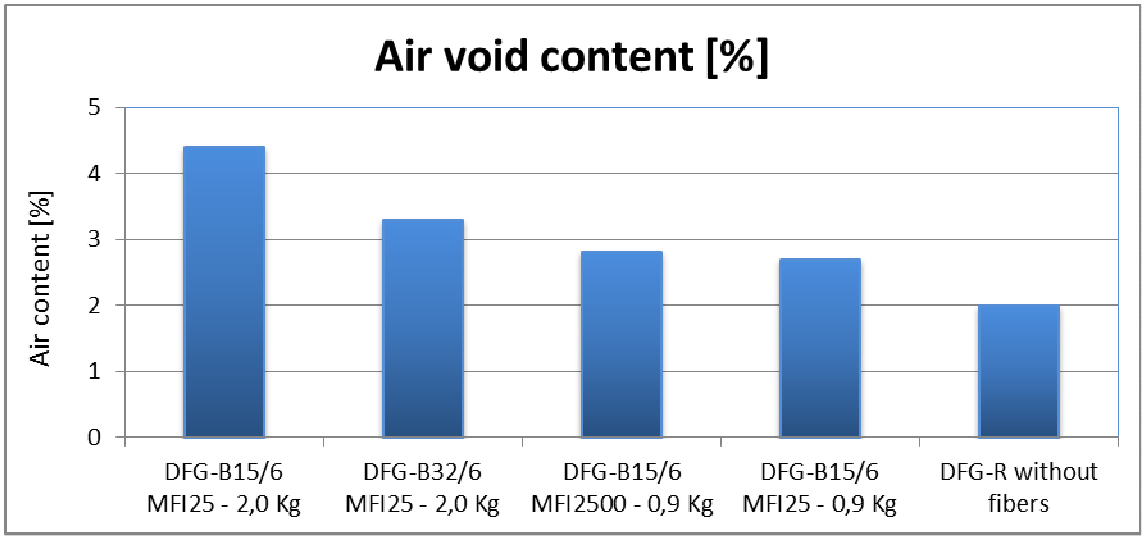

Figure 10-7: Air void content of fresh concrete increase with higher dosage of PP-fibres

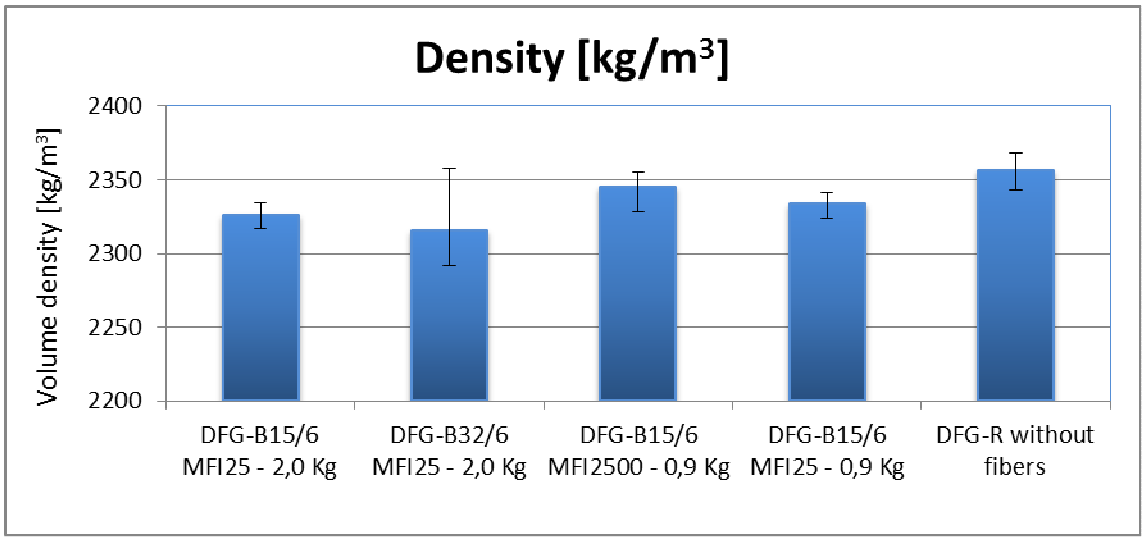

Figure 10-8: Fresh concrete properties - Density of fresh concrete

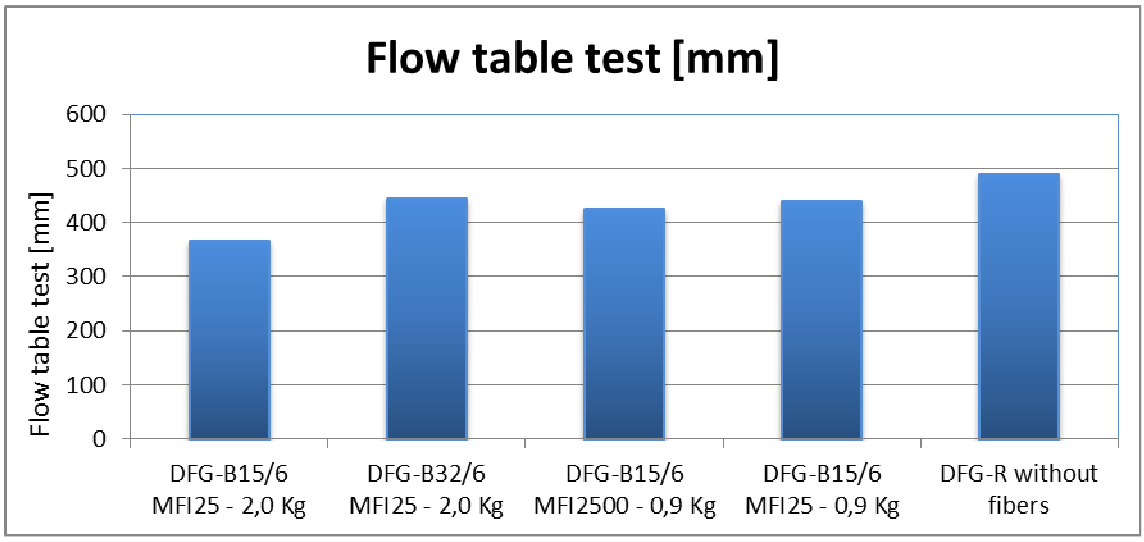

Figure 10-9: Fresh concrete properties - workability of concrete tested by flow table test

10.4.2 Properties of hardened concrete

Specimens	***DFG-B15/6 MFI25 - 2,0 Kg***	***DFG-B32/6 MFI25 - 2,0 Kg***	***DFG-B15/6 MFI2500 - 0,9 Kg***	***DFG-B15/6 MFI25 - 0,9 Kg***	***DFG-R without fibers***
Compressive strength [N/mm²] *	65,6	66	70,9	70,9	72
Water content [mass%]	3,88	3,96	3,81	3,88	3,27
Density [Kg/m³]	2310	2315	2326	2350	2355

** Tested on 28th day*

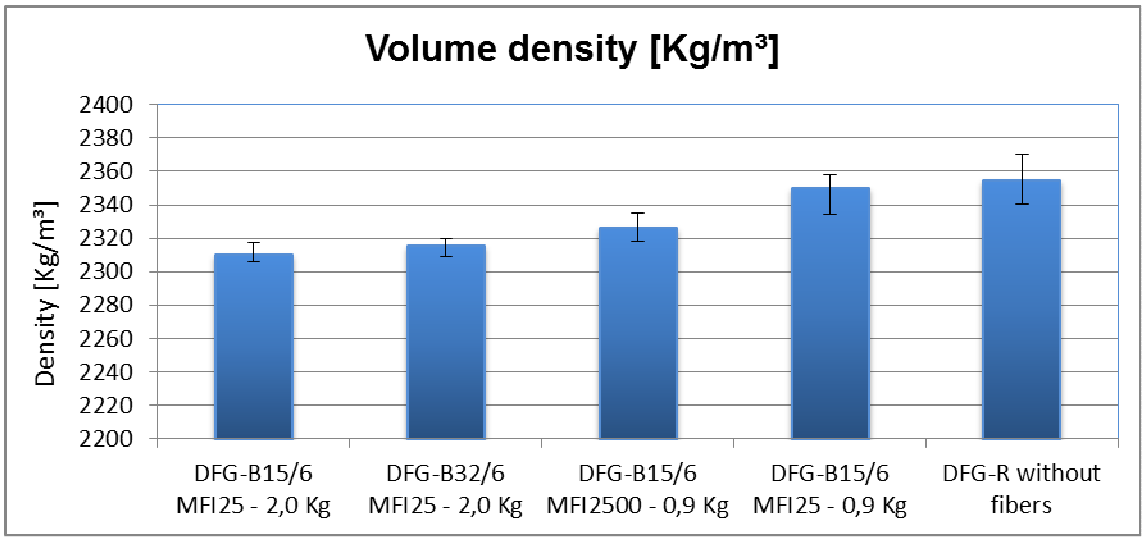

Figure 10-10: Hardened concrete properties – volume density

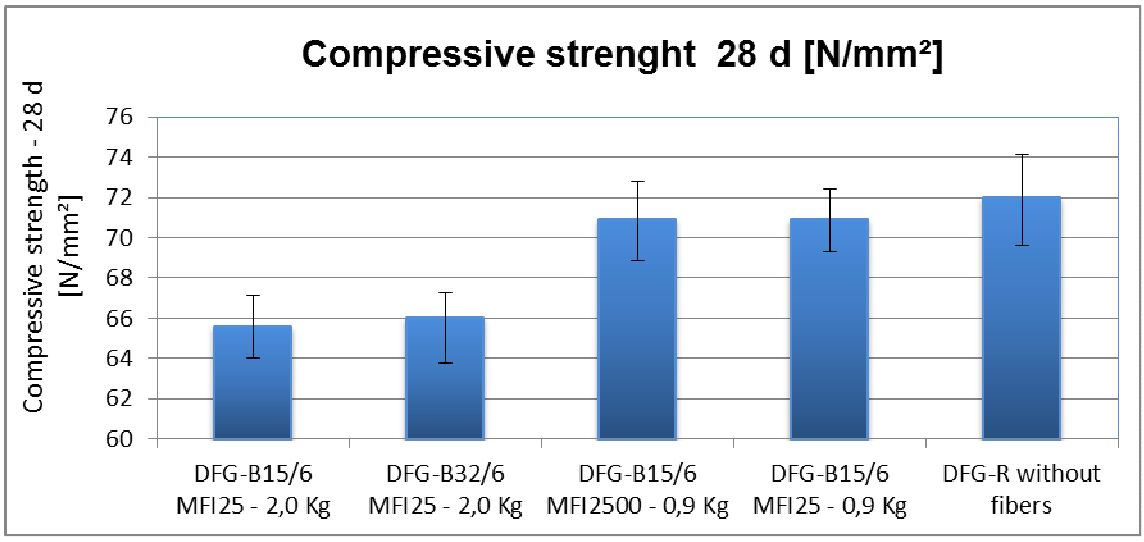

Figure 10-11: Hardened concrete properties – compressive strength

Additional micro-pores are created during the addition and mixing of fibres in the fresh concrete mix. Addition of PP fibres influences the porosity due to so called “foaming effect” developed during mixing of fresh concrete. The higher amount of fibres the higher porosity. Figure 10-7 shows that air void content [vol.%] increased with increased amount of fibres. With increasing air void content the density and workability decrease (Figure 10-8, Figure 10-9). Same trend is observed in compressive strength and density of hardened concrete.

10.5 Testing of explosive spalling

Testing was undertaken at sample age of min. 90 days. Weight, photos of the surface and photogrammetric pictures of the surface has been taken before installing the specimen in

the furnace. Testing procedure has been supervised by specialist from division 7.3. Fire engineering at BAM. The HydroCarbon temperatute-time curve has been used to simulate ventilated oil fire with a high initial temperature increase of 1100°C C after 30 minutes and then constant temperature 1100°C hold up to 180 [14].

The temperature T (°C) in hydrocarbon fire curve is given by:

$$T = 1080 \cdot (1 - 0.325 \cdot e^{-0.167t} - 0.675 \cdot e^{-2.5t}) + T_o \qquad 1.2.$$

t….. *time (min)*

T_o… *ambient temperature (°C)*

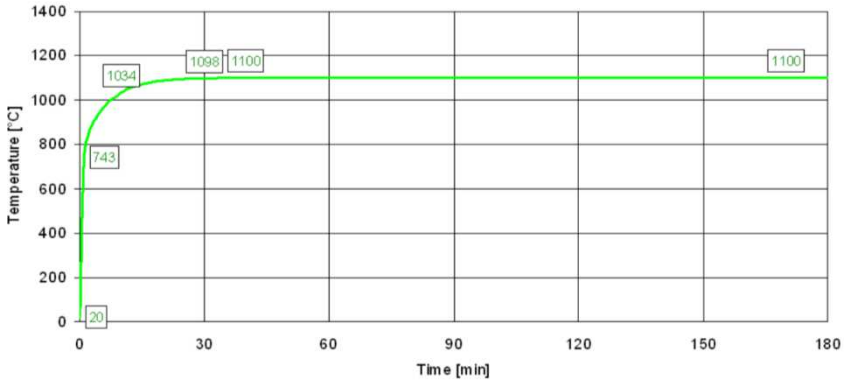

Figure 10-12: HydroCarbon temperature-time curve [14]

10.5.1 Testing devices - 1m^3 furnace

Explosive spalling tests were carried out in the furnace with volume 1 m^3 with two oil burners in simultaneous operation. Two thermocouples measuring temperature are placed in the furnace. The entire testing process is carried out by using computer software ensuring the temperature level in accordance with the hydrocarbon curve.

Figure 10-13: Testing 1m^3 furnace (by author)

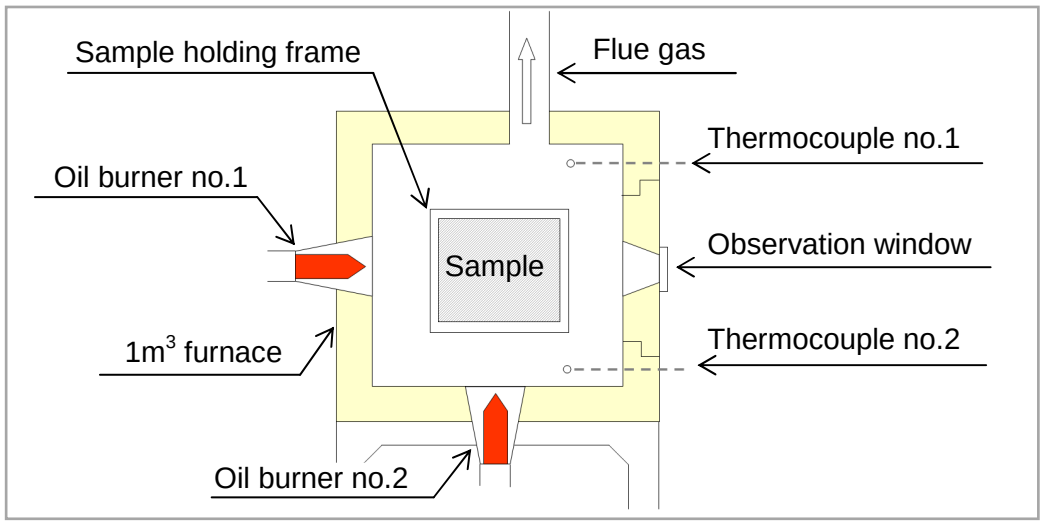

Figure 10-14: Schema of testing furnace

Any measuring device to record beginning, duration and the end of explosive spalling was not install and therefore explosive spalling during the testing is identify only by sounds and observation via observation window. Applied device to record entire course of spalling could be for example the sensors measuring the acoustic emission.

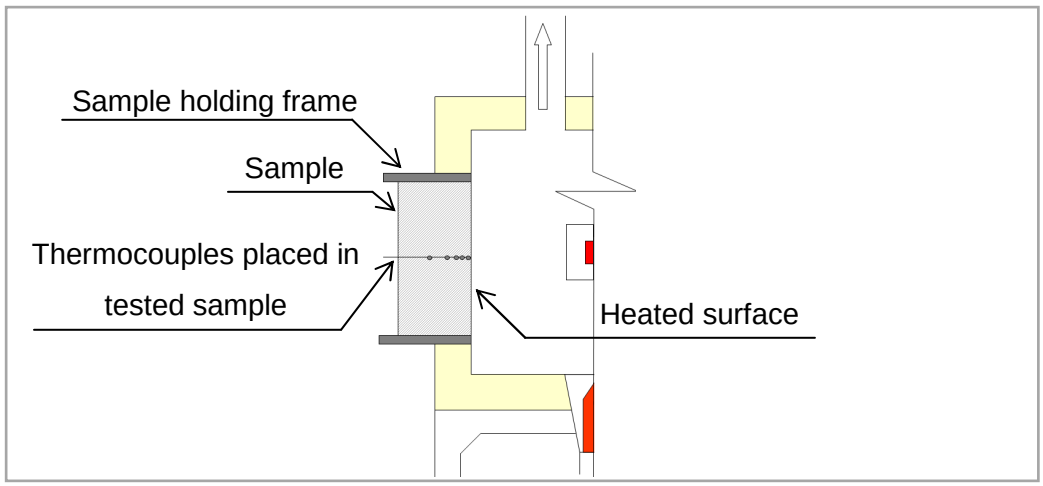

Figure 10-15: Schema of testing set-up

10.5.2. Results of experimental work

For better orientation in the result it will be necessary to explain and describe “composition of identification title of the samples”:

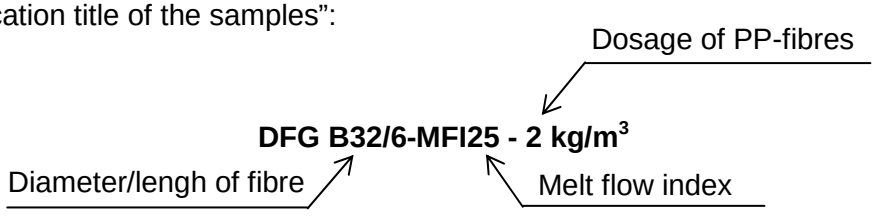

Duration of test procedure

1. Before fire test (00:00)

2. First cracks occurred on the all side walls generally in two-thirds (5 min)

3. Water vaporization and condensation on the top surface of specimen (26 min)

4. Water vaporization and condensation on the top surface of specimen (45 min)

5. Water vaporization and condensation on the bottom surface of specimen (47 min)

6. Cool down specimen after fire test

Figure 10-16: Test procedure of specimen with 2 kg/m^3 PP-fibres of diameter 32 µm and length 6 mm with MFI 25

Figure 10-17: Left: Detail of exposed surface before fire test; Right: Cool down specimen after fire test

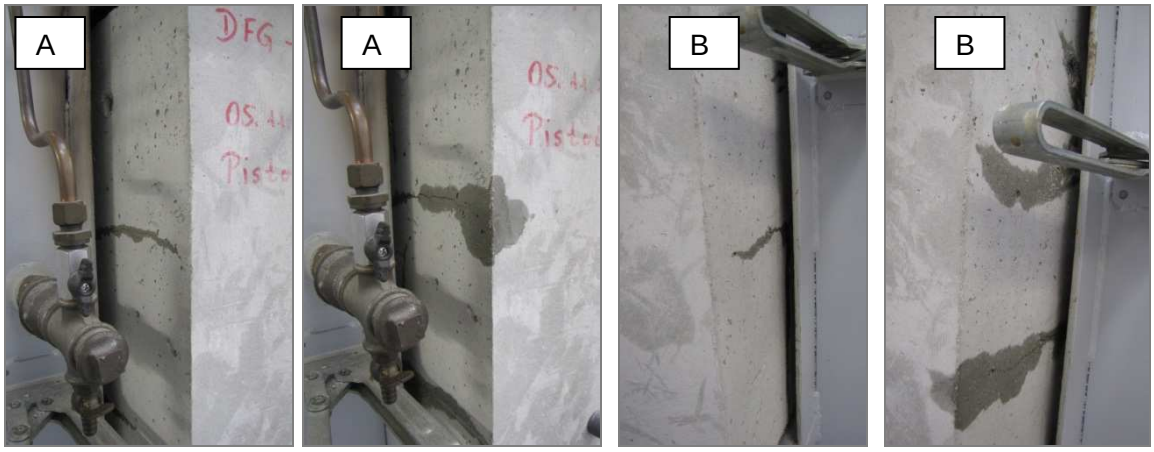

Figure 10-18: Crack formation and water vaporization (00:05 – 00:28) – speciment DFG B15/6 - MFI25 - 2 kg/m^3

Figure 10-19: Left: Water vaporization and intensive condensation on the top surface of specimen (00:47); Right: Location of crack formation occurred in first 5 minutes (DFG B15/6 - MFI25 - 2 kg/m^3) (by author)

Test procedure and the effect of high temperatute on speciment with PP-fibre exposed to hydrocarbon fire cuve is clearly desctibe in Figure 10-16, Figure 10-17 and Figure 10-18 together with time stamps. Within first 25 minutes crack formation and water vaporization take place. During the testing we have not experienced any explosive spalling except the reference sample without PP-fibres. Explosive spalling occurred within first 5 minutes when temperature reached 200°C. In fact the spalling behaviour can be estimate and define only by adequate fire tests. The basic parameter of explosive spalling is the depth of spalling, spalled off area and also time of spalling. Surface of tested specimen was scanned by photogrammetry device before and after fire exposure. Fotogrammetry picture provides a clear impression of surface defects and therefore will be used for final evaluation, comparison of the surfaces and determining the explosive spalling depth (volume).

Figure 10-20: Photogrammetry device (by author)

Volume of spallining in relation to dosage of PP-fibres:

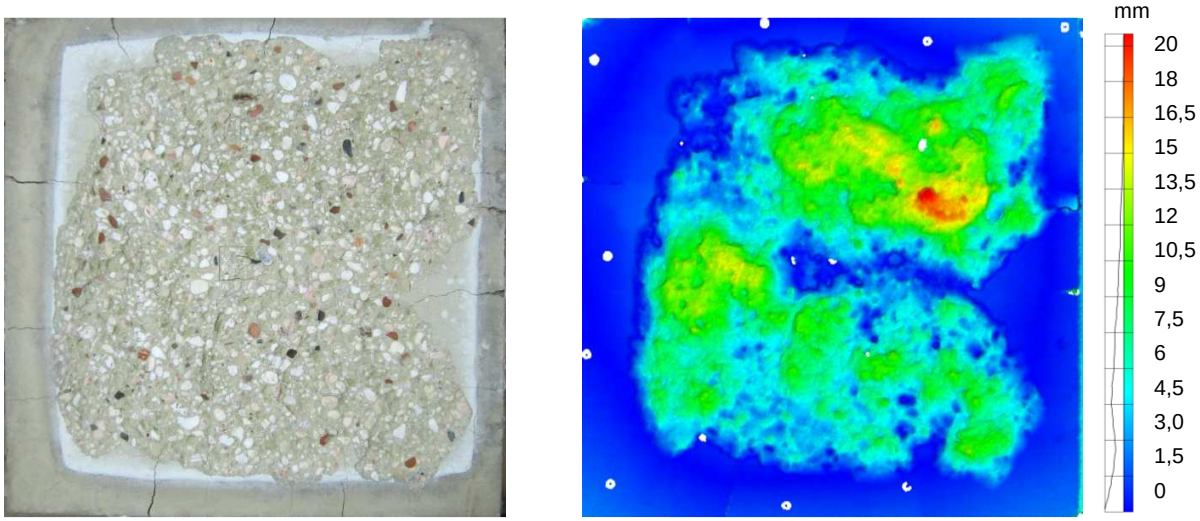

Figure 10-21*:* DFG-R- without fibers – spalling depth up to 20 mm

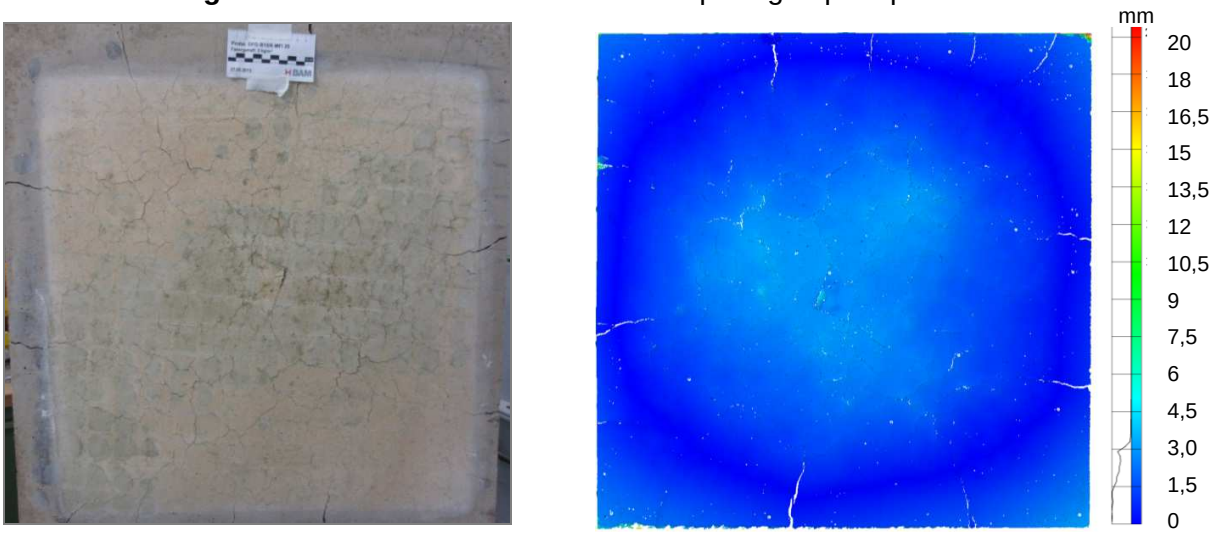

Figure 10-22: DFG-B15/6 - MFI25-2 kg/m3 - spalling volume 0%, only cracks and deformation

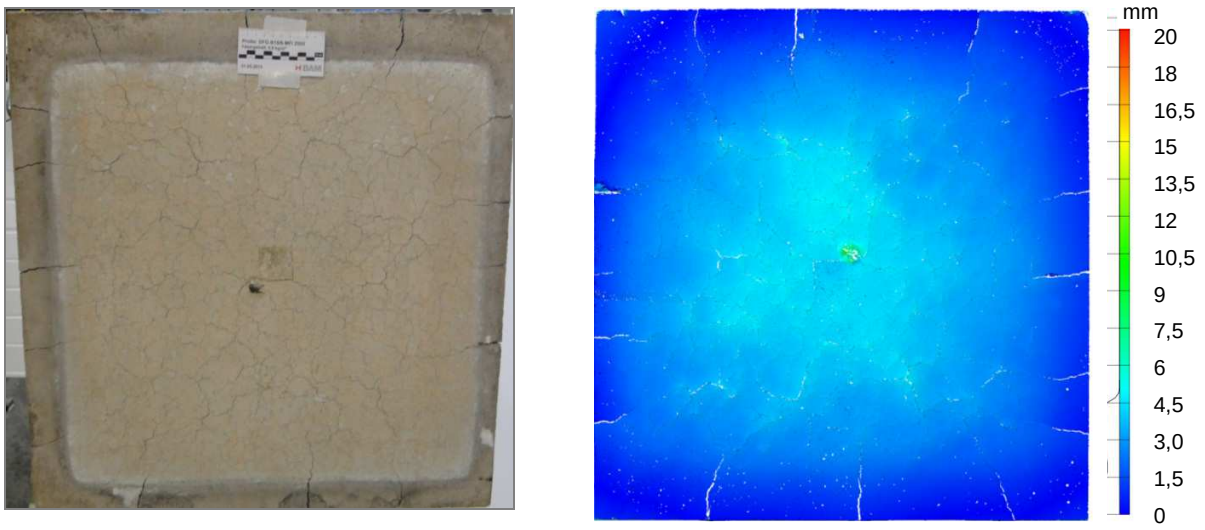

Figure 10-23*:* DFG-B15/6 - MFI2500 – 0,9 kg/m3 - spalling volume 0%, only cracks and deformation

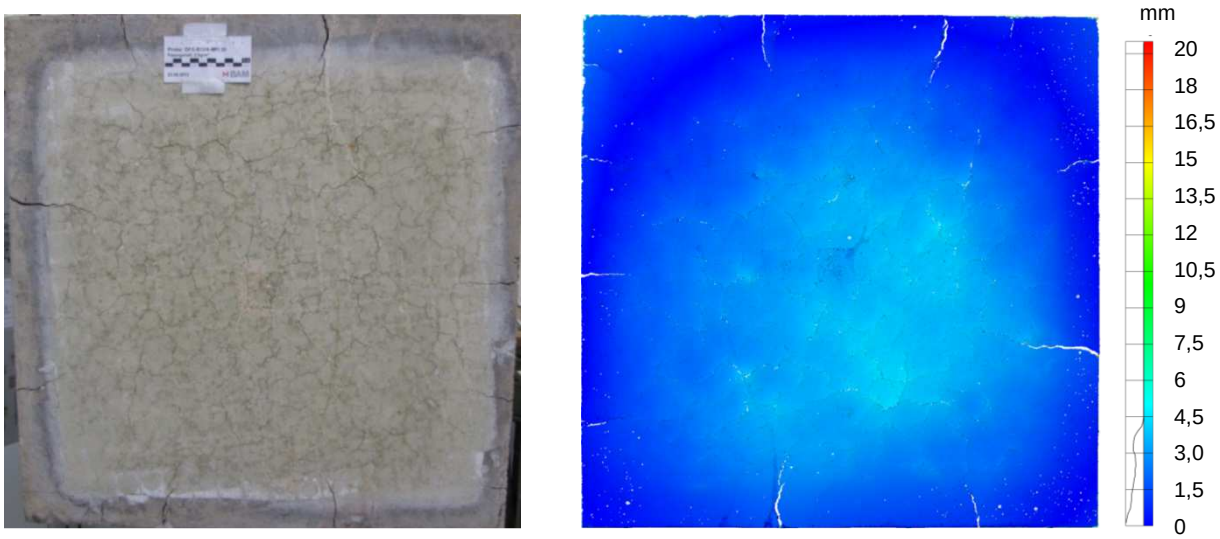

Figure 10-24: DFG-B32/6 - MFI25 – 2 kg/m3 - spalling volume 0%, only cracks and deformation

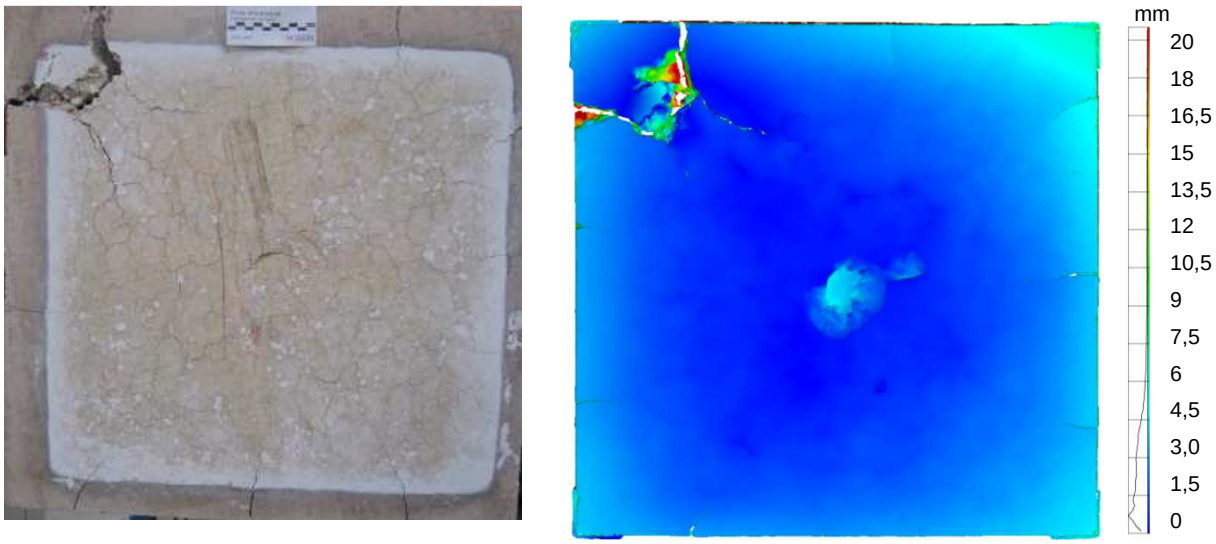

Figure 10-25: DFG-B15/6 - MFI25 – 0,9 kg/m^3 - spalling volume 0%, cracks and deformation

10.5.3 Summary and conclusions

Behaviour of high performance concrete exposed to hydrocarbon fire cuve was determine by photogrametry. Fibre dosage of 2 kg/m^3 PP-fibres has been already established as sufficient amount for high performance concrete and therefore explosive spalling has not been presumed at specimens with this dosage of standard fibres (DFG B15/6-MFI25-2.0 kg/m^3, DFG B32/6-MFI25-2.0kg/m^3). Specimen with modified fibres with MFI 2500 and reduced dosage 0,9 kg/m^3 has showed resistance on the similar course as sample with standard PP-fibres with MFI 25 and dosage 2.0 kg/m^3. Fibre dosage of 0.9 kg of PP-fibres per m^3 has been proven as sufficient for that modified fibres and therefore the explosive spalling did not occurred. In order to clarify this phenomenon the high temperature microscopy method was undertaken to establish properties of PP-fibres and analyze their

different mode of action. The main aim of the application of high temperature microscopy was characterization of material properties as softening and melting processes and temperatures (**Figure 10-26**). High contrast, high dynamic resolution to aid observation of melting and softening processes and software-supported measurement of wetting angles are the main the requirements to the microscope camera.

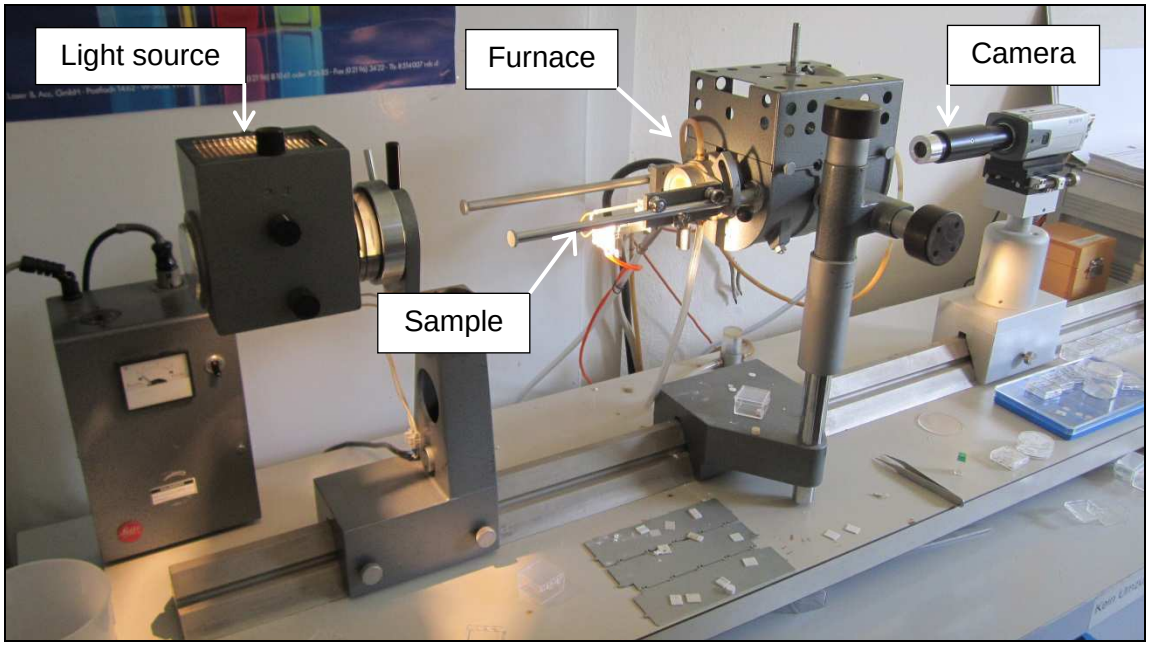

Figure 10-26: High-temperature microscopy (by author)

High temperature microscopy has been used to characterize the properties of PP-fibres at temperatures up to 200°C, particularly to identify softening and melting point of fibres, wetting properties (wetting angle) of polypropylene and interaction between PP-fibers and cement matrix. The substrate was positioned in the middle of the tube furnace where the external thermo element is located. The sample structure is heated up in the furnace to the specified solder softening temperature. The wetting angle was measured at several temperature points in the softening range. Observed temperature, important in term of PP-fibres was 171°C, which is define as melting point of PP-fibres and therefore a melting and interaction between polypropylene and cement stone has been monitored at temperature range. The first aim of study was also to distinguish thermal properties of modified PP-fibres with MFI2500 from standard PP-fibres with MFI25.

Temperature	PP-fibres with MFI 25	PP-fibres with MFI 2500
20 – 135°C		
150°C		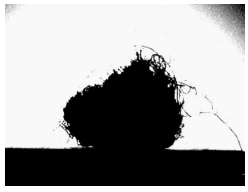
155°C		
160°C		
165°C		
170°C		
180°C		
185°C	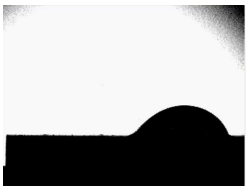	
194°C		

Figure 10-27: Identification of melting point of PP-fibres with different melt flow index.

Melting started with difference of about 10°C. PP-fibres with MFI 25 start to melt at 160°C and build a drop at temperature 174°C whereas modified PP-fibres with MFI 2500 start to melt in the range 147 - 150°C and build a drop at temperature 160°C (Figure 10-27). Since temperature increases with time (therefore is time dependent) enhanced permeability is reached sooner in concrete with modified fibres which results in decrease of pore pressure and explosive spalling is therefore prevented. This fact may be an explanation for higher resistance against explosive spalling due to higher permeability of heated concrete with reduced dosage of 0.9 kg/m^3 modified PP-fibres in comparison with concrete with addition of 2.0 kg/m^3 of standard PP-fibres. The second goal was to observe and analyze the interaction between PP-fibres and cement matrix. State of the art of polypropylene fibres and its mode of action was not fully understood up to now. In present work no interaction in form of absorption of melted PP fibres into the cement matrix has been observed. It can be explained as follow: increased pore pressure and flow of water vapour and enclosed air are required or molecular size is large to be absorbed into the cement matrix. Figure 10-27 clearly demonstrates melting properties of polypropylene fibres with different melt flow index. Monitoring of melting mechanism was performed for three times in total with different amounts of fiber to ensure accuracy of this method.

Figure 10-28 shows photogrammetric picture of specimen with reduced dosage of standard PP-fibres (with MFI 25) down to 0.9 Kg/m^3. Despite the fact that explosive spalling was expected did not occur. This may be caused by insufficient density and strength of concrete required for explosive spalling. Tested specimens with compressive strength around 70 MPa belong to category of high performance concrete but also are at the interface of ordinary concrete and high-performance concrete. Water/cement ratio over 0,3 (0,37 in tested specimens) leads to presence of capillary pores and therefore structure has been porous enough to limit build-up pore pressure.

Figure 10-29 illustrates increases of temperature during heating. Thermocouples located in the middle of specimen in depth 2 mm showed higher increase of temperature in sample without fibres results from exposed surface after explosive spalling. Temperature inside the specimens decreases with depth in all samples similarly (Figure 10-29). In depth of 80 mm temperature inside specimens with PP-fibres differ by 100°C from sample without fibers where temperature in sample without fibres reaches 700°C and in samples with fibres 600°C. Similar increase of temperatures in all samples (with/without fibres) was observed in depth 150 mm where reached temperature was between 110 and 130°C. If the thickness of concrete cover is min. 150 mm its distinctive damage and reduced function of reinforcement would not be anticipate.

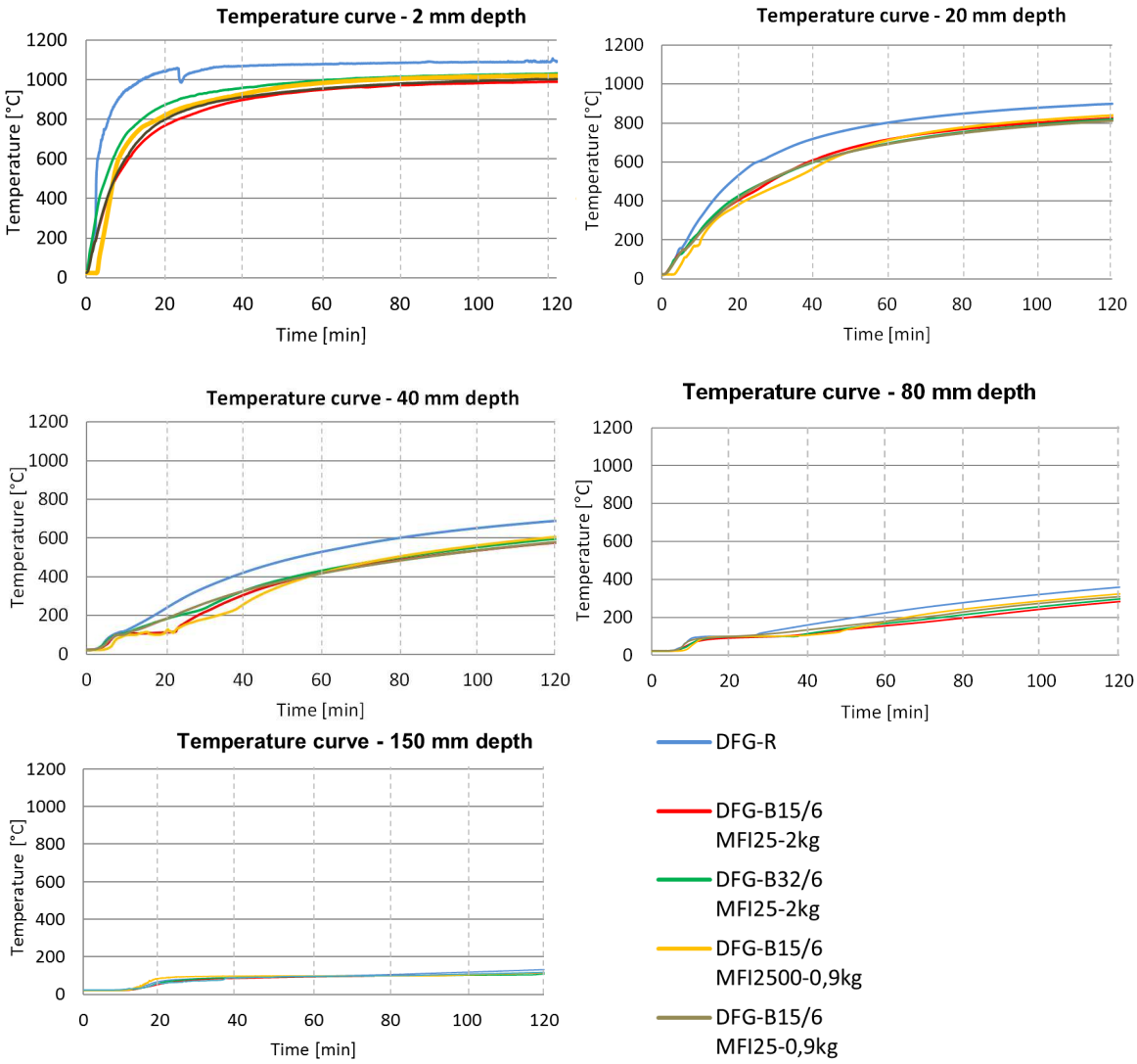

Figure 10-29: Temperature inside specimen decreases with depth

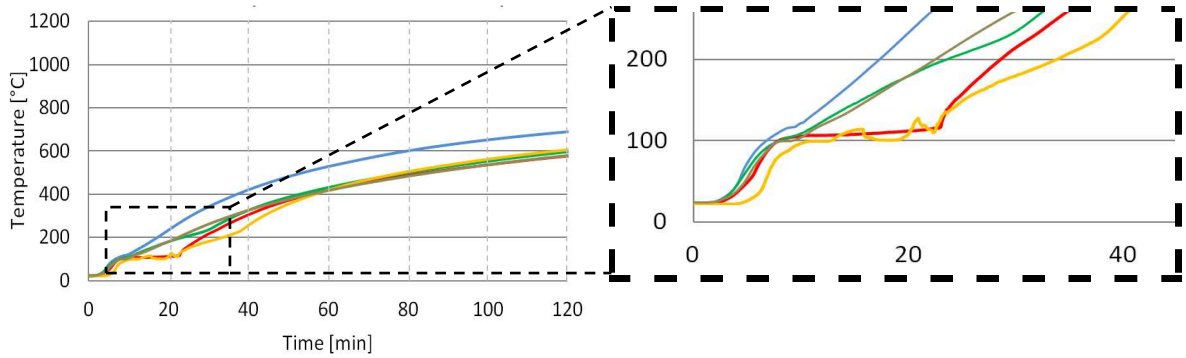

Figure 10-30: Temperature curve

Thermocouples located in depth 40 mm show endothermic delay in specimen with standard PP-fibres of dimension 15/6 mm and dosage 2 kg/m^3 (red colour curve) and specimen with modified fibres and dosage 0.9 kg/m^3 (yellow colour curve) at temperature 100°C. At that temperature energy is consumed by transition of state of water from liquid

to gas and thereby cool down effect is generated. This endothermic delay has taken place between 8th and 23th minute since the beginning. Due to explosive spalling of plain concrete thermocouples were uncovered and therefore any anomalies in form of endothermic delay were not obtained in the sample without PP-fibres.

Deformation of surface was obtained in all samples (Figure 10-32). This deformation of the surface could be explain as so called „bimetal effect" (Figure 10-31), where two different metal materials under the thermal load deforms due to different thermal expansion α. In the case of concrete the thermal expansion α is the same but due to different temperature tension on one side and compression on other side is caused.

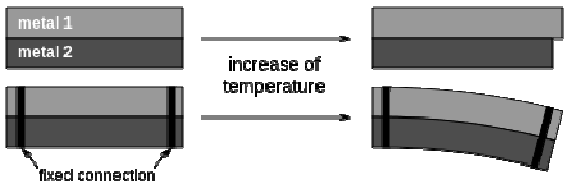

Figure 10-31: Bimetal effect

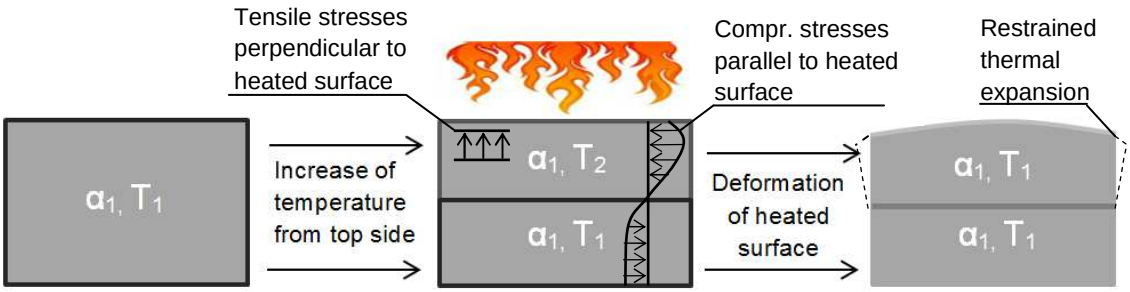

Figure 10-32: Graphical representation of surface deformation after fire exposure

Compression stresses parallel to heated surface together with tensile stresses perpendicular to heated surface cause deformation and restrained thermal expansion [49]. Another possible explanation could be the thermal expansion of the aggregate causing the deformation of the heated side. Deformation is most pronounced in the middle of the heated surface and exhibits a bulging of surface. This is due to the intensity of the thermal load which is the most intense in the middle of the sample surface where a crossing of horizontally a vertically positioned burner area is.

11 Permeability of concrete

11.1 Preparation of experiment

It was important to determine an adequate number of samples and compile testing plan which would clearly interpret the target temperature applied to each sample. Therefore six specimens of each mix design were produced.

It was also necessary to understand the principle of testing equipment and the theoretical basic of fluid transport in porous media.

In order to define the temperature reached in the core of the specimen we created four samples with thermocouples. Measurement of target temperature is situated in the oven and do not give an exact temperature value in the core of sample. According to the specimens with thermocouples the interval of temperatures obtained for an experiment (Table 11-1).

Table 11-1: Temperature loading adjustment

Target temperature [°C]	Temperature adjusted during measurement [°C]
95	100 → 105
150	155 → 175
175	180 → 195
200	205 → 225
225	230 → 255
250	255 → 290

11.2 Preparation of specimens

Before producing the specimens itself the thermocouples as sensors for measuring a temperature were prepared at the same way as describe previously. Concrete mixture was placed in the steel rings with diameter approximately 100 mm and thickness of 50 mm. During a testing the air pressure is applied on the top side of sample and therefore a steel ring has a different diameter of bottom side and upper side as illustrated as d_1 and d_2 in the table with dimensions of sample in order to keep concrete in the steel ring.

Figure 11-1: Concrete samples placed in steel rings (left: specimen with thermocouple)

11.3 Materials

Concrete

In this investigation a HPC with siliceous aggregates was created in mixing plants TEKA 250 l with a compressive strength of 72,5 MPa (for concrete with 2 kg/m^3 of PP-fibres), 73 MPa (for concrete with 0,9 kg/m^3 of PP-fibres with MFI 25), 67,9 MPa (for concrete with 0,9 kg/m^3 of PP-fibres with MFI 2500)and 73,4 MPa (for concrete without PP-fibres) measured after 28 days. The water content 3.44 mass% for concrete without PP-fibres and 3.5 mass% for concrete with PP-fibres were defined. The specimens were stored in a climate chamber with temperature 20°C and relative humidity of 65%. The proportions of the mixures are given in Table 1.

Table 1: Mix design

PP-Fibres		***DFG-R without fibres***	***DFG-B15/6 MFI25***	***DFG-B15/6 MFI2500***	***DFG-B15/6 MFI25***
Dosage of PP-fibres [kg/m^3]*		-	2	0,9	0,9
Cement CEM I 42,5 R [kg/m^3]		450			
Water [kg/m^3]		167			
Additive FM 21/BV 21 [kg/m^3]		9			
Aggregates (siliceous) [kg/m^3]	**0,0-0,5 mm (Quarz)**	241			
	0,5-1,0 mm (Okrilla)	121			
	1,0-2,0 mm (Okrilla)	155			
	2,0-4,0 mm (Okrilla)	224			
	4,0-8,0 mm (Okrilla)	328			
	8,0-16,0 mm (Dorsten)	655			
Melt flow index of PP fibres		-	25	25	2500
Superplasticizer FM 21/BV 21 [kg/m^3]		9	9	10,1	11,2**

Aggregate, Polypropylene fibres, Superplasticizer

Individual components of the concrete for determining permeability are identical with mixture for the determination of the explosive spalling (see chapter 10.3.).

- aggregate - siliceous aggregates - dry quartz gravel from Ottendorf – Orilla,
- polypropylene fibres - standard fibres PB EUROFIBRES with MFI 25,
  - modified fibres PB EUROFIBRES HPR with MFI 2500,
- superplasticizer - FM 21 (FM) / BV 21 (BV) based on naphthalene sulfonate and melamine sulfonate.

11.4 Material properties

Specimens		***DFG-B15/6 MFI25***	***DFG-B15/6 MFI2500***	***DFG-B15/6 MFI25***	***DFG-R without fibers***
Dosage of PP-fibers [kg/m^3]		2	0,9	0,9	-
The test specimens w_1-w_3 [mm]		150/150/150			
Flow table test [mm] - a		430 (F3)	430 (F3)	450 (F3)	490 (F4)
Air void content [%]		2,4	2,8	2,2	1,9
Volume density [kg/m^3]	w_1	2344	2336	2328	2349
	w_2	2352	2340	2331	2359
	w_3	2342	2323	2324	2365
Average [kg/m^3]	w_1-w_3	2346	2333	2328	2358
Time of vibration [s]		30	30	30	30

11.4.1 Properties of fresh concrete

Specimens	***DFG-B15/6 MFI25 - 2,0 Kg***	***DFG-B15/6 MFI2500 - 0,9 Kg***	***DFG-B15/6 MFI25 - 0,9 Kg***	***DFG-R without fibers***
Air void content [%]	2,4	2,8	2,2	1,9
Volume density [kg/m^3]	2350	2330	2330	2360
Flow table test [mm] - a	430 (F3)	430 (F3)	450 (F3)	490 (F4)

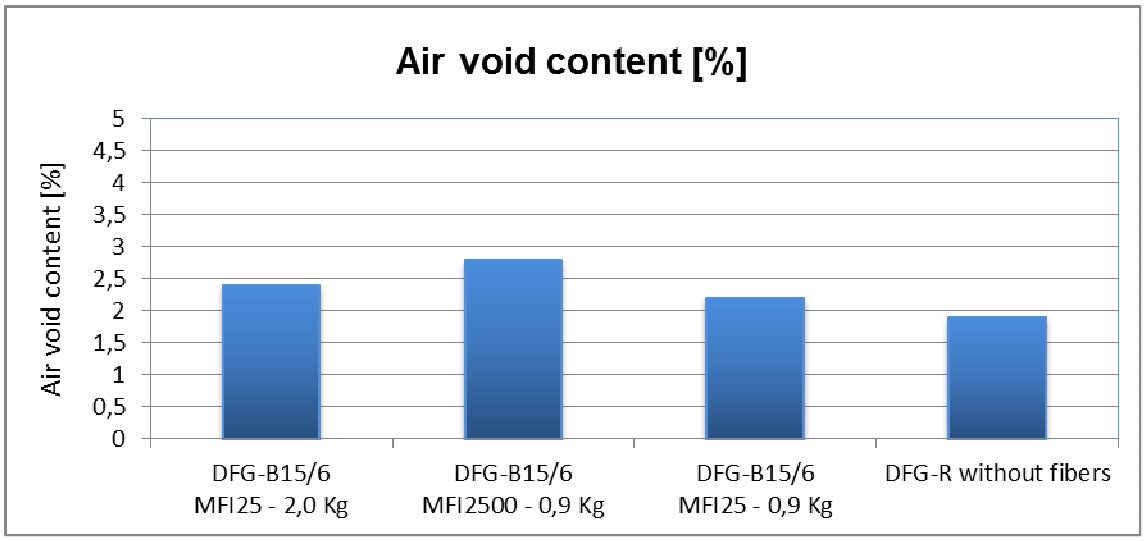

Figure 11-2: Fresh concrete properties – air void content [%]

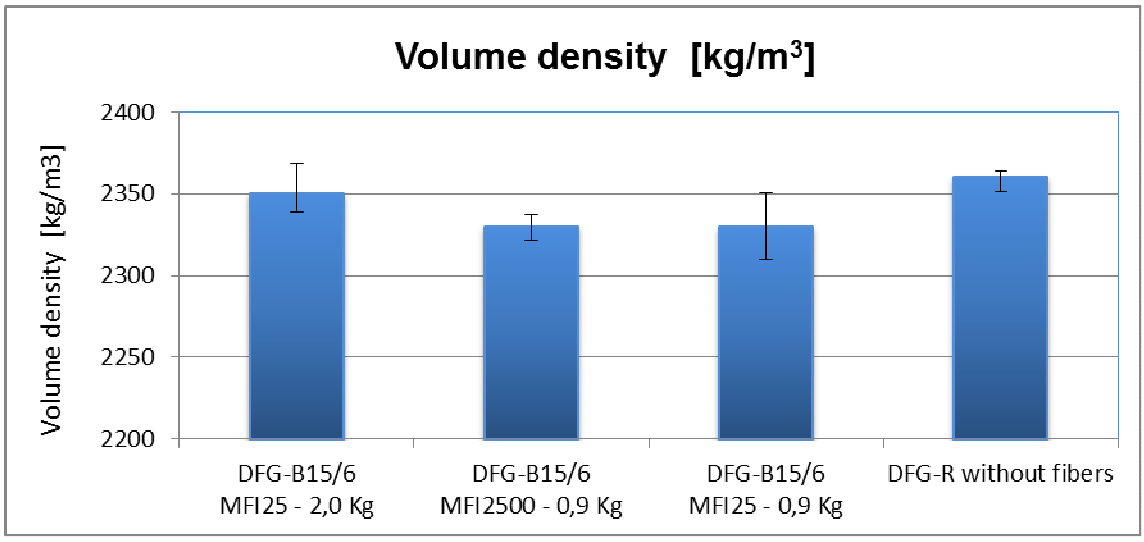

Figure 11-3: Fresh concrete properties – volume density [kg/m^3]

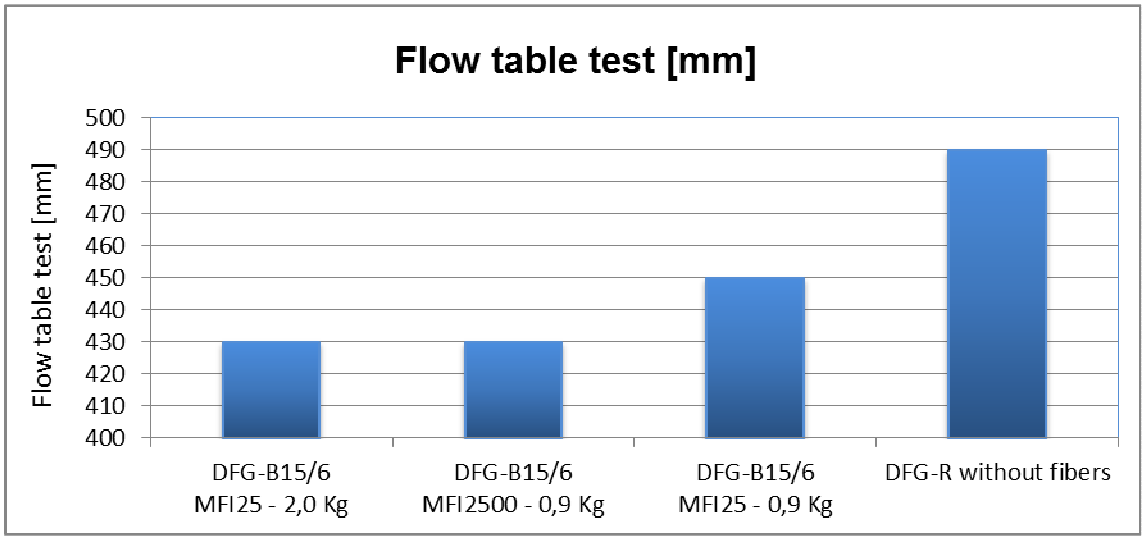

Figure 11-4: Fresh concrete properties – flow table test [mm]

11.4.2 Properties of hardened concrete

Specimens	*DFG-B15/6 MFI25*	*DFG-B15/6 MFI2500*	*DFG-B15/6 MFI25*	*DFG-R without fibers*
Dosage of PP-fibers [kg/m^3]	2	0,9	0,9	-
Compressive strenght [N/mm^2]	72,5 (28d)	67,9 (28d)	73 (28d)	73,4 (28d)
Density [Kg/m^3]	2330	2330	2320	2340
Water absorption [mass%]	3,51	3,5	3,51	3,44

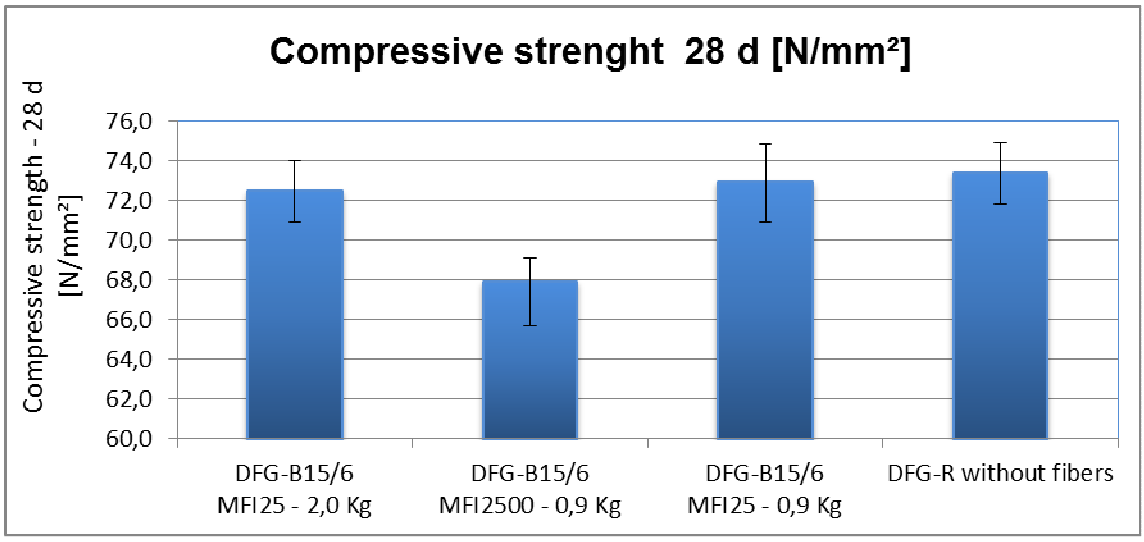

Figure 11-5: Hardened concrete properties – compressive strength [N/mm^2]

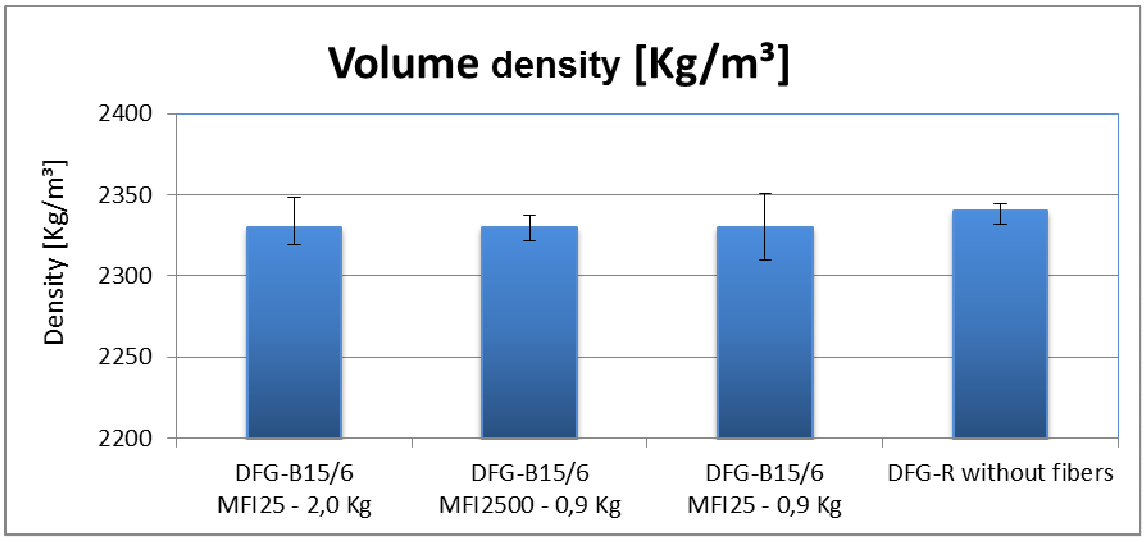

Figure 11-6: Hardened concrete properties – volume density [kg/m^3]

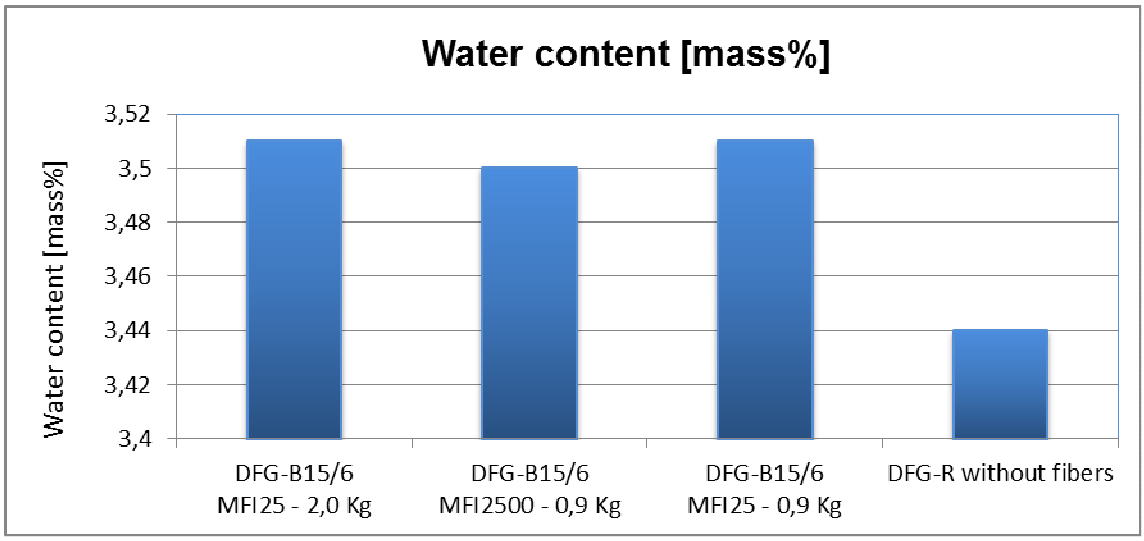

Figure 11-7: Hardened concrete properties – water content [mass%]

11.4.3 Dimensions of samples:

Fibres	Temperature [°C]	Weight [mm]	d1 [mm]	d2 [mm]	Height [mm]	Average d [mm]
Without fibres	20	1750.5	102.3	100.2	46.0	101.3
	150	1757.7	103.8	99.8	45.3	101.8
	175	1789.4	104.0	99.0	47.0	101.5
	200	1757.6	104.2	100.9	45.4	102.5
	225	1776.7	103.8	99.8	47	101.8
	250	1802.9	104.2	101.0	47.2	102.6
MFI 25-0.9 kg	150	1782.4	104.4	100.8	47.6	102.6
	175	1758.4	103.8	101.2	47.4	102.5
	200	1804.4	103.8	101.1	48.0	102.4
	225	1773.4	104.5	101.2	48.1	102.8
	250	1794.7	105.6	101.6	48.1	103.6
MFI 25-2.0 kg	20	1783.4	104.3	101.0	46.7	102.7
	150	1766.1	104.5	100.5	46.8	102.5
	175	1757.7	104.1	101.3	45.6	102.7
	200	1754.7	103.3	103.3	47.5	103.3
	225	1759.6	103.7	100.8	46.1	102.2
	250	1787.7	104.3	100.9	47.2	102.6
MFI 2500-0.9 kg	20	1757.3	103.9	99.7	46.6	101.8
	150	1768.7	104.1	100.4	46.6	102.3
	175	1757.5	105.0	100.1	45.6	102.5
	200	1773.5	104.1	101.0	47.5	102.5
	225	1763.7	104.6	101.4	46.8	103.0
	250	1743.6	104.7	100.0	46.8	102.4

11.5 Testing of permeability

11.5.1 Testing procedure

1. The permeability was measures at initial state at room temperature (around 22°C) and applied pressure of 2 bara (0.2 MPa).

2. Consequently the temperature was increased to temperature level one step under the target temperature marked in the table by *"+ intermediate temperatures"* (if target temperature is 175°C then temperature level measured before is 150°C) and permeability was measured under pressure of 2 bara.

3. Subsequently, the temperature was increased to the target temperature and the procedure was repeated. Permeability at target temperature was measured at pressure of 2, 4 and 6 bara (0.2, 0.4 and 0.6 MPa).

4. Finally, the "residual permeability" at 2 bars is measure at samples cooled-down to room temperature around 25°C

All measurement were carried out with heating rate of 2 $K \cdot min^{-1}$.

Attention should be paid to the fact that distinction is made in the measurement of the pressure in "bar" or "bara". "Bar" refers to the pressure on the ruling, relative atmospheric pressure and "bara" (or bar (a))refers the absolute pressure.

"absolute pressure = relative pressure + atmospheric pressure" where atmospheric pressure is 98066 Pa which is close to 100 000 Pa (100 000 Pa = 1 bar) and therefore unit use as atmospheric pressure was 1bar (0.1 MPa).

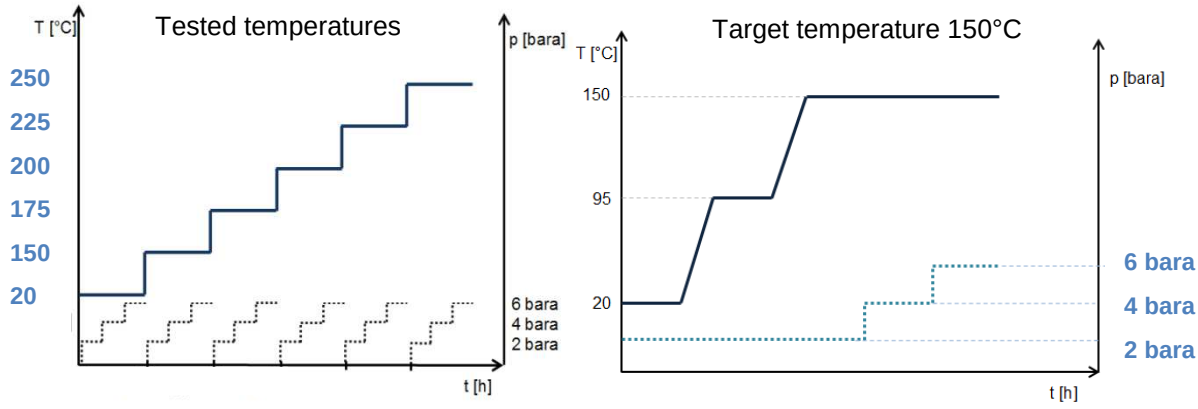

Figure 11-8: Testing procedure of the permeability experiments

Table 11-2: Testing plan

Nr	Mixture	Target temperature [°C] Permeability measurement at 2, 4, 6 bara	Intermediate temperature [°C] permeability at 2 bara					
			20	**(95)**	**150**	**175**	**200**	**225**
1	**Without PP-fibres**	**20**						
2		**150**	+	(+)				
3		**175**	+	(+)	+			
4		**200**		(+)	+	+		
5		**225**				+	+	
6		**250**					+	+
1	**MFI 25 2 kg/m³**	**20**						
2		**150**	+	(+)				
3		**175**	+	(+)	+			
4		**200**		(+)	+	+		
5		**225**				+	+	
6		**250**					+	+
1	**MFI 2500 0,9 kg/m³**	**20**						
2		**150**	+	(+)				
3		**175**	+	(+)	+			
4		**200**		(+)	+	+		
5		**225**				+	+	
6		**250**					+	+
1	**MFI 25 0,9 kg/m³**	**150**	+	(+)				
2		**175**	+	(+)	+			
3		**200**		(+)	+	+		
4		**225**				+	+	
5		**250**	+				+	+

11.5.2 Permeability testing device

The equipment for measurement of permeability under temperature load has been constructed and developed at Technical University in Vienna, Institute for Building materials, building physics and fire protection. This measuring device allows to measure air flow rates at different temperatures and simultaneously at different pressure levels. In the past a multiple devices to measure the permeability of concrete exposed to different thermal loads were constructed, but often allowed the measurement of cooled-down sample only.

Measurement of three main values (factors):

- Temperature
- Pressure differential
- Flow velocity

Testing device

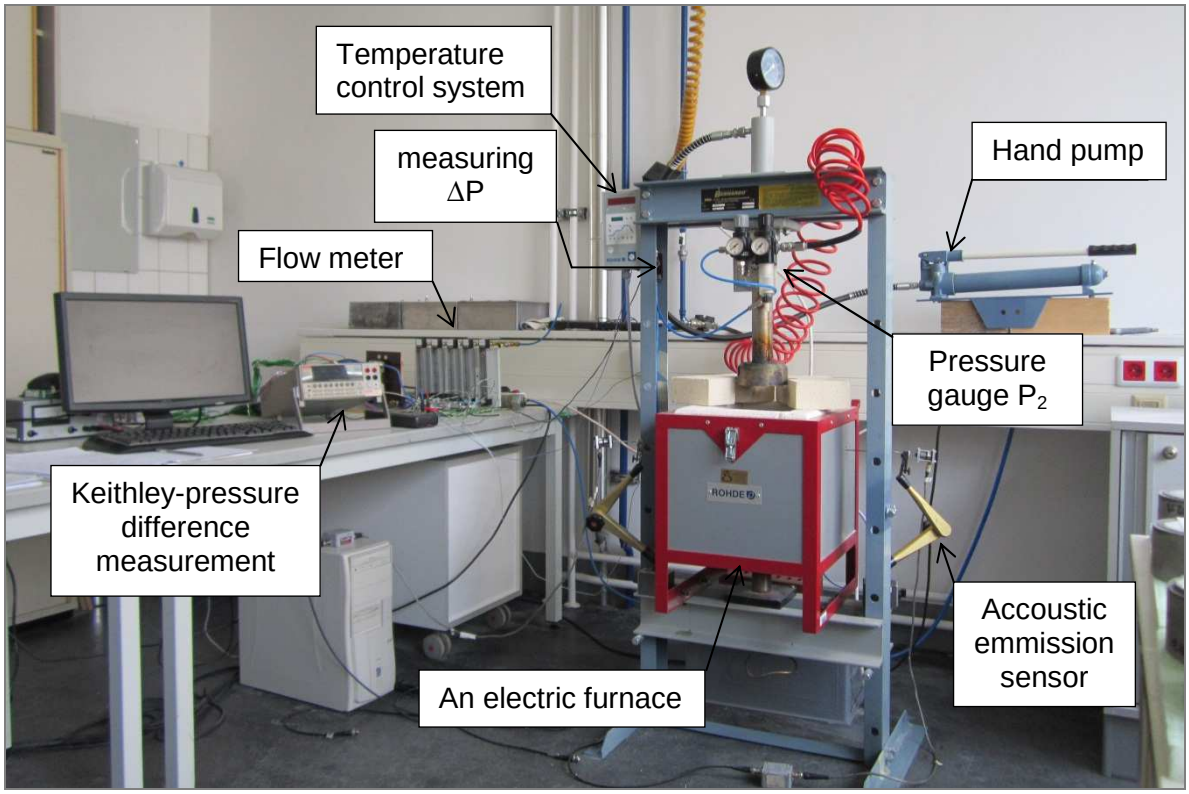

Figure 11-9: Tester for determining the permeability of temperature (by author)

The system consists essentially of the following parts (**Figure 11-9**):

- An electric furnace
- Frame holding the electric furnace
- A compressed air supply
- Sample holder, sample ring and pressure plunger
- Compressed air supply
- Differential pressure gauge
- Flow meter (rotameters)
- Computer programme

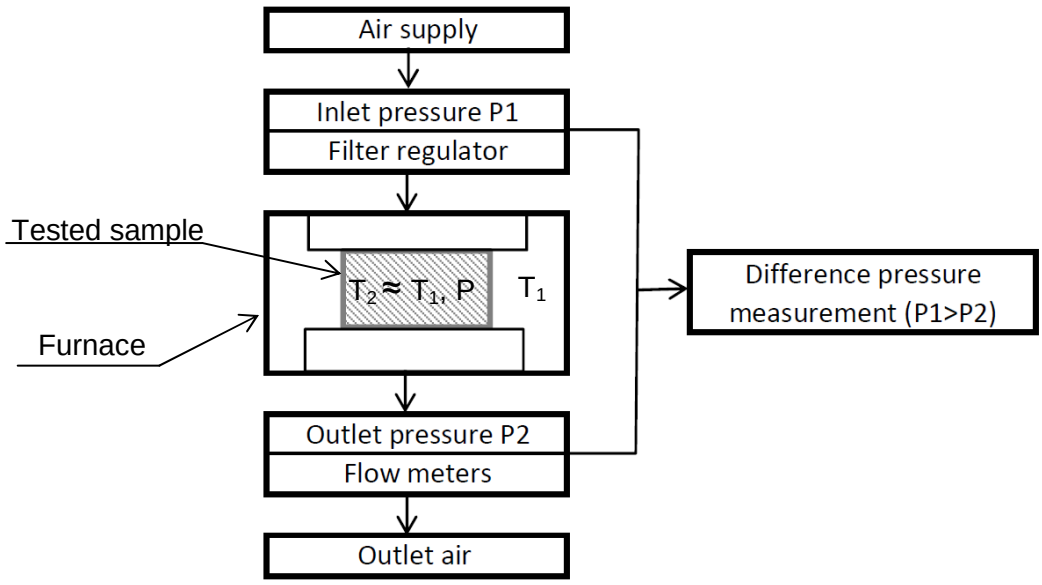

Figure 11-10: Scheme of experimental set-up

Frame holding the electric furnace

The electric furnace is fixed centrally in the Frame WK 12 F Bernardo (Figure 11-11) with compressive load max.10 tons. Maximum working height of frame is 940 mm and max. working width 510 mm. The individual components of the test apparatus as thermo computer TC 504 and manual pump are from company Bernardo.

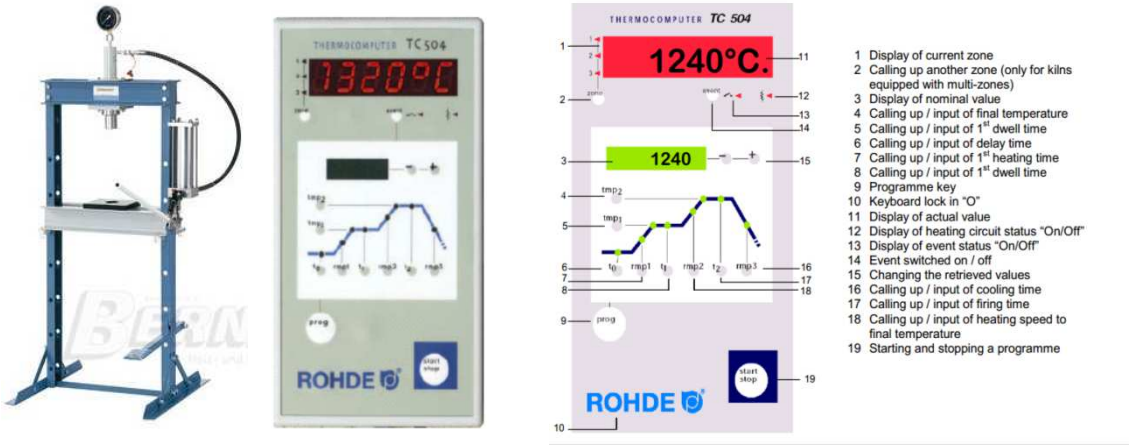

Figure 11-11: left: frame WK 12 F Bernardo ; right: thermo computer TC 504

Thermo computer TC 504

Thermo computer TC 504 (Figure 11-11) is installed on the left side. This control system allows a sufficiently accurate heating and holding the desired temperature. The furnace is heated up with the pre-set speed in degree Celsius per hour. Heating rate was set up to 2 K^{-1}/min.

Manual pump

The plunger is used, the necessary load on the sample holder and sample ring applied so that the required sealing between the individual components can be ensured. Furthermore, its role is to guide the air into the tester (**Figure 11-12**).

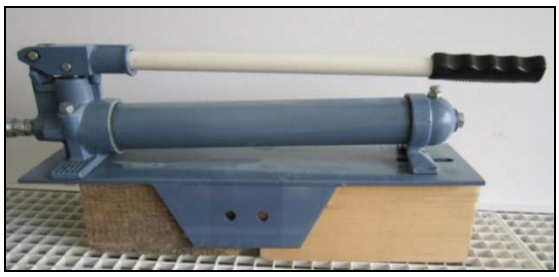

Figure 11-12: Manual pump (by author)

An electric furnace

An electric furnace Rohde TE 10 Quattro (**Figure 11-13**) of external dimensions (500 x 430 x 500) mm and internal dimensions (230 x 180 x 230) mm has about ten liters capacity. It is a control by system Rohde TC with maximum temperature 1250 °C and heating rate 2 K/min. This control system allows a sufficiently accurate heating and holding the desired temperature. The maximum temperature of the furnace is 1320°C. Constant pressure in the furnace is set up to 1 bar. This pressure acts on the sample surface.

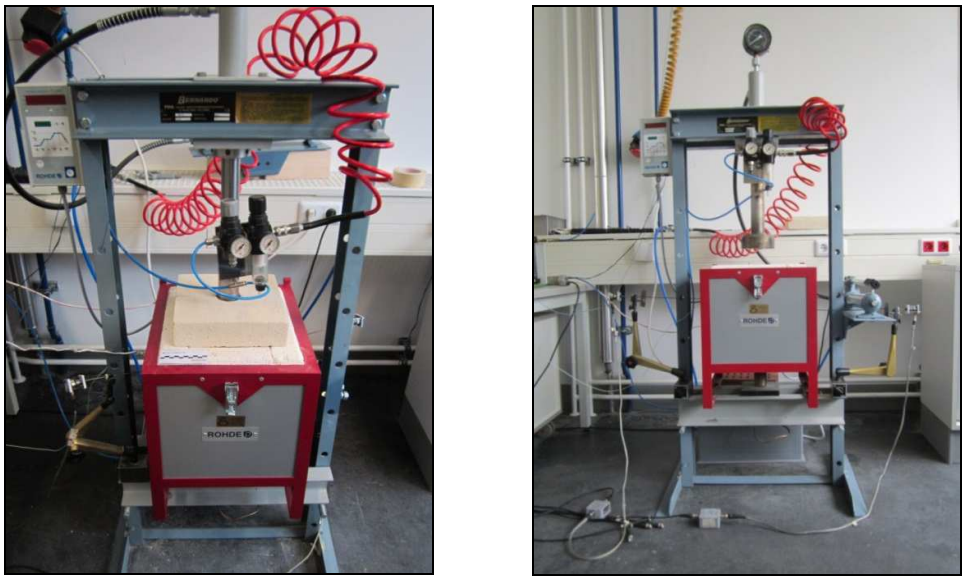

Figure 11-13: Electric furnace ROHDE in the frame (by author)

Compressed air supply, pressure gauge

The air system allows application of maximum pressure of 10 bars. The compressed air coming from the compressed air system disposed in the laboratory. A coiled cable leads to the filter regulator which cleans the air as well as controls the inlet pressure. The inlet air can be preheated to max. temperature of 80°C (85°C).

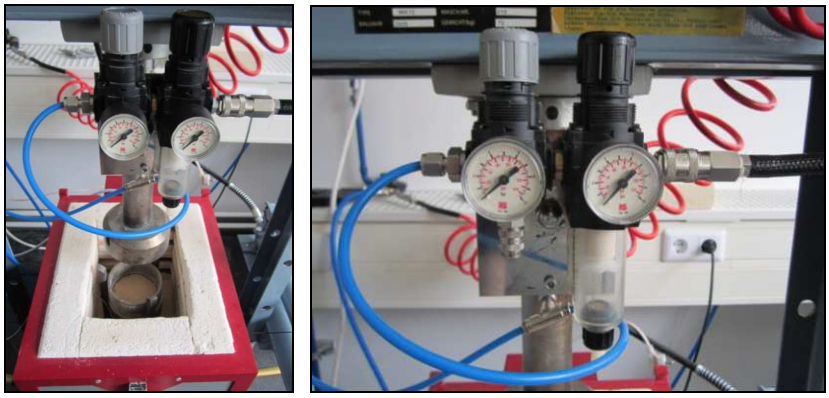

Figure 11-14: left: sample holder, right: pressure gauge (by author)

Sample holder, sample ring and pressure plunger

The plunger transmits required load on the sample holder and the sample ring. In order to ensure tightness between the plunger and the sample the sealing rings are used. The sealing rings are cut from a plate of the heating protection. The sample steel rings are cut from a steel tube having a diameter of 116.4 mm to 50 mm wide rings.

Figure 11-15: from left: sample holder, pressure plunger and sample ring (by author)

Flow meter (rotameters)

To measure the flow rate the 5 rotameters Vögtlin were used with measuring unit Bl/h. The value is read in the middle of the float. All 5 float flowmeters have a millimeter scale of 0 - 120 mm. This is the model V 100. By multiple distributor and ball valves, the air flow is directed to the appropriate rotameter.

Following rotameter were used:

- K140 E01**:** Measuring glass: 140mm length; Float: Glass material, black, d= 1,191 mm; calibration medium: nitrogen, 1,5 bars; Flow (20°C, 2 bas, air): 0 – 3,3 Nl/h
- K140 E08G**:** Measuring glass: 140mm length; Float: Glass material, black, d= 3,175 mm; calibration medium: nitrogen, 1,013 bars; Flow (20°C, 2 bas, air): 0 – 26,9 Nl/h
- K140 E11G**:** Measuring glass: 140mm length; Float: Glass material, black, d = 3,175 mm; calibration medium: nitrogen, 1,5 bars; Flow (20°C, 2 bas, air): 0 - 3.3 Nl/h
- K140 H14**:** Measuring glass: 140mm length; Float: Material steel, metallic, d= 6,35 mm; calibration medium: water, 20°C, flow rate (20°C, 2 bas, air): 103,2 –1118,1 Nl/h
- K140 B15: Measuring glass: 140mm length; Float: Material Ceramic, white, d= 9,525 mm; calibration medium: water, 20°C, flow rate (20°C, 2 bas, air): 5 - 3423.7 Nl/h

Figure 11-16: Rotameters (by author)

Computer programme

With the computer program FlowCalc 1.0 from Vögtlin the measured data can be evaluated. The readings of the rotameter in millimeters are converted with the help of the program to liter per hour [Bl/h]. **F**ormula for input into the Excel spreadsheet:

$$k = \frac{\dot{m}_2 * l}{A} * v * \frac{2p_2}{p1^2 - p2^2} \qquad 1.17.$$

k… permeability k [m^2]

$\dot{m}_2$ … flow rate =dm/dt [Bl / h]

l… perfused specimen length [m]

A… surface of the sample [m]

ν… kinematic viscosity [m/s]

p_1… inlet pressure [bara]

p_2 … outlet pressure [bara]

11.5.3 Results of experimental work

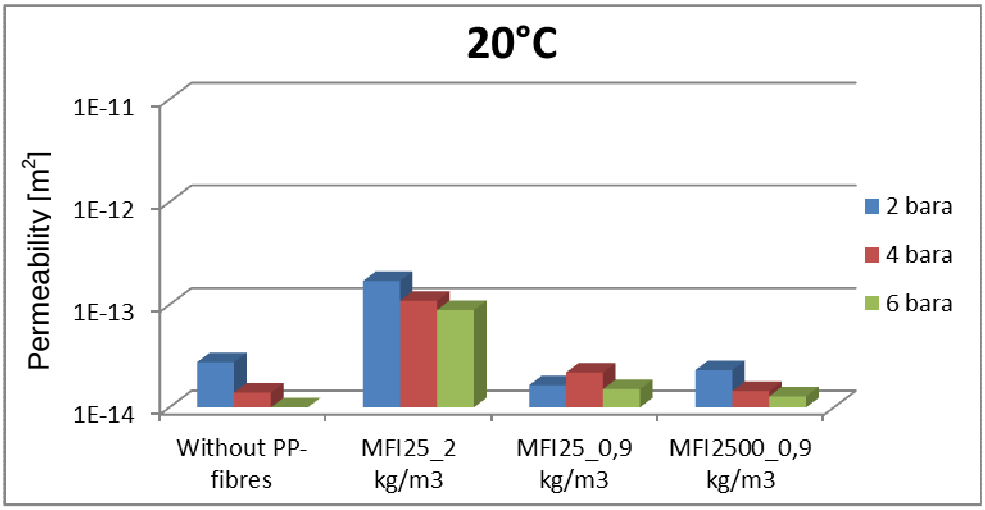

Figure 11-17: Permeability measured at 20°C with applied pressure 2, 4, 6 bara

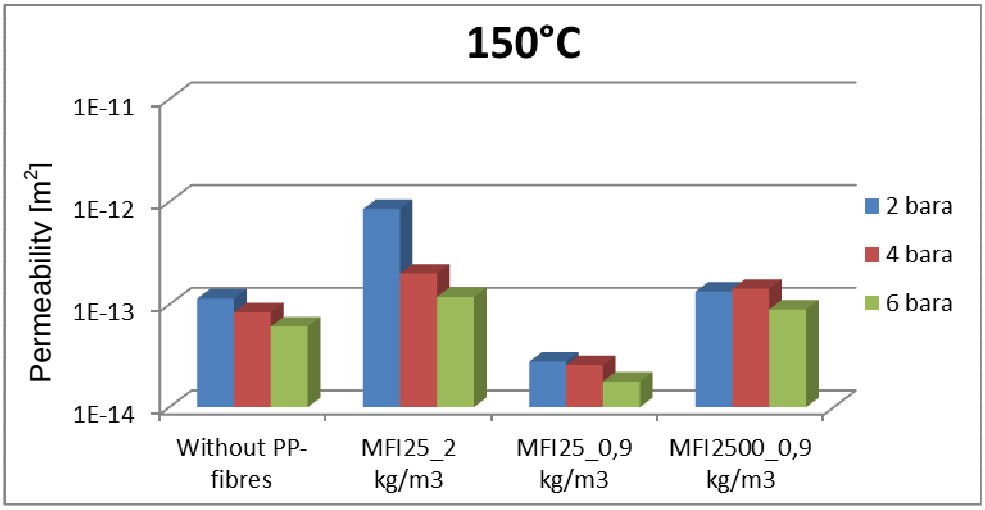

Figure 11-18: Permeability measured at 150°C with applied pressure 2, 4, 6 bara

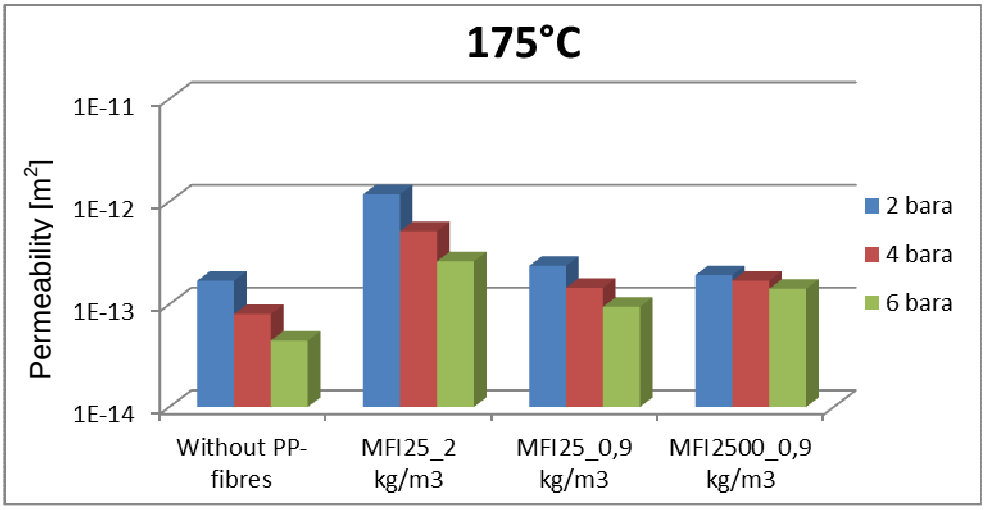

Figure 11-19: Permeability measured at 175°C with applied pressure 2, 4, 6 bara

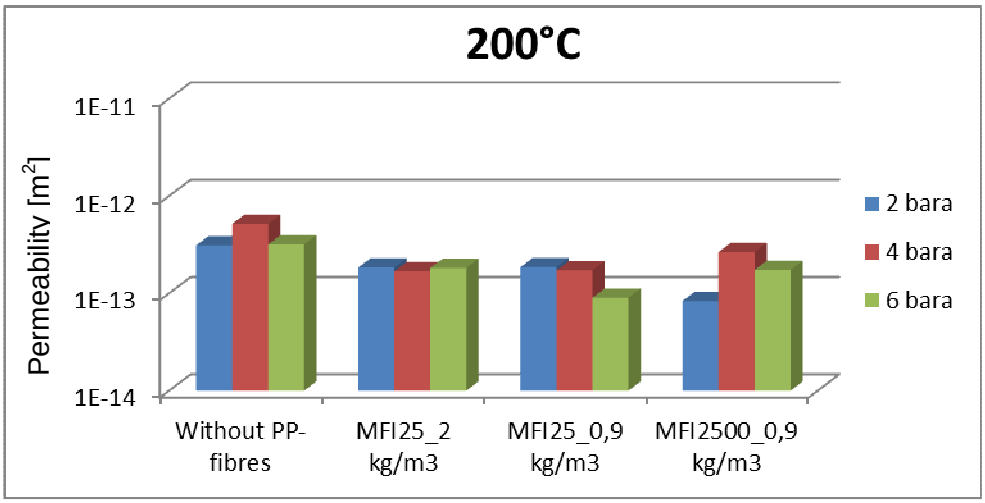

Figure 11-20: Permeability measured at 200°C with applied pressure 2, 4, 6 bara

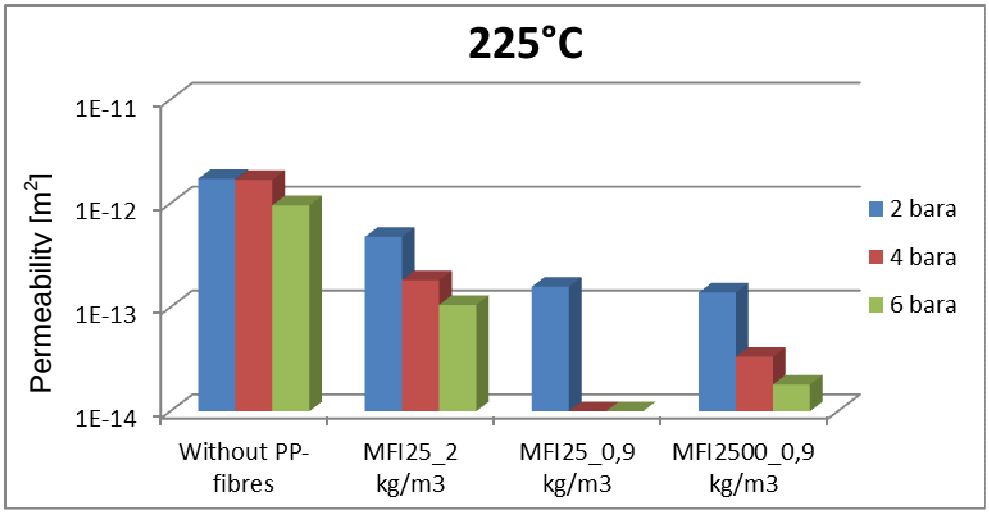

Figure 11-21: Permeability measured at 225°C with applied pressure 2, 4, 6 bara

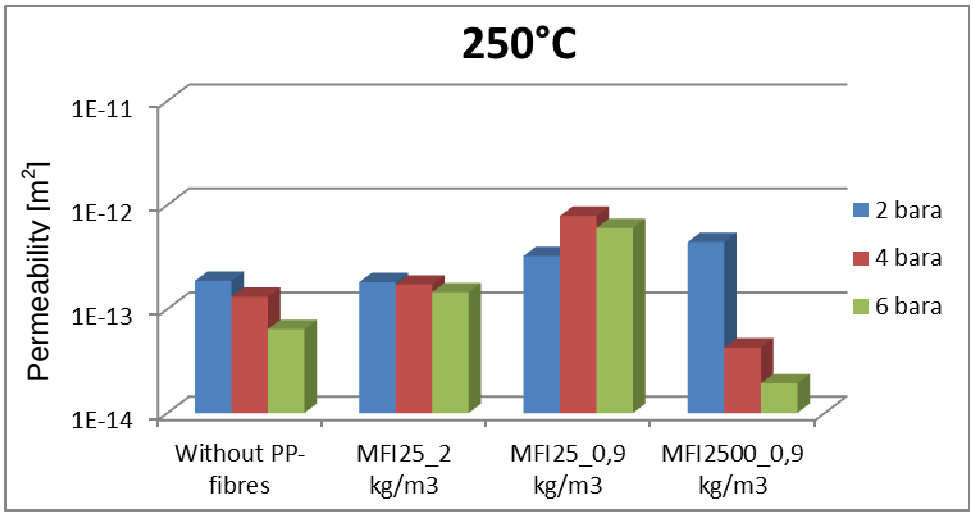

Figure 11-22: Permeability measured at 250°C with applied pressure 2, 4, 6 bara

11.5.4 Summary and conclusion

Diagrams showed in **Figure 11-17** - **Figure 11-22** demonstrate permeability measured at 2, 4 and 6 bara. Lower initial permeability of plain concrete (without fibres) in comparison to fibre reinforced concrete was expected. The highest permeability $1.7 \cdot 10^{-13}$ m^2 measured at 20°C (before heating) has been measured in specimen with standard fibres with MFI 25 and dosage 2 kg/m^3. That was expected due to the essential mode of action of fibres that increase porosity during a mixing of fresh concrete. Initial permeability of plain concrete (without fibres) is close to $2.7 \cdot 10^{-14}$ m^2 and therefore is higher than permeability of specimens with standard fibres of reduced dosage of 0.9 kg/m^3 that is $1.6 \cdot 10^{-14}$ m^2. This anomaly may be a result of initial shrinkage of concrete that was in other specimens restricted by addition of fibres. This initial shrinkage could have disturbed sealing of the sample concrete ring and therefore permeability is slightly higher than assumed.

Figure 11-18 shows rapid increase of permeability of specimen with modified fibres at 150°C. Earlier softening and melting of fibres is cause by higher melt flow index. Permeability of concrete with standard PP-fibres is increased later at 175°C and thus mode of action of modified and standard PP-fibres differ in melting point.

Permeability of plain concrete at increasing temperature is almost constant up to 175°C and then rapidly increases at range between 200°C and 225°C. Permeability of concrete without fibers measured at 225°C differs one order of magnitude from fibre reinforced concretes. It may result from crack formed due to high pressure build-up in pores. Subsequent rapid decrease of one order of magnitude at 250°C was likely caused by measurement error. Permeability of different concrete mixtures measured at 2 bara showed one interesting common point at temperature 200°C where permeability reaches around 10^{-13} m^2. Permeability of samples with fibres have increasing trend up to 175°C compared to the sample without fibers which has almost constant permeability up to this temperature. It could be a result of mode of action of fibres that increase permeability just before 175°C.

Noticeable increase of permeability and melting point of fibres is marked in Figure 11-23. Temperature peaks obtained from permeability measurement are in consistent with results gained from high temperature microscopy. PP-fibres with MFI 25 reached the highest permeability at 175°C. This permeability was $2.37 \cdot 10^{-13}$ m^2 for sample with reduce dosage of 0.9 kg/m^3 fibres and $5.71 \cdot 10^{-13}$ m^2 for standard dosage of 2 kg/m^3. Rapid increase of permeability of sample with fibres with higher melt flow index (MFI 2500) was recorded at 150°C. Permeability at this temperature peak was $1.33 \cdot 10^{-13}$ m^2 and thus

higher than permeability of samples with a same dosage of standard fibres that was $9.43 \cdot 10^{-14}$ m^2.

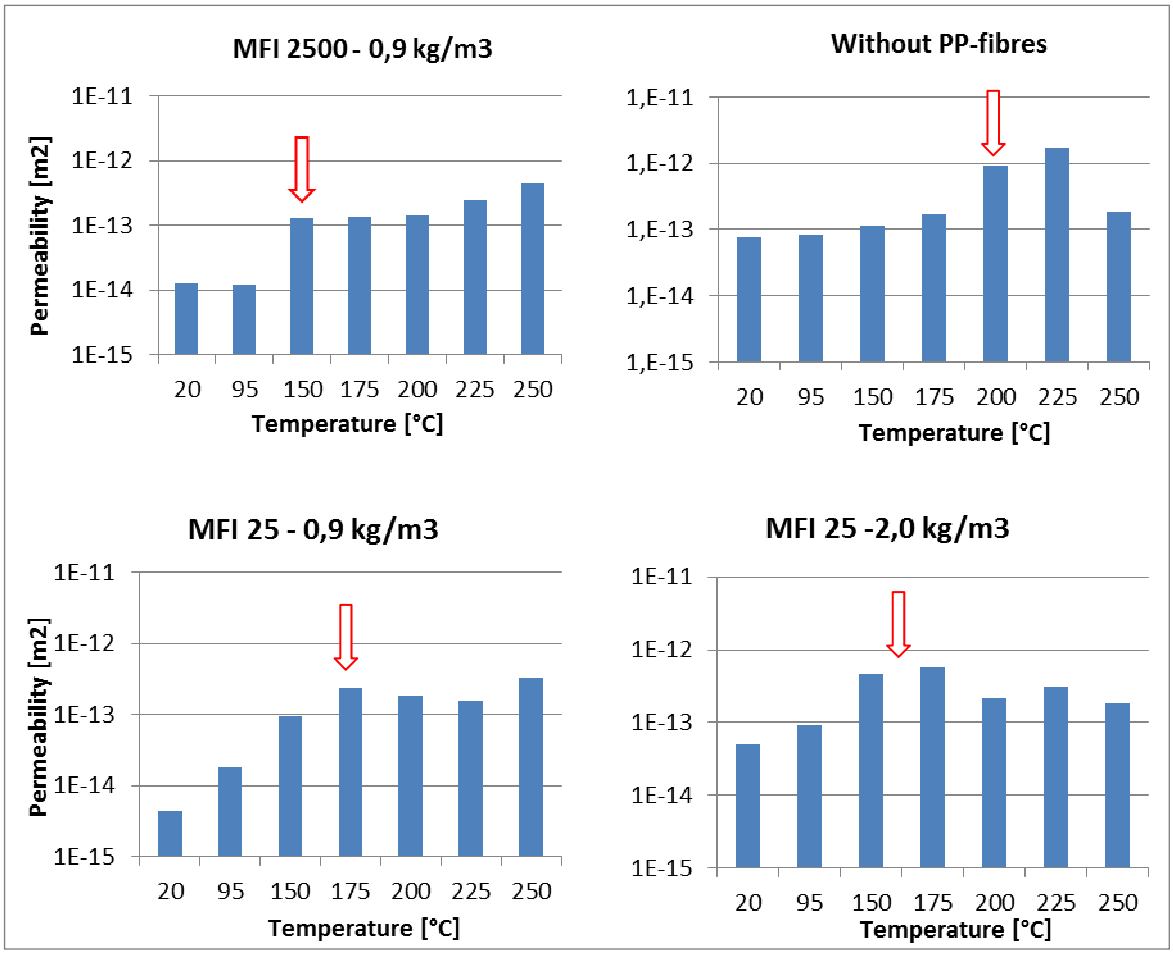

Figure 11-23: Permeability increase related to measured temperature steps

The evaluation was based on the results obtained from measurements, researches carried out and published so far ([1]-[2][3], [21]-[23]).

12 Overall assessment of present work

Explosive spalling of concrete was intensively studied during the last decade. Spalling of concrete, especially in the case of high performance concrete (HPC), may be prevented by technological measures based on the addition of small amounts of PP-fibres. This amount various according to the density of concrete which is mainly influence by water-cement ratio. The effect of fibre addition was originally explained by the vapour flow theory and the theory of permeation. Due to our experience to eliminate explosive spalling of concrete structures exposed to elevated temperature, we propose say the following that emerged from the experiments carried out:

- for ordinary concrete (OC), generally 1 kg/m^3 of polypropylene fibres are enough to avoid spalling,
- for high performance concrete (HPC), generally 2.0 kg/m^3 of polypropylene fibres with melt flow index 25 (MFI25) are enough to avoid spalling,
- for high performance concrete (HPC) 0.9 kg/m^3 of polypropylene fibres with melt flow index 2500 (MFI2500) are enough to avoid spalling.

Behaviour of concrete subjected to high temperatures is not entirely understand today and attempt to clarify this issue is still in process. Even though many experiments and reported test results has been already released but it is difficult to interpret the results due to the facts that tested concretes are different, test procedures are different, the test condition are not comparable, interpretation of results is not clear enough, description of test procedures are incomplete, size and shape of specimens are incomparable etc. Mode of action of PP fibres, fibre-matrix interaction, permeability of concrete, micro-cracking, macro-cracking, the crack population and other aspect are necessary to investigate and clarify in detail.

Further permeability measurements should be done between 150°C and 170°C to distinguish properties and behavior of polypropylene fibers with different melt flow index. Also further microstructure analysis may bring to the light major contribution of fibres, fibre-matrix interaction and formation of micro-cracks and/or macro-cracks.

Permeability measurement has proved to be very time consuming and therefore it was not possible to obtain sufficient amount of results within the diploma thesis that would determine the permeability of different concrete mixtures with high accuracy.

Finally, it would be appropriate to note that deeper experience of permeability measurements was acquired based on course of measurement and gained results that allowed modification of testing equipment. Arrangement, which will ensure the more accurate results and simplify measuring process.

13 LIST OF REFERENCES

[1] Kalifa, P.; Chéné, G and Gallé, C: 'High-temperature behaviour of HPC with polypropylene fibres – From spalling to microstructure', Cement and Concrete Research 31 (2001) 1487-1499.

[2] Zeiml, M.; Leithner, D.; Lackner, R.; Mang, H. A.: 'How do polypropylene fibers improve the spalling behavoir of in-situ concrete?', Cement and Concrete Research 36 (2006) 929-942.

[3] Schneider U. Properties of material at high temperatures-concrete. 2nd RILEM Report, Gesamthochule Kassel, Germany; 1986.

[4] Hertz KD. Limits of spalling of fire-exposed concrete. Fire Safety Journal 2003;38:103–16.

[5] Kodur VKR, Bilodeau A, Hoff GC. Optimization of the type and amount of polypropylene fibres for preventing the spalling of lightweight concrete subjected to hydrocarbon fire. Cem Concr Compos 2004;26(2):163–74.

[6] List of historical tunnels fire by Promat: http://www.promat-tunnel.com/en/lijst2.html

[7] Directive 2004/54/EC of the European Parliament and of the Council on Minimum Safety. Requirements for Tunnels in the Trans-European Road Network, April 2004, Brussels, Belgium

[8] Commission Decision of 20 December 2007 concerning the technical specification of interoperability relating to ‘safety in railway tunnels’ in the trans-European conventional and high-speed rail system, no. 2008/163/EC

[9] Schulte C., Schaab A.; Fire protection requirements and solution for international tunnel projects. Proceedings of 2nd International RILEM Workshop on Concrete Spalling due to Fire Exposure, 5-7 October 2011, Delft, The Nedherlands

[10] Eurocode 1: Actions on structures - Part 1-2: General actions - Actions on structures exposed to fire; German version EN 1991-1-2:2002 + AC:2009

[11] Eurocode 2: Design of concrete structures- Part 1-2: General rules- Structural fire design; German version EN 1992-1-2:2004 + AC:2008

[12] EN 13501-1:2007: Fire classification of construction products and building elements - Part 1: Classification using test data from fire reaction to fire tests

[13] ČSN 73 7507 Desing of road tunnels, January 2006, Czech Republic

[14] Types of fire exposure. Online [2013-08-06]. Available from: <:http://www.promat-tunnel.com/en/hydrocarbon-hcm-hc/rabt-rws.aspx#>

[15] EUREKA-Bericht zu EU 499 Firetun: Fire inTransport Tunnels, Report on Full-Scale Tests, Studiengesellschaft für Stahlanwendung, Düsseldorf, 1996.

[16] Smith, K., Atkinson, T.; PP fibres to resist fire-induced concrete spalling, Propex Concrete System, UK, November 2010. Online [2013-08-06]. Available from: <http://www.tunneltalk.com/Polypropylene-fibres-Nov10-Resistance-to-concrete-spalling-under-fire.php>

[17] Cit. [2013-09-12]. Available from: < http://www.promat-tunnel.com/en/index.aspx>

[18] Mikulinec, D.; Betony s vzšší odolností vůči vysokým teplotám, Diplomová práce, VUT v Brně, Fast, 2012

[19] Schneider U., Horvath J., Behavior of Ordinary Concrete at High Temperatures. Institutsheft 9, Institut für Baustofflehre, Bauphysik und Brandschutz, TU – Wien, 2003

[20] SIČÁKOVÁ A. a kolektiv, New generation cement concretes – Ideas, Design, Technology and Aplications, 1. vydání Košice, červen 2008, 156 str., ISBN 978-80-553-0040-5

[21] K. Pistol, F. Weise, B. Meng, U. Schneider, The mode of action of polypropylene fibres in high performance concrete at high temperature, 2nd International Rilem Workshop on Concrete and Spalling due to Fire Exposure - Proceedings, Delft, (The Netherlands), (2011).

[22] P. Kalifa, G. Chéné, C. Gallé, High temperature behaviour of HPC with polypropylene fibres: from spalling to microstructure, Cement and Concrete Research 31 (2001) 1487–1499.

[23] P. Kalifa, F.D. Menneteau, D. Quenard, Spalling and pore pressure in HPC at high temperature, Cem. Concr. Res. 30 (2000) 1 – 13.

[24] R. Cerný; Properties of cementitious composites at high temperatures. Czech Technical University in Prague, Faculty of Civil Engineering, Department of Materials Engineering and Chemistry, Prague, Czech Republic

[25] J. Procházka, CSc. ČVUT - stavební fakulta, katedra betonových konstrukcí – Trvanlivost a životnost betonových konstrukcí

[26] U.Diederichs, U.M. Jumppannen, V.Penttala, Behaviour of high strength concrete at high temperatures, Espoo 1989, Helsinki University of Technology, Department of Structurat Enfineering, Report 92, 1992

[27] U.Diederichs – prezentation

[28] R. Drochytka, Trvanlivost stavebních materiálů, Brno 2007

[29] Thomas J., Jennings H. The science of concrete. Online [2013-08-06]. Available from: <http://iti.northwestern.edu/cement/monograph/Monograph7_2.html>

[30] Prof. Ing. Jaroslav Procházka, CSc. ČVUT - stavební fakulta, katedra betonových konstrukcí – Trvanlivost a životnost betonových konstrukcí

[31] K. Gornik, Einfluss der Temperatur auf die Permeabilität von Beton, Master´s thesis, Technical University TU Wien, 2006

[32] U. Schneider, Research Report vol.9, Vienna University of Technology, Institute for building materials, buildings physic and fire protection, Institute 206.

[33] http://www.bernardo-maschinen.com/WK-12-F-Bernardo-Werkstattpresse.html

[34] Neville A. M., Properties of concrete, Fourth Edition

[35] One seven. [online]. [cit. 2013-09-20]. Available from: <http://www.oneseven.com/references/stationary-references/>

[36] Fire protection for new and existing underground structures [online]. 2009-7 [cit. 2013-09-20]. Available from: <http://www.tunnel- online.info/en/artikel/tunnel_Fire _Protection_for_new_and_existing_Underground_ Structures_329612.html>

[37] Clement F., Zámečník M. Fire protection option for concrete tunnel linings [online]. 2007-1-16.ročník. [cit. 2013-08-20]. Available from: <http://www.ita-aites.cz/files/tunel/2007/1/tunel-0701-6.pdf>

[38] Z. Liu, A. Kashef, G. Lougheed, J. Z. Su and N. Benichou; An Overview of the International Road Tunnel Fire Detection Research Project. Available from: <www.nfpa.org/~/media/Files/proceedings/an_overview_of_the_international_road _tunnel_fire_deteciton_.pdf

[39] Fire design of concrete structures : materials, struktures and modelling. 2007. Lausanne, Shwitzerland : Case Postale, 2007. 91 s. ISBN 978-2-88394-078-9

[40] Image of monofilament polypropylene fibres [online]. [cit. 2013-09-24]. Available from:<http://jiataiexport.en.made-in-china.com/product/bodEZHrjSeRB/China-PP-Monofilament-Fiber.html>.

[41] ABC Polymer IndustriesTM an international plastics group. Image of polypropylene fibres [online]. [cit. 2013-09-24]. Available from:<http://www.abcpolymerindustries.com/concrete-fibers.php>.

[42] Persson B.; Mitagation of fire spalling of concrete with fibres, Presentation in technical committee “Durability of Self-Compacting Concrete”, Ghent (Belgium), April 2005

[43] Liu X.; Ye G.; De Schutter G.; Yuan Y.; Taerwe L.; On the mechanism of polypropylene fibres in preventing fire spalling in self-compacting and high-performance cement paste, Delf (The Netherland), November 2007

[44] Adhesives Toolkit. Capillary rheometers [online]. [cit. 2013-12-23]. Available from:<http://www.adhesivestoolkit.com/Docs/test/Physical%20Analysis%20-%20Capillary%20Rheometers.xtp#ref21>

[45] Castellotea M., Alonsoa C., Andradea C., Turrillasa X., Campoc J.: Composition and microstructural changes of cement pastes upon heating, as studied by neutron diffraction, Cement and Concrete Research 34 (2004) 1633–1644

[46] J. Horvath, C. Hertel, F. Dehn, U. Schneider,; Einfluß der Vorlagerung auf das Temperaturverhalten von selbstverdichtendem Beton, Berlin, 2004

[47] J.Válek, L. Bodnárová, R. Hela,; Vytvoření postupů a receptur pro použití betonu s vyšší trvanlivostí vůči působení vysokých teplot v konstrukcích; Dílčí vyzkumná práce za rok 2011, CIDEAD 2011

[48] S. Werner, A. Rogge,; Effect of the dimension of a fire exposed surface upon the spalling of concrete specimens, Fire and Materials, 2014

[49] Z. P. Bažant. Analysis of pore pressure, thermal stress and fracture in rapidly heated concrete. In L. T. Phan, N. J. Carino, D. Duthinh, and E. Garboczi, editors, Proceedings of the International Workshop on Fire Performance of High-Strength Concrete, pages 155–164. NIST, Gaithersburg, Maryland, 1997.

[50] From Wikipedia, free encyclopedia. Bimetal 2013-12 [online]. [cit. 2013-09-24]. Available from:<http://en.wikipedia.org/wiki/Bimetal>

14 LIST OF ACRONYMS AND SYMBOLS

PP polypropylene

MFI melt flow index

HPC high performance concrete

OC ordinary concrete

SCC self compacting concrete

15 LIST OF ANNEXES

A. Concrete permeability results

B. Methodology of experimental work

ANNEXES

A.CONCRETE PERMEABIILTY RESULTS

A.1. Permeability of concrete with 0.9 kg/m^3 PP-fibres with MFI 25 (MFI25-0.9kg/m^3)

No	Date	Start [hh:mm]	Oven temp. [°C]	P_1 [bara]	Rotam.	Δp [bara]	P_2 [bara]	Permeability K [m²]	Test durati. [h]
20°C									
1	24.6.13	08:20	27,7	2,0	3/64	0,8090	1,19	**1,648E-14**	
2	24.6.13	13:00	27,8	4,0	4/44	2,5092	1,49	**2,196E-14**	5,0
3	24.6.13	14:45	27,6	6,0	4/61	4,1757	1,82	**1,508E-14**	2,0
4	25.6.13	15:35	27,2	2,0	3/92	0,9374	1,06	**1,838E-14**	1,0
150°C									
1	12.6.13	15:30	22,9	2,0	2/40	0,9138	1,09	**7,266E-16**	
2	13.3.13	08:05	23,6	2,0	2/58	0,9142	1,09	**1,327E-15**	16,5
3	13.3.13	14:30	171,5	2,0	3/79	0,7760	1,22	**2,776E-14**	6,5
4	14.3.13	08:10	169,6	4,0	4/40	2,5376	1,46	**2,577E-14**	17,5
5	14.6.13	13:10	166,6	6,0	4/55	4,1809	1,82	**1,784E-14**	5,0
6	23.6.13	11:00	28,3	2,0	2/26	1,3137	0,69	**2,186E-16**	
175°C									
1	26.6.13	15:30	26,0	2,0	2/59	0,8071	1,19	**1,642E-15**	
2	27.6.13	08:45	107,0	2,0	3/63	0,8559	1,14	**1,762E-14**	17,0
3	27.7.13	15:45	169,5	2,0	4/40	0,6208	1,38	**1,608E-13**	7,0
4	28.6.13	08:00	193,3	2,0	4/49	0,4653	1,53	**2,829E-13**	16,0
5	28.6.13	11:35	184,2	4,0	4/81	1,3092	2,69	**1,451E-13**	3,5
6	29.6.13	13:30	184,9	6,0	4/97	2,2801	3,72	**9,469E-14**	26,0
7	01.07.23	08:00	24,4	2,0	3/39	1,0713	0,93	**6,876E-15**	42,0
200°C									
1	1.7.13	13:00	25,0	2,0	2/116	0,8557	1,14	**4,290E-15**	
2	2.7.13	07:30	185,8	2,0	4/32	0,4753	1,52	**1,919E-13**	19,0
3	2.7.13	17:00	214,2	2,0	4/32	0,6952	1,30	**1,249E-13**	9,5
4	3.7.13	10:30	216,0	4,0	4/83	1,2131	2,79	**1,717E-13**	17,5
5	3.7.13	15:45	26,8	6,0	4/102	1,9682	4,03	**9,009E-14**	5,0
6	4.7.13	09:00	32,2	2,0	3/41	1,7813	0,22	**1,362E-15**	17,0
225°C									
1	22.7.13	14:00	27,0	6,0	2/38	1,9865	4,01	**3,561E-16**	
2	23.7.13	06:40	226,7	6,0	4/11	4,5506	1,45	**4,994E-15**	17,0
3	23.7.13	13:05	254,0	2,0	2/67	0,9848	1,02	**2,234E-15**	5,5
4	23.7.13	16:50	255,5	4,0	3/98	2,8134	1,19	**6,398E-15**	4,0
5	24.7.13	07:00	255,0	6,0	4/24	4,5701	1,43	**8,062E-15**	14,0
6	24.7.13	15:10	42,4	2,0	2/41	0,9783	1,02	**6,967E-16**	8,0
250°C									
1	11.9.13	13:00	25,0	2,0	3/30	1,0200	0,98	**6,155E-15**	
2	12.9.13	08:40	205,2	2,0	4/51	0,5463	1,45	**2,460E-13**	19,5
3	12.9.13	13:10	228,0	2,0	4/55	0,4832	1,52	**3,138E-13**	4,5
4	13.9.13	10:30	257,2	2,0	4/56	0,4930	1,51	**3,229E-13**	21,0
5	13.9.13	12:00	252,5	4,0	4/102	0,3942	3,61	**7,838E-13**	1,5
6	14.9.13	07:55	275,3	6,0	5/44	0,5800	5,42	**6,001E-13**	20,0
7	15.9.13	13:30	22,0	2,0	4/49	0,6792	1,32	**1,286E-13**	28,5

A.2. Permeability of concrete with PP-fibres of dosage 2 kg/m^3 with MFI 25 (MFI25-2 kg/m^3)

No	Date	Start [hh:mm]	Oven temp. [°C]	P_1 [bara]	Rotam.	Δp [bara]	P_2 [bara]	Permeability K [m²]	Test durati. [h]
20°C									
1	17.7.13	09:30	25,9	2,0	4/42	0,4892	1,51	**1,704E-13**	
2	17.7.13	15:50	25,9	4,0	4/81	1,2975	2,70	**1,092E-13**	6,0
3	18.7.13	11:25	26,0	6,0	4/102	1,9865	4,01	**8,885E-14**	19,5
150°C									
1	4.10.13	07:25	23,8	2,0	3/82	0,9847	1,02	**1,514E-14**	
2	4.10.13	12:00	105,6	2,0	4/32	0,9609	1,04	**6,554E-14**	4,5
3	7.10.13	08:00	173,3	2,0	4/105	0,3202	1,68	**8,517E-13**	20,0
4	7.10.13	12:55	173,2	4,0	4/58	1,0016	3,00	**2,008E-13**	5,0
5	7.10.13	16:00	168,4	6,0	5/65	1,6961	4,30	**1,186E-13**	3,0
6	8.10.13	08:15	27,4	2,0	4/39	0,9333	1,07	**6,803E-14**	16,0
175°C									
1	26.6.13	15:30	26,0	2,0	2/59	0,8071	1,19	**1,642E-15**	
2	27.6.13	08:45	107,0	2,0	3/63	0,8559	1,14	**1,762E-14**	17,0
3	27.7.13	15:45	169,5	2,0	4/40	0,6208	1,38	**1,608E-13**	7,0
4	28.6.13	08:00	193,3	2,0	4/49	0,4653	1,53	**2,829E-13**	16,0
5	28.6.13	11:35	184,2	4,0	4/81	1,3092	2,69	**1,451E-13**	3,5
6	29.6.13	13:30	184,9	6,0	4/97	2,2801	3,72	**9,469E-14**	26,0
7	1.07.13	08:00	24,4	2,0	3/39	1,0713	0,93	**6,876E-15**	42,0
200°C									
1	29.7.13	13:05	29,7	2,0	3/77	0,8931	1,11	**1,696E-14**	
2	29.7.13	18:10	175,4	2,0	4/38	0,6756	1,32	**1,402E-13**	5,0
3	30.7.13	07:30	196,0	2,0	4/41	0,6120	1,39	**1,746E-13**	13,5
4	30.7.13	13:50	225,7	2,0	4/41	0,6078	1,39	**1,839E-13**	6,5
5	31.7.13	06:50	222,6	4,0	4/84	1,2580	2,74	**1,681E-13**	17,0
6	31.7.13	12:00	217,9	6,0	4/107	1,5343	4,47	**1,823E-13**	5,0
	31.7.13	15:00	74,0	2,0	4/53	0,4788	1,52	**2,388E-13**	3,0
225°C									
1	8.10.13	13:40	25,3	2,0	3/76	0,8381	1,16	**1,817E-14**	
2	9.10.13	08:15	193,0	2,0	4/73	0,5175	1,48	**3,559E-13**	18,5
3	9.10.13	11:00	225,7	2,0	4/78	0,5412	1,46	**3,768E-13**	3,0
4	9.10.13	15:00	253,4	2,0	4/81	0,4723	1,53	**4,781E-13**	4,0
5	10.10.13	07:10	265,8	4,0	5/53	1,1730	2,83	**1,827E-13**	16,0
6	10.10.13	13:20	262,6	6,0	5/63	2,0180	3,98	**1,057E-13**	6,0
7	11.10.13	09:55	26,4	2,0	4/13	0,9807	1,02	**3,055E-14**	19,5
250°C									
1	6.5.13	10:20	22,0	2,0	3/87	0,9913	1,01	**1,838E-14**	
2	6.5.13	15:40	87,0	2,0	4/14	0,9262	1,07	**3,959E-14**	5,5
3	7.5.13	08:28	138,0	2,0	4/31	0,8273	1,17	**8,510E-14**	16,0
4	7.5.13	14:18	179,0	2,0	4/37	0,7542	1,25	**1,186E-13**	6,0
5	8.5.13	08:20	208,0	2,0	4/42	0,6687	1,33	**1,612E-13**	18,0
6	8.5.13	14:20	225,0	2,0	4/43	0,6367	1,36	**1,796E-13**	6,0
7	13.5.13	12:45	225,0	2,0	4/39	0,7331	1,27	**1,373E-13**	
8	14.5.13	07:40	250,0	2,0	4/43	0,6494	1,35	**1,809E-13**	19,0
9	14.5.13	10:20	250,0	4,0	4/83	1,2564	2,74	**1,716E-13**	2,5
10	14.5.13	13:55	250,0	6,0	4/104	1,8601	4,14	**1,450E-13**	3,5
11	15.5.13	08:07	22,0	2,0	4/24	0,8819	1,12	**5,169E-14**	18,0

A.3. Permeability of concrete with 0.9 kg/m^3 PP-fibres with MFI 2500 (MFI2500-0.9kg/m^3)

No	Date	Start [hh:mm]	Oven temp. [°C]	P_1 [bara]	Rotam.	Δp [bara]	P_2 [bara]	Permeability K [m²]	Test durati. [h]
20°C									
1	7.8.13	17:35	33,9	2,0	3/107	0,9055	1,09	**2,310E-14**	
2	8.8.13	06:20	30,3	4,0	4/32	2,6967	1,30	**1,444E-14**	12
3	8.8.13	10:30	30,4	6,0	4/54	4,2732	1,73	**1,281E-14**	4
150°C									
1	9.9.13	12:15	24,1	2,0	2/116	0,9891	1,01	**3,417E-15**	
2	9.9.13	15:03	105,7	2,0	3/55	0,9891	1,01	**1,244E-14**	3
3	10.9.13	08:10	176,5	2,0	4/41	0,7324	1,27	**1,336E-13**	17
4	10.9.13	11:20	170,5	4,0	4/92	0,9634	3,04	**1,424E-13**	3
5	10.9.13	14:30	170,7	6,0	5/41	1,5077	4,49	**8,972E-14**	3
6	11.9.13	08:00	27,5	2,0	4/26	0,8848	1,12	**5,489E-14**	17,5
175°C									
1	26.9.13	12:15	23,3	2,0	3/5	1,0251	0,97	**2,835E-15**	
2	27.9.13	08:05	174,4	2,0	4/39	0,7120	1,29	**1,326E-13**	20
3	27.9.13	14:30	190,9	2,0	4/41	0,6811	1,32	**1,924E-13**	6,5
4	28.9.13	16:20	193,1	4,0	4/95	0,8760	3,12	**1,696E-13**	2
5	29.9.13	09:55	187,4	6,0	5/68	1,5597	4,44	**1,415E-13**	17
6	30.9.13	08:00	25,6	2,0	4/43	0,8885	1,11	**7,930E-14**	22
200°C									
1	3.9.13	12:45	23,1	2,0	3/37	0,8384	1,16	**9,745E-15**	
2	4.9.13	10:30	165,5	2,0	4/17	0,7097	1,29	**7,432E-14**	22
3	5.9.13	13:10	226,2	2,0	4/24	0,8182	1,18	**8,342E-14**	2,5
4	6.9.13	08:00	218,0	4,0	4/98	0,6233	3,38	**2,655E-13**	19
5	6.9.13	11:40	216,7	6,0	5/42	0,8306	5,17	**1,740E-13**	3,5
6	9.9.13	08:05	24,2	2,0	4/33	0,7871	1,21	**7,632E-14**	68
225°C									
1	30.9.13	14:30	24,7	2,0	3/55	0,8894	1,11	**1,243E-14**	
2	1.10.13	08:25	223,6	2,0	4/33	0,7814	1,22	**1,105E-13**	18
3	1.10.13	12:15	249,4	2,0	4/40	0,7579	1,24	**1,388E-13**	4
4	1.10.13	14:35	246,1	4,0	4/58	2,7288	1,27	**3,339E-14**	2
5	2.10.13	07:40	245,6	6,0	4/65	4,5369	1,46	**1,807E-14**	17
6	3.10.13	10:50	25,2	2,0	3/21	1,0567	0,94	**4,632E-15**	3
250°C									
1	20.9.13	08:00	21,2	2,0	3/114	0,8689	1,13	**2,517E-14**	
2	22.9.13	12:40	221,8	2,0	4/50	0,5601	1,44	**2,397E-13**	52,5
3	23.9.13	08:00	250,0	2,0	4/57	0,4513	1,55	**3,601E-13**	19
4	23.9.13	11:40	287,6	2,0	4/58	0,4002	1,60	**4,411E-13**	4
5	23.9.13	15:35	287,3	4,0	4/52	2,4127	1,59	**4,261E-14**	4
6	23.9.13	21:35	284,8	6,0	5/53	4,2709	1,73	**1,920E-14**	6
7	24.3.13	08:40	22,2	2,0	3/40	1,0497	0,95	**7,233E-15**	11
7	24.3.13	08:40	22,2	2,0	3/40	1,0497	0,95	**7,233E-15**	11

A.4. Permeability of concrete without PP-fibres (Without PP-fibres)

No	Date	Start [hh:mm]	Oven temp. [°C]	P_1 [bara]	Rotam.	Δp [bara]	P_2 [bara]	Permeability K [m²]	Test durati. [h]
20°C									
1	4.7.13	13:00	26,8	2,0	4/11	0,9915	1,01	**2,762E-14**	
2	4.7.13	15:45	27,3	4,0	4/29	2,6510	1,35	**1,391E-14**	2,5
3	5.7.13	07:10	25,4	6,0	4/34	4,4351	1,56	**7,626E-15**	15,5
4	5.7.13	11:30	26,9	2,0	3/52	1,0047	1,00	**9,810E-15**	4
150°C									
1	16.9.13	07:55	21,3	2,0	4/46	0,7302	1,27	**1,101E-13**	
2	16.9.13	12:45	174,3	2,0	4/42	0,9049	1,10	**1,002E-13**	5
3	16.9.13	15:05	168,6	4,0	4/83	1,5583	2,44	**8,415E-14**	2,5
4	16.9.13	21:40	162,4	6,0	5/39	1,9351	4,06	**6,115E-14**	6,5
5	17.9.13	08:45	31,7	2,0	4/50	0,6812	1,32	**1,331E-13**	11
175°C									
1	24.9.13	12:20	25,3	2,0	2/68	0,9133	1,09	**1,757E-15**	
2	24.9.13	16:10	177,2	2,0	4/7	0,8713	1,13	**3,736E-14**	4
3	25.9.13	08:05	197,2	2,0	4/41	0,6980	1,30	**1,467E-13**	16
4	25.9.13	12:00	191,1	4,0	4/82	1,6388	2,36	**8,021E-14**	4
5	25.9.13	15:00	180,2	6,0	4/98	2,7155	3,28	**4,442E-14**	3
6	26.9.13	07:55	27,4	2,0	3/40	1,0220	0,98	**7,668E-15**	15
200°C									
1	5.8.13	12:25	28,6	2,0	4/23	0,7693	1,23	**6,231E-14**	
2	5.8.13	15:35	176,6	2,0	4/44	0,5893	1,41	**1,890E-13**	3
3	6.8.13	06:30	192,9	2,0	4/52	0,4898	1,51	**2,809E-13**	14,5
4	6.8.13	12:40	217,4	2,0	4/52	0,4643	1,54	**3,106E-13**	6
5	6.8.13	14:50	218,8	4,0	4/97	0,3337	3,67	**5,176E-13**	2
6	7.8.13	06:45	198,8	6,0	5/45	0,4885	5,51	**3,185E-13**	15,5
225°C									
1	17.9.13	11:30	21,9	2,0	4/53	0,4774	1,52	**2,117E-13**	
2	17.9.13	16:00	188,1	2,0	4/68	0,1411	1,86	**1,365E-12**	4,5
3	18.9.13	08:10	206,1	2,0	4/70	0,0720	1,93	**2,881E-12**	16
4	18.9.13	12:35	228,1	2,0	4/70	0,0653	1,93	**3,285E-12**	4
5	18.9.13	16:05	230,3	4,0	4/106	0,1146	3,89	**1,693E-12**	3,5
6	19.9.13	08:00	240,2	6,0	5/46	0,1779	5,82	**9,623E-13**	16
7	19.9.13	15:45	28,3	2,0	4/72	0,1100	1,89	**1,386E-12**	7,5
250°C									
1	5.6.13	14:40	20,1	2,0	4/22	0,8154	1,18	**5,435E-14**	5
2	6.6.13	08:00	105,9	2,0	4/27	0,7518	1,25	**8,339E-14**	17
3	6.6.13	13:30	166,7	2,0	4/34	0,6582	1,34	**1,302E-13**	5,5
4	7.6.13	08:30	191,5	2,0	4/38	0,5834	1,42	**1,719E-13**	19
5	8.6.13	04:45	221,3	2,0	4/38	0,5853	1,41	**1,789E-13**	20
6	9.6.13	08:30	242,6	2,0	4/37	0,5955	1,40	**1,769E-13**	4
7	10.6.13	08:00	281,2	2,0	4/36	0,5856	1,41	**1,862E-13**	23,5
8	10.6.13	12:10	301,6	4,0	4/79	1,2432	2,76	**1,307E-13**	4
9	10.6.13	15:45	297,0	6,0	4/90	2,0263	3,97	**6,406E-14**	3,5
10	11.6.13	16:00	24,9	2,0	4/27	0,7473	1,25	**7,127E-14**	24

B. METHODOLOGY OF EXPERIMENTAL WORK

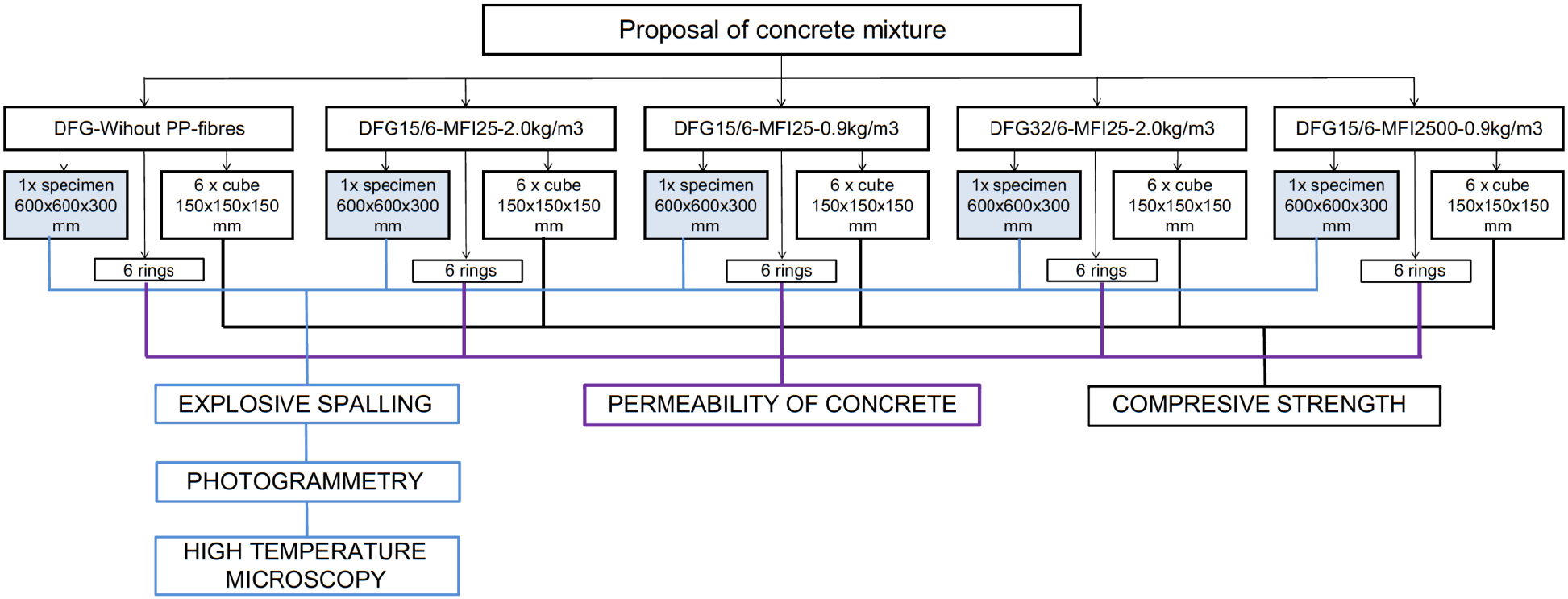
Proposal of concrete mixture
DFG-Wihout PP-fibres
DFG15/6-MFI25-2.0kg/m3
DFG15/6-MFI25-0.9kg/m3
DFG32/6-MFI25-2.0kg/m3
DFG15/6-MFI2500-0.9kg/m3
1x specimen 600x600x300 mm
6 x cube 150x150x150 mm
6 rings
EXPLOSIVE SPALLING
PERMEABILITY OF CONCRETE
COMPRESIVE STRENGTH
PHOTOGRAMMETRY
HIGH TEMPERATURE MICROSCOPY